Complementary Strategies to Promote Mesenchymal Stem Cell Differentiation for Ligament Tissue Engineering

Robyn Denise Shaffer

Dissertation Submitted to the Faculties of Virginia Polytechnic Institute and State University and Wake Forest University in partial fulfillment of the requirement for the degree of

Doctor of Philosophy
in
Biomedical Engineering

Aaron S. Goldstein, Co-Chairman
Linda A. Dahlgren, Co-Chairman
Mark E. Van Dyke
William R. Huckle
James Y. Yoo

11/1/2010
Blacksburg, Virginia

Keywords: tendon, regenerative medicine, electrospun, topography, nucleofection

Complementary Strategies to Promote Mesenchymal Stem Cell Differentiation for Ligament Tissue Engineering

Robyn D. Shaffer

Abstract

Anterior cruciate ligament (ACL) ruptures and tears are significant orthopedic problems that result in discomfort and limited mobility. Fully functional tissue engineered ligament replacements are promising alternatives to current graft choices for repair of ACL disruptions. The cell-based approach to construct engineered ligament grafts presented herein involves the culture of mesenchymal stem cells (MSC) on biodegradable, fibrous polymeric scaffolds to promote tissue formation. Multipotent MSCs are advantageous because of their *in vitro* proliferative capacity and ease of harvest; however; the promotion of MSC differentiation into mature fibroblasts and subsequent extracellular matrix (ECM) development is unknown. The proposed studies utilized three complementary methods to promote differentiation of MSCs: scaffold architecture, mechanical stretch, and over-expression of the transcription factor, scleraxis. First, elastomeric scaffolds were fabricated by electrospinning a segmented poly(esterurethane urea) with variations in fiber diameter and fiber alignment. Primary mesenchymal stem cells and the mesenchymal stem cell line, C3H10T1/2, were seeded on these scaffolds and assumed spindle-shaped morphologies and oriented with the direction of fiber alignment. Fiber diameter affected cellular responses, including the expression of ECM genes (e.g. collagen type I and decorin) which were elevated on smaller mean fiber diameter scaffolds initially. However, scleraxis gene expression was greatest on larger mean fiber diameter scaffolds at the end of two weeks. Second, cyclic stretch was applied to C3H10T1/2 cells on semi-aligned scaffolds using a novel bioreactor. Cell attachment was verified during and after the application of mechanical stress by confocal microscopy. Cyclic stretch induced cells to assume a highly elongated morphology; however, ECM gene expression changes were moderate. Third, forced constitutive expression of scleraxis was accomplished by nucleofection of C3H10T1/2 cells with plasmid DNA. Transient mRNA expression, accumulation of the gene product in the cell nucleus, and cell death were observed. Future work will seek to refine the experimental methods, including the development and testing of an inducible scleraxis transgene and the application of longer periods of mechanical stimulation. Finally, these complementary approaches may be combined to further extend this work in pursuit of directed differentiation of stem cells and the ensuing generation of a robust tissue graft.

Acknowledgements

My graduate school experience has been blessed with a number of people who have taught me the ropes in becoming a researcher as well as a better person. I would first like to thank Dr. Goldstein, my co-advisor, for his guidance, support and writing expertise during my tenure. I also thank my co-advisor Dr. Dahlgren for her support and always being my cheerleader – your help and direction were greatly appreciated! Thanks to Dr. Van Dyke and Dr. Yoo for advice and willingness to serve on my graduate committee as well as hosting me during my semester at WFRIM. I am grateful to Dr. Huckle for not only serving on my committee but also for assistance in many laboratory procedures. Many thanks to Dr. Eyestone for numerous discussions and advice during the scleraxis project.

I sincerely appreciate Dr. David Kaplan and the entire Tufts University BME department for graciously allowing me to work in their labs, as well as being great friends when I was far from home. I am especially grateful to Jon Kluge for taking the time to assist in my bioreactor project. I would also like to thank Dawn Delo O'Reilly for being my first research mentor and great friend – I strive to have the work ethic and attitude you do. To Christy Jones – thanks for being the best undergrad student I could have. I also thank the SBES department for support and assistance during my time at Virginia Tech.

I am fortunate to have very loving and supportive friends and family, including my new extended family (Sharon and Wes). I am eternally grateful to my Mom and Dad for providing moral support, lifting my spirits and doing anything for me, including those homemade meals during the homestretch!

To Nick, the best husband a girl could have. We finally made it through graduate school together, through the highs and lows, near and far. Thank you supporting me, I'm not sure what I would have done without you. I am so grateful to have you as my best friend. Thanks for being so great. You are the shore; I am the ocean.

Table of Contents

List of Figures

List of Tables

Chapter 1: Background & Literature Review

Ligament Structure, Function and Composition

Tendons and ligaments are dense connective tissues with the function of stabilizing active motion through the joints and providing mechanical reinforcements to the musculoskeletal system. Tendons connect muscle to bone, while ligaments connect bone to bone. In particular, the anterior cruciate ligament (ACL) stabilizes the knee joint and prevents excessive translation of the tibia during normal and athletic activity. Tendons and ligaments share similar biochemical composition, organizational structure and mechanical properties exhibiting a clear structure-function relationship. Not surprisingly, tendons and ligaments also share similar developmental pathways during embryogenesis.

The extracellular matrix is complex network of structural and functional proteins that provides a substrate to support cell and tissue differentiation and organization. In ligaments and tendons, approximately 80% of the total tissue volume is ECM while the remaining 20% contains specialized fibroblasts [137]. The ECM of ligaments and tendons is composed of collagens, elastins, proteoglycans and connective tissue glycoproteins. Collagens comprise ~60-85% of the tendon dry weight with a majority (approximately 75% in ligament) being type I collagen [45]. The second most abundant collagen in ligaments and tendons is type III collagen, comprising 9-12% of the tissue dry weight in ligaments and less 5% in tendons [9]. In addition, there is a very low percentage (1-2%) of elastin present in native ligaments and tendons. Collagen type III concentrations during early tendon development decline as the tendon matures while established ligaments contain substantially greater levels of this immature element suggesting that ligaments have more active matrix remodeling processes [9, 25, 33]. In addition, high collagen type

III levels are correlated with smaller collagen fibril diameters [33]. Other non-fibrillar collagens, such as type XII collagen, are also present. Type XII collagen is hypothesized to provide a temporary crosslink during collagen fibrillogenesis, thereby stabilizing the fibril during development and healing and permitting fibril growth [25]. Fibrils are the structural building block of collagen-rich tendons and ligaments.

The collagen molecules in tendons and ligaments are organized into a structural hierarchy as pictured in Figure 1.1. Collagen molecules aggregate to form fibrils (less than 100 nm diameter), bundles of fibrils form fibers (1-20 μm in diameter), groups of fibers are then packed into larger fascicles (100-250 μm in diameter). This process, known as fibrillogenesis, forms the primary tendon unit arranged predominately parallel to the direction of mechanical force [25, 137]. Collagen fibrils form a periodic "crimp" pattern due to local deformations that can be visualized using light microscopy. In tendons this crimp pattern is more uniform while ligaments display a less packed arrangement [85]. Moreover, ligaments display more collagen fiber heterogeneity throughout the length of the tissue than tendons. Near the ligament-bone interface of the ACL, collagen fascicles of varying lengths surround the parallel fascicles in a helical pattern that allows the tissue to withstand tensile, rotational and shear loading at varying degrees [137]. Collagen fibril formation is regulated by other small ECM proteins within the tissue including proteoglycans and glycoproteins.

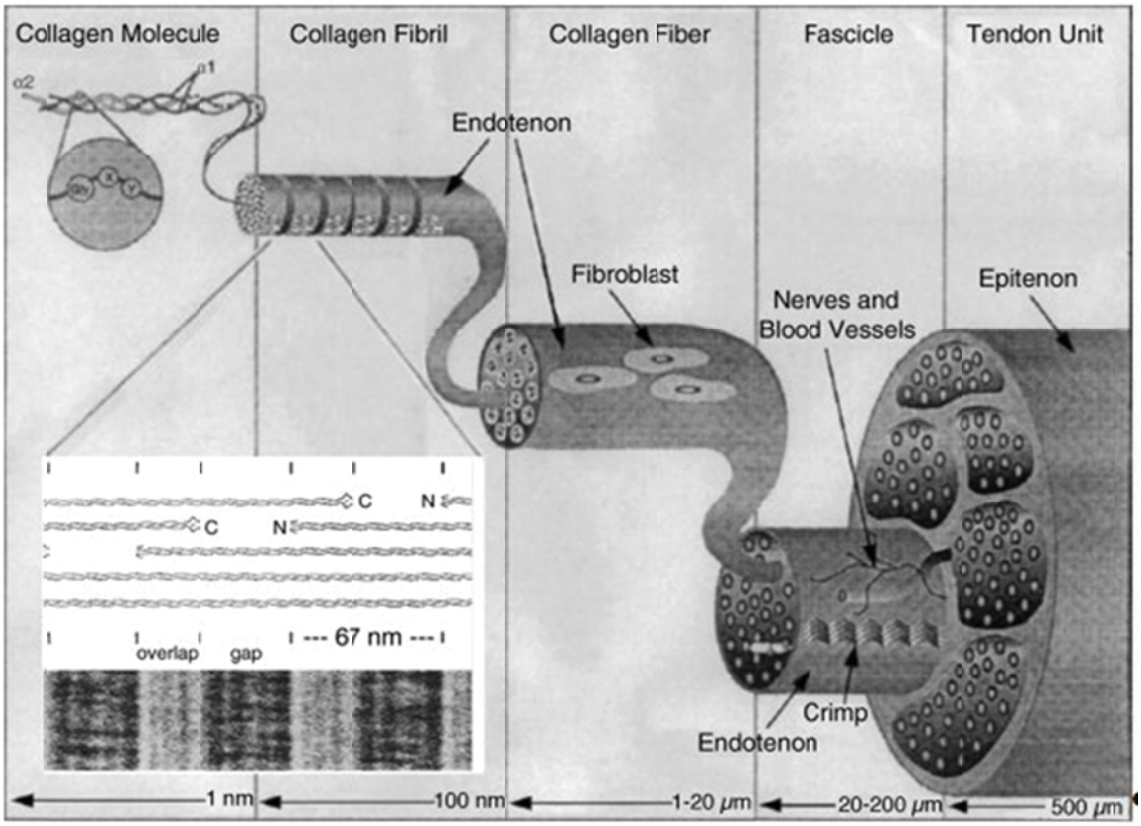

Figure 1.1: Structural hierarchy of collagen in tendon. Collagen molecules aggregate to form fibrils; fibrils group together to form fibers; fibers bundle together to form fascicles; fascicles group together to form tertiary fiber bundles which act as the primary tendon unit. Connective tissue called endotenon surrounds the bundles and fascicles [219].

Proteoglycans (PGs) such as decorin, biglycan, and fibromodulin contribute to the structure and function of tendons and ligaments primarily by assisting in collagen fibrillogenesis. PGs comprise a small portion of the tendon and ligament ground substance, approximately 5% of dry weight; however, they are important to the structural composition of the tissue. Decorin - the most abundant proteoglycan in tendons and ligaments - has been shown to inhibit fibrillogenesis of type I and type III collagen, thereby reducing the average diameter of collagen fibrils [25, 244, 245]. However, decorin is theorized to be a mediator, not an inhibitor, by aligning fibrils end-to-end, thus decreasing the speed of lateral fusion of fibrils [25]. Similar in structure to decorin, biglycan also

regulates collagen fibril formation but has been hypothesized to play the complementary role of promoting fibril fusion [25, 268]. Fibromodulin, another type of PG, has been shown to delay aggregation of collagen molecules with growing fibrils [106].

Structural glycoproteins including tenascin-c and cartilage oligomeric matrix protein (COMP) are also present in ligaments and tendons, making up a very small portion the dry weight. Initially thought as a protein localized to cartilage only, COMP has been shown to be present in vascular smooth muscle, ligaments and tendons [25]. COMP molecules are hypothesized to catalyze collagen fibril formation by promoting binding of individual collagen molecules thereby increasing the rate of collagen fibrillogenesis [104, 224]. Tenascin-C is an important glycoprotein in the ligament extracellular matrix that gives elasticity to the tissue while providing additional binding sites for other matrix proteins and cell adhesion receptors [118]. While only a small percentage of the total ligament or tendon dry weight, PGs and glycoproteins are very important in regulating collagen organization, which directly influences the mechanical properties of the tissue.

The cell type responsible for the secretion and maintenance of ECM in tendons and ligaments is a specialized fibroblast, sometimes known as a tenocyte or fibrocyte. These cells are primarily arranged longitudinally between collagen fiber bundles and are sparsely distributed along the length of the tissue. The anterior and posterior cruciate ligaments (ACL and PCL, respectively) have been found to have the highest DNA concentration, and therefore a higher cell population than the Achilles and patellar tendons [9]. Tendon and ligament fibroblasts are spindle-shaped and have cell extensions that extend deeply into the ECM. Cell-cell communication is accomplished via gap junctions on these projections [162]. In addition to elongated fibroblasts, ligaments also contain groups of larger ovoid

cells, primarily in regions that resemble fibrocartilage [9, 193]. In the cruciate ligaments, these regions experience compression during normal joint function and may explain the appearance of these chondrocyte-like cells and localized type II collagen expression [193]. Indeed, tendon and ligament cells regulate matrix components in order to respond to *in vivo* stresses.

The collagen fibrils are the primary load-bearing component of tendons and ligaments and are responsible for the unique stress-strain curves of the tissue. As shown in Figure 1.2, a typical stress-strain curve of tendons and ligaments has three main regions: 1) toe-in, 2) linear and 3) yield segments. The nonlinear toe-in region of the curve involves the un-crimping or geometrical alignment of collagen fibers and removal of water from the tissue. In the linear region, the collagen fibers are stretched until they finally fail in the yield area of the curve. Tendons and ligaments also demonstrate viscoelastic behavior wherein loading and unloading of the tissue results in differing paths of the load-elongation curve (N-mm). From the load elongation curve, the ultimate load and elongation prior to failure can be determined. The elastic modulus of the tissue can be found from the slope of the stress-strain curve.

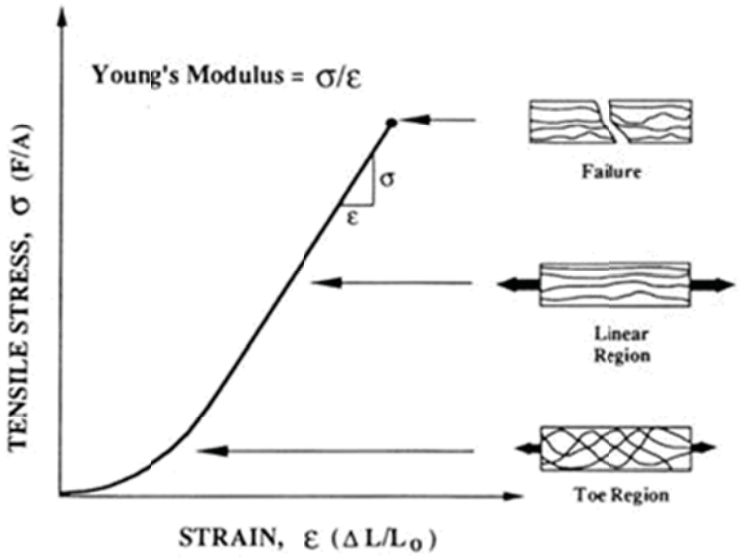

Figure 1.2: Stress-strain curve for collageneous tissues such as ligaments and tendons [173]

The biomechanical properties of the ACL have been evaluated extensively, mainly for designing replacement grafts of similar characteristics. The length of human ACL ranges from 27-32 mm [137]. The fibril crimp pattern in the ACL prevents permanent damage to the tissue by allowing 7-16% relaxation prior to deformation [246]. The ultimate tensile load of the ACL, measured by tensile testing of the femur-ACL-tibia complex, has been reported to be 2160 ± 157 N for humans, aged 22 to 35 years [261]. The elastic modulus of the human ACL can vary from 65-111 MPa depending on the age and health of the tissue [221]. The ACL is capable of withstanding tensile forces between 67-630 N for common activities such as ascending stairs and jogging [246]. Micro strain transducers implanted on the ACL have also measured *in vivo* strains. Strains ranging from 1 to 4% were found for common activities such as stationary biking and squatting [31].

The nerve, lymphatic and vascular supply to tendons and ligaments varies in each specific tendon or ligament. In general, connective tissue layers surrounding the collagen bundles provide the nutrients to tendons and ligaments. The thin connective tissue layer

surrounding the entire tendon or ligament is also known as the epitenon. The epitenon is continuous with internal layers, called endotenon, surrounding individual collagen bundles and thus providing necessary vascular supplies. The soft tissues within the knee joint capsule (the intrapatellar fat pad and synovial membrane) supply blood to the cruciate ligaments [12]. The intra-articular location restricts the natural regenerative capability of the ACL as compared to an extra-articular ligament, like the medial collateral ligament (MCL) [195].

Individual tendons and ligaments differ slightly in their cell and matrix composition; however, all tendons and ligaments share the same basic cell types, patterns of innervation and vascular supply, and framework of proteins that is dominated by the same primary matrix macromolecule, type I collagen. Development and regulation of the extracellular matrix in ligaments and tendons is a dynamic process that imparts and maintains functional viscoelastic properties throughout the life of the individual from embryonic formation to adulthood. Attempts at repair or replacing ligament tissue has focused on achieving native biological composition and biomechanical strength to restore normal joint kinematics [137]. While there are no specific markers for tendon or ligament tissue, the presence of ligament- or tendon-like matrix, cellular morphology and the levels of so-called "selective" markers of tendon/ligament, such as scleraxis and tenomodulin, are considered indicative of stem cell differentiation towards a ligament/tendon phenotype [10, 246]. Scleraxis and tenomodulin are the most specific proteins in tendon/ligament tissue based on studies of embryological development; however, their specific roles are not clearly understood.

Developmental Biology of Tendon and Ligaments

Embryonic ligament and tendon formation remains less defined than other musculoskeletal tissues such as bone and muscle. Scleraxis, a basic helix-loop-helix transcription factor, is a highly localized for the connective tissues that mediate attachment of muscle to bone as shown in Figure 1.3 [212]. Scleraxis was found to be expressed at high levels in murine mesenchymal precursors of the axial skeleton in advance of chondrogenesis and then downregulated at the onset of ossification. The highest levels were found in regions of cartilage and dense connective tissue development, including ligaments and tendons [60]. Brent et al. determined through *in vivo* experimentation that tendon progenitor populations are localized to the syndetome, a fourth compartment of the somite [36]. The interactions between the myotome and sclerotome, precursors to muscle and skeletal structures, respectively, are necessary for specification of the tendon lineage (Figure 1.4). Fibroblast growth factor-4 and fibroblast growth factor-8 signaling from the myotome and sclerotome has been shown to induce scleraxis expression [36, 71]. Progenitors of ligament tissue are also hypothesized to be localized in similar areas of the somite [212, 238]. This theory is based on expression of scleraxis which is present in all tendons, rotator cuff primorida and collateral and anterior cruciate ligaments in developing chicks [212].

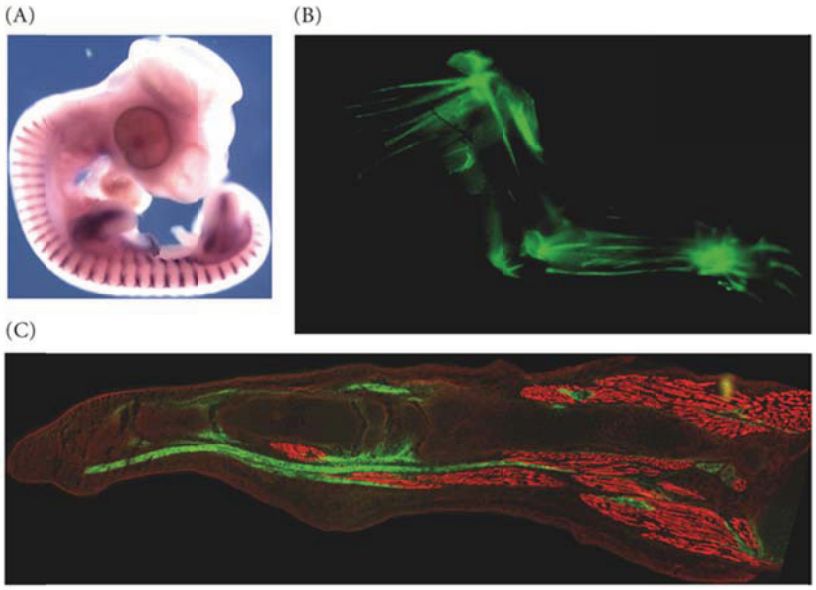

Figure 1.3: Scleraxis expression during tendon development. (A) *In situ* hybridization showing scleraxis pattern in developing chick embryo. (B) Areas of scleraxis expression seen in tendons of newborn mouse forelimb (ventral view). Green fluorescent protein has fused to the scleraxis enhancer. (C) Wrist and finger of a newborn mouse showing scleraxis in the tendons connecting those muscles to the digit and wrist [212].

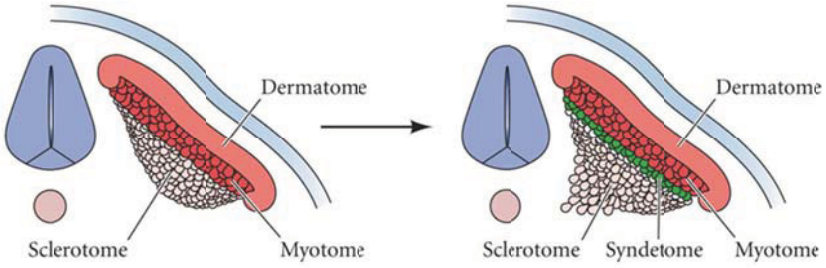

Figure 1.4: Embryonic localization of tendon precursors. Tendon precursors (syndetome) are located between the myotome (muscle) and sclerotome (bone) during embryological development. The dermatome, myotome and sclerotome are established before tendon precursors are specified. Reproduced from Developmental Biology, 8th edition, Figure 14.19 with permission [94].

Recent studies using scleraxis knockout mice have demonstrated that scleraxis expression is essential for tendon differentiation, organization of tendon progenitor cells into functional tendons and the development of mature tendon extracellular matrix [175]. The identification of this tendon/ligament transcription factor has led to *in vitro* studies to

define scleraxis activity. Early mechanistic studies showed that scleraxis mRNA expression in the rat osteoblastic osteosarcoma cells, ROS17/2.8, is regulated by transforming growth factor β1 (TGFβ-1) in a dose- and time-dependent manner [148]. In these same cells, aggrecan and osteopontin expression levels were enhanced by scleraxis over-expression while type I collagen and alkaline phosphatase levels were suppressed [150]. Scleraxis has also been implicated as a positive regulator of tenomodulin, a glycoprotein that is expressed in tendon, ligament and cornea [218]. However, Lejard et al. demonstrated that over-expression of scleraxis enhances the activity of the COL1A1 promoter in NIH/3T3 cells which is further increased with co-overexpression of E47, forming a heterodimer [141].

Few studies have measured the effect of environmental cues on scleraxis expression. In one study, scleraxis expression is maintained at higher levels in human MSCs in a 3D environment while planar cultures have diminished over time [134]. Cyclic strain (10%, 0.33 Hz) of MSCs on porous 3D scaffolds also increased mRNA expression of scleraxis over 48 hours [80]. The effect of scleraxis over-expression in undifferentiated stem cells has not been determined and may provide new information for the development of ligament/tendon tissue engineering strategies.

Tenomodulin (TeM) is a type II transmembrane protein, similar to chondromodulin-I (ChM-I), with expression limited to hypovascular, dense connective tissues including tendons, ligaments, epimysium of skeletal muscle, sclera and cornea. TeM has anti-angiogenic activities, similar to ChM-I. TeM initiates anti-angiogenic responses by inhibition of capillary tube-formation of vascular endothelial cells *in vitro* [190]. TeM is primarily expressed in tendons and ligaments [35, 216, 217]. *In situ* hybridization of chick

embryos showed regions of TeM expression co-localized with expression of type I collagen [217]. The onset of tenomodulin expression follows scleraxis expression and is associated with tenocyte differentiation at later stages of development [218]. This has prompted study of the interaction of tenomodulin and scleraxis in tendon and ligament maturation. Scleraxis knockout mice have severe tendon defects including a disorganized extracellular matrix and absence of tenomodulin, suggesting a complementary role of scleraxis and TeM in tendon and ligament matrix formation [175]. Similarly, TeM-deficient mice exhibit reduced tenocyte density and a wider distribution of collagen fibril diameters with a greater maximum diameter [66]. Induced expression of scleraxis in isolated tenocytes resulted in upregulation of TeM [218]. However, TeM has not been shown to activate the scleraxis gene directly. Thus, TeM is likely important for organization of mature ECM by developing tendon or ligament fibroblasts.

Clinical Problem

An estimated 200,000 anterior cruciate ligament (ACL) tears or ruptures occur each year, making it among the most common knee injuries in the United States, with approximately 50% undergoing ACL surgical reconstructions [37, 165]. ACL injuries can occur following a change in directional movement or sudden stops such as landing from jumping or slowing down after a sprint [255]. The injuries often occur in young athletes in high-impact sports such as soccer, basketball, skiing and volleyball [200]. In addition, women have an increased risk for ACL injuries compared to men which is hypothesized to be a result of hormonal or biomechanical differences [109]. As the individuals place more emphasis on physical activity to combat obesity and the level of intensity in individual sports increases, the number of ACL injuries could continue to rise.

Surgical repair of a torn or ruptured ACL is often performed to stabilize tibial translation. Without surgical reconstruction, high-risk of pain, meniscal injury, chronic laxity and early osteoarthritis due to anterior tibial instability can result [83, 195]. Non-operative treatments for ACL ruptures or tears are typically unsuccessful due the poor healing response of this intra-articular ligament [89]. In a 20-year follow up of conservatively treated ACL injuries (non-surgical), Nebelung et al. found that 95% of the ACL-compromised knees had severe osteoarthritis [182]. They also showed that the injured ACLs fail to restore biomechanical strength and biochemical composition of intact tissues that often results in re-injury.

Surgical Repair of ACL

Autograft and allograft reconstructions are currently the only surgical methods approved for primary ACL reconstruction to restore stability to the knee. Historically, synthetic grafts or prosthetic ligaments were an option for primary repair. Synthetic replacements of the ACL are classified as grafts, augmentation devices or total prostheses. Grafts, including carbon fiber and Gore-Tex, are sutured at each end and are intended to provide immediate stability to the knee while allowing for tissue in-growth and remodeling. Ligament augmentation devices (LADs), such as the Kennedy Ligament Augmentation Device, provided mechanical support during the healing process when used in conjunction with living tissue. However, these LADs decreased the strength of the new tissue as a result of stress-shielding. Total prostheses, such as the Leeds-Keio, made of polyester, were used as a permanent ACL replacement, preventing an *in vivo* remodeling process. Most of the prosthetics for ACL repair have had good short-term results but ultimately exhibited graft failure [72, 155]. A more recent synthetic ACL in development,

the Ligament Advanced Reinforcement System (LARS) made of the common polymer polyethylene terephthalate, has had promising early clinical results. Long-term studies of LARS have not been completed to address the concern of graft rupture common to synthetic ligaments [181]. Among the synthetics once used for clinical repair, only the Gore-Tex ACL graft is currently approved by the Food and Drug Administration (FDA) and is only for use in patients that have had a previous failed reconstruction [155]. Thus, primary reconstructions currently involve the use of either autologous or allogenic tissue grafts, typically chosen at the discretion of the surgeon.

The current gold standard in ACL surgical repair is the autologous tissue graft (autograft). Autograft choices include bone-patellar tendon-bone (BTB), bone-quadriceps tendon or quadruple semitendionus/gracilis tendon. Autografts are advantageous in that they are immunologically compatible and have no risk for disease transmission; however, they are associated with donor-site morbidity wherein the site of autograft harvest also must heal resulting in increased postoperative pain and extended rehabilitation [246]. Allogenic tissue grafts (allografts) are also used for ACL reconstruction to circumvent donor-site morbidity associated with autografts. Allografts are obtained from human cadavers, then sterilized and stored until use, usually by cryopreservation. During these processes, the soft tissue can lose mechanical strength and integrity thereby lessening the grafts ability to restore stability to the knee joint [88]. Although the risk has decreased over the years, allografts are also associated with disease transmission. In addition, allografts have limited availability and cannot be adequately sized to suit the recipient.

Tissue Engineering Strategies

Tissue engineering is a promising alternative to current surgical graft choices for the repair of ACL disruptions. Defined by Langer and Vacanti in 1993, tissue engineering is "an interdisciplinary field that applies the principles of engineering and life sciences toward the development of biological substitutes that restore, maintain, or improve tissue function or a whole organ" [135]. Concepts of biomaterials, cell biology, mechanics, developmental biology, physiology and anatomy are often applied together to design and successfully engineer a replacement tissue. Generally, tissue engineering, sometimes called regenerative medicine, combines suitable cells and a biomaterial scaffold that can be used for clinical repair of injured or diseased tissue. Additional factors such as cytokines, pharmaceuticals and gene therapies can also be included in the engineered tissue to improve functionality *in vivo*.

The aforementioned ACL reconstruction strategies are not sufficient for successful long-term clinical outcomes and a new approach to repair the ACL-deficient knee is needed. Tissue engineering is a promising alternative to the current repair techniques. The ideal neoligament would alleviate anterior tibial instability and initiate the endogenous healing process, permitting limited activity. An engineered neoligament capable of providing mechanical strength and stability to the knee joint initially would allow the patient's own regenerative capabilities to remodel and further strengthen the tissue. Eventually, the neoligament would become remodeled into a fully regenerated ligament with biomechanical strength and stability for full physical activity. For a the ACL, a tissue-engineered strategy would incorporate three critical components: a cell population capable of producing the appropriate ECM proteins, a robust scaffold on which cells may adhere

and deposit these proteins and environmental cues such as mechanical strain to direct cell differentiation and ECM deposition and organization.

Cell Sources

A cell population capable of producing the appropriate ECM proteins and enhanced proliferation *in vivo* is necessary to generate a functional ACL replacement. Differentiated ACL and MCL fibroblasts produce the desired ECM proteins and would be acceptable for ACL repair [57]. However, clinical studies have routinely demonstrated deficiencies in the ability of ACL to heal following injury in contrast to the MCL, which heals spontaneously due to an intrinsic blood supply [260]. Intrinsic properties of the constituent cells in the ACL have been implicated as possible a factor for differential the differential repair mechanisms [179]. Subsequent studies have shown that ACL fibroblasts to have slower proliferation and migration rates *in vitro* as compared to MCL fibroblasts. Explant cultures of ACL cells demonstrated a slower growth rate as passage number increased and lower cell numbers at each passage than explanted MCL cells at all passages measured [179]. In the same study, MCL fibroblasts were observed to migrate into an artificial wound site faster than ACL fibroblasts. More recently, MCL fibroblasts were shown to increase type I collagen expression levels throughout subsequent passages than ACL fibroblasts [4]. Terminally differentiated cell sources are limited in availability for tissue engineering strategies.

Additional differentiated cell sources have been suggested for use in tissue-engineered ligaments. Other potential sources include the Achilles tendon (AT) and patellar tendon (PT). AT and PT fibroblasts have been compared to ACL and MCL fibroblasts in regards to cell proliferation and gene expression. PT fibroblasts seeded onto

collagen fiber scaffolds proliferated more rapidly but synthesized similar amounts of collagen as compared to ACL fibroblasts on the same scaffold [69]. On 3D poly(l-lactic acid) scaffolds, AT and PT fibroblasts proliferated faster than ACL and MCL fibroblasts while ACL fibroblasts had the greatest gene expression of fibronectin, collagen type I and collagen type III, compared to all cell types studied [57]. Skin fibroblasts have also been proposed as a cell source for tissue engineered ligaments. Skin fibroblasts have comparable viability to ACL fibroblasts when implanted into the intra-articular knee joint or subcutaneous space [29]. Isolation of differentiated tendon or ligament fibroblasts from the patient is difficult and their capacity to proliferate and maintain a ligamentous phenotype *in vitro* is diminished over time [4, 57]. Therefore, use of another cell source, such as bone marrow stem cells (BMSCs) or MSCs has been suggested [242].

Mesenchymal Stem Cells

Multipotent mesenchymal stem cells (MSC) offer many advantages as compared to terminally differentiated cell types. Mesenchymal stem cells are adult stem cells residing in numerous mesenchyne tissues such as bone marrow, skin, muscle and fat [3]. As depicted in Figure 1.5, MSCs has been shown to form a variety of musculoskeletal tissues including bone, cartilage, fat, tendon, and muscle [42]. Mesenchymal stem cells are an attractive cell source for cell-based tissue engineering strategies. MSCs may be readily harvested from bone marrow, are highly proliferative *in vitro* and are able to maintain a stable multipotent phenotype [197]. Autologous MSCs used in cell-based tissue engineering strategies also decreases the possibility of immune rejection [47]. However, the promotion of MSC differentiation into mature ECM-producing ligament fibroblasts is a crucial factor in the

engineering of a functional tissue replacement. To date, the knowledge of the biological factors that promote MSC differentiation along a ligament lineage is limited.

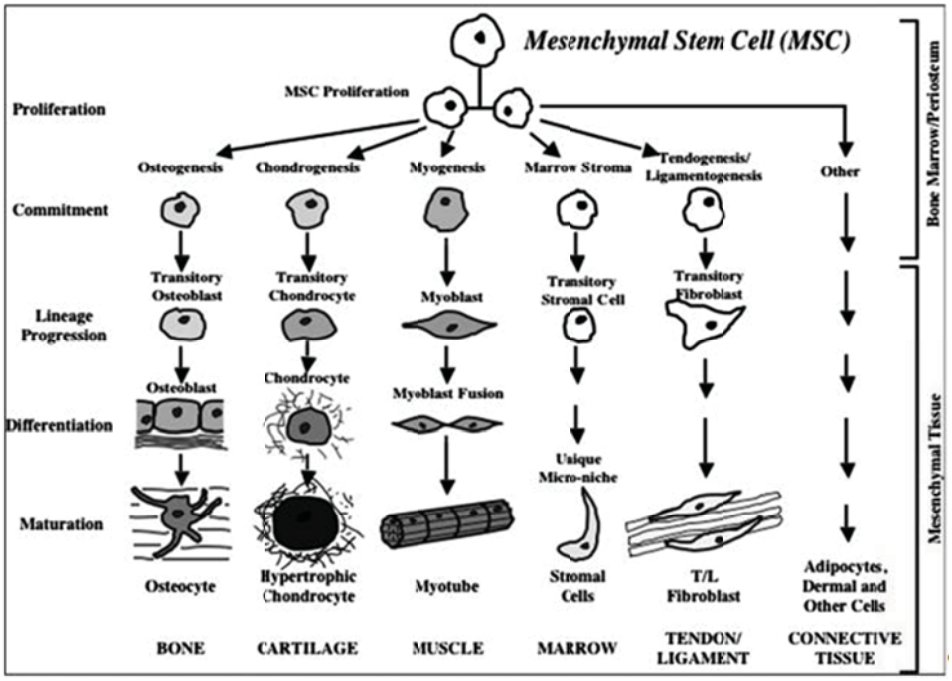

Figure 1.5: The mesengenic process diagram. The original diagram appeared first in Caplan (1989) based on what was known about mesenchymal progenitors in embryos [42].

Mesenchymal stem cells have been compared to terminally differentiated fibroblasts for use in ligament tissue engineering applications. Comparing skin fibroblasts, ACL fibroblasts and MSCs, MSCs showed the greatest proliferation and collagen production on PLGA scaffolds [242]. In a recent study by Liu et al., rabbit MSCs proliferated significantly faster than ACL fibroblasts cultured on silk scaffolds from 1 week to 2 weeks in culture. Initially, the ACL fibroblasts had greater gene expression of ECM markers, collagen type I, collagen type III and tenascin-C, compared to MSCs. However, after 2 weeks of culture on the silk scaffolds, MSCs had significantly upregulated expression of these matrix genes while expression levels in ACL fibroblasts remained approximately the same. MSCs also demonstrated greater viability than ACL fibroblasts once implanted in the

knee joint [145]. Accordingly, rabbit MSCs on composite silk scaffolds have shown prominent type I collagen ECM development and adequate mechanical strength for *in vivo* ACL regeneration [78]. Several research groups have investigated the factors regulating *in vitro* MSC differentiation into ligament fibroblasts.

Biochemical and mechanical stimuli have been applied to MSCs to enhance their differentiation along the tendon/ligament lineage. The expression of matrix components, growth factors and signaling molecules found in tendons and ligaments are indicative of cell differentiation along these lineages, as no specific marker is known. MSCs cultured in growth media supplemented with either epidermal growth factor (EGF) or FGF-2 followed by addition of TGFβ-1 showed optimal MSC differentiation as evidenced by increased expression of collagen types I and III, in contrast to individual growth factor supplements [170]. However, administration of growth factors (FGF-2, EGF, TGFβ-1) in extended culture (3-4 weeks) of MSCs did not significantly increase collagen type I and III mRNA transcript levels or total collagen accumulation [171].

Other attempts to differentiate MSCs along a tendon or ligament fibroblast lineage have employed static tension or external mechanical stimuli in 3D type I collagen gels. MSCs in pre-tensioned 3D collagen gels have been shown to undergo significant changes cellular morphology and such cell shape rearrangements is hypothesized to alter the cell state from proliferative to differentiating [17]. Altman et al. used multi-dimensional strain (uniaxial stretch at 10% elongation and rotational 90°) applied concurrently to increase expression of collagen type I, collagen type III and tenascin-c in MSCs cultured in a collagen gel anchored between bone anchors [7]. Recently, MSC differentiation was shown to be enhanced in a static 3D collagen gel environment, compared to planar culture, while

dynamic loading regulated the expression of matrix metalloproteinases (MMPs) and Wnt signaling molecules that are critical components in skeletal embryogenesis [134]. Sequential combination of growth factor supplementation and mechanical stimulation has also been shown to enhance MSC differentiation and matrix deposition [169]

Biomaterial Matrices

The design of the scaffold is also essential to functional tissue replacements. The scaffold permits deposition of extracellular matrix proteins by seeded cells, thus facilitating the healing process. Biomaterial scaffolds are not inert; they can influence transport of nutrients and metabolites as well as affect cell differentiation and function. Scaffolds are a template for tissue formation and an important component of a tissue engineering strategy.

Numerous biomaterials for tissue-engineered ligaments are currently under investigation as scaffolds that maintain mechanical integrity while promoting matrix production *in vitro* and *in vivo*. For a tissue-engineered ligament, the scaffold ideally should approximate the mechanical properties of the ACL at initial implantation, allow for tissue in-growth and cellular proliferation and degrade at a similar rate to the development of robust extracellular matrix [246]. Natural biomaterials such as silk, collagen, decelluarized allograft tendon and small intestine submucosa have been studied by various research groups [4, 6, 20, 46, 257]. In addition, poly(lactide-co-glycolide acid) (PLGA), poly(l-lactide acid) (PLLA), poly(ε-caprolactone) (PCL), and combinations of these are synthetic materials currently being studied as scaffolds for a tissue engineered ligament [80, 87, 194, 241]. However, a relatively low range of tunable properties limits these biomaterials.

Polyurethanes and poly(esterurethane urea)s (PEUURs) have been studied extensively as biomaterials, primarily for soft tissue applications, including ligament,

cartilage, nerve, smooth muscle and cardiovascular regeneration [34, 53, 96, 144, 161, 167, 226]. PEUURs demonstrate good biocompatibility and biodegradation rates *in vitro* and *in vivo* [99, 100]. These polymers have unique chemistries that make them suitable for biomedical applications. PEUURs have been synthesized by a two-step process that creates segmented elastomers with a hard and soft segment [101]. The soft segment consists of degradable polyester, such as PCL, PLGA or PLA while the hard segment is made of a diisocyanate and an aliphatic or aromatic chain extender. The degradation rates and mechanical stiffnesses or elasticities can be varied to match the target tissue by varying the ratio of soft to hard segments or changing the composition of the chain extender and the soft segment in the PEUUR. The morphology and structure of the segments can also affect biodegradation and mechanical properties. For example, amorphous soft segments will degrade more rapidly than semi-crystalline soft segments [223]. PEUURs are designed to biodegrade through hydrolytic or enzymatic breakdown into α-hydroxy acids and urea and urethane fragments, depending on the composition of the polymer [101]. Additionally, the degradation products of PEUUR synthesized with aliphatic diisocyanates are known to be non-toxic [100]. A segmented polyurethane elastomer prepared from MDI, an aromatic diisocyanate, and a PCL 530 g/mol (known as Artelon®) maintains the necessary tensile strength and modulus during for ACL reconstructions while slowly degrading [96]. For tissue engineering applications, PEUUR scaffolds can be fabricated into flexible, yet strong, scaffolds using a variety of techniques including electrospinning.

Electrospinning is a simple method that has been used extensively in biomedical applications [139, 143]. The merit of electrospinning is that it can produce nano-fibrous scaffolds with structural features required for cell growth and tissue organization [178]. In

this technique, an electrode is placed on syringe containing a polymer solution. A grounded collector is placed at 10-20 cm from the syringe. The large voltage potential, typically 15-30 kV, is applied overcome the surface tension of the solution, and causes ejection of a fiber to a grounded collector. By varying the distance to the collector, the voltage, the polymer solution properties or motion of the collector, fiber composition and organization can be controlled. Random fiber orientation in a fused fiber mesh is achieved with a stationary collector. Fiber alignment can be achieved by rotating a collector such as a drum (Figure 1.6). The rotational speed of the collector determines the degree of fiber orientation in the mesh. Other parameters, such as viscosity/polymer concentration, polymer flow rate and environmental conditions, can all affect the resultant fiber morphology and thus influence cellular behavior and subsequent tissue development.

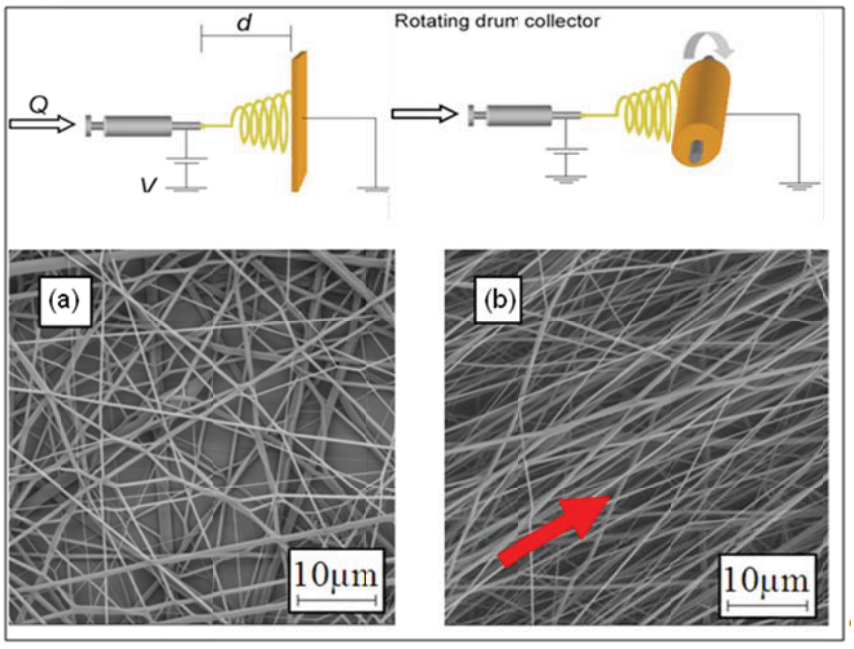

Figure 1.6: Electrospinning setups to produce (a) randomly oriented or (b) aligned fiber mesh.

The effect of fiber diameter and fiber alignment on cell attachment and individual cell morphology has been studied on electrospun meshes. NIH/3T3 fibroblasts seeded

onto electrospun fibers adhered significantly better and had a more elongated morphology on 500 nm diameter fibers than fibers over 3 μm in diameter, presumably by limitations of the cell membrane curvature [236]. Fibroblasts also exhibit an increase in cell aspect ratio as the fiber diameter is increased [27, 149].

In multiple cell types, gene expression and the development of ECM on electrospun scaffolds is altered as fiber architecture is changed. Total collagen production of human ACL fibroblasts was shown to be significantly increased on aligned electrospun scaffolds (angular deviation of 6.5°) as compared to randomly oriented scaffolds (angular deviation of 41.7°) but cell proliferation is similar on the two scaffold types [139]. Conversely, chondrocytes on either aligned or non-aligned electrospun scaffolds contained comparable amounts of total collagen content but the aligned scaffolds demonstrated a greater increase in modulus [22]. Human skin fibroblasts had a significantly higher rate of cell proliferation and collagen type III gene expression on electrospun matrices with fiber diameters ranging from 0.35 to 1.1 μm than the fiber matrices below and above this fiber diameter range [133]. Isolated human Schwann cells cultured on electrospun fibers of approximately 1 μm diameter demonstrated a more mature phenotype, as evidenced by upregulation of early markers of myelin-differentiation, that was further enhanced by alignment of the electrospun scaffold [52]. MSC gene expression of collagen 1α1, decorin and tenomodulin was highest on electrospun fiber scaffolds with an average diameter of 0.28 μm than scaffolds with 0.82 μm or 2.3 μm average fiber diameter. In the same study, scleraxis expression was not significantly affected by either fiber diameter or degree of fiber alignment; however a general trend of increased scleraxis expression with increasing fiber diameter was observed [28].

Mechanical Stimuli

Mechanical environment is an important regulator of ligament and tendon extracellular matrix development, remodeling and maintenance *in vivo*. Mechanical stretch is also thought to be a critical environmental factor that signals developing ligament progenitor cells to differentiate into mature ligament fibroblasts. The ACL and MCL are stretched to 4-5% strain during normal activity and up to 7.7% strain during externally applied loads [31, 251]. Following ACL injury and reconstruction, rehabilitation exercises are recommended to improve healing [259]. Through exercise, the ligament cells are stimulated to produce and remodel the injured tissue. To mimic this *in vivo* environment, native fibroblasts from the ACL, MCL or patellar tendon have been used for many experimental stretching studies. Cyclic stretch has been shown to stimulate the expression and synthesis of collagen type I and III, tenascin-C, TGF β1 and α-smooth muscle actin (α-SMA) in explanted fibroblasts [2, 7, 54, 108, 112, 126, 139, 140, 191, 252]. The frequency, magnitude and duration of applied cyclic strain has been demonstrated to be an important regulator of cell behavior [250]. Cell source (e.g. MCL or ACL fibroblasts) may also show marked differences in gene expression after cyclic stretch.

Mesenchymal stem cell response to mechanical stretch has also been studied, but to a lesser degree than terminally differentiated fibroblasts. Rabbit mesenchymal stem cells cultured in collagen sponges and subjected to 2.4% cyclic uniaxial stretch demonstrated significantly higher type I collagen gene expression and increased mechanical properties, including linear stiffness, at the end of two weeks [121]. Using a mesenchymal stem cell line, mRNA relative expression of scleraxis, collagen types I and III and tenascin-c was increased following cyclic strain (10%, 0.33 Hz) on PCL-based porous 3D scaffolds over 48

hours [80]. MSCs co-cultured with ACL fibroblasts and then subjected to uniaxial stretch (1Hz, 10%, 2 days) showed upregulation of mRNA expression of collagen type I and III, and tenascin-C as compared to non-stretched cells with and without co-culture [140], suggesting beneficial effects of signaling molecules secreted by the ACL fibroblasts. However, the 10% strain applied in these last two studies may be considered injurious because it was above the normal loading for ACL. Indeed, Chew et al. examined the effect of strain magnitude and showed that low-magnitude cyclic stretching increased mRNA expressions of early markers of osteoblastic differentiation of human MSCs, whereas high-magnitude stretching upregulated the mRNA expressions of tendon/ligament-related genes [51].

Cellular responses are dependent not only on the magnitude, duration and frequency of stretch but also the substrate on which they reside. In two similar studies, fibroblasts cultured on patterned silicone substrates either aligned with the direction of stretch or perpendicular to it, depending on the size and width of the micropattern [191, 252]. Lee et al. demonstrated that human ACL fibroblasts increased collagen production on aligned, nanofiber sheets under mechanical stretch (0.2Hz, 5%, 24 hr) compared to unaligned nanofibers [139]. This study, however, was conducted with electrospun 1 mm thick meshes that were supported by the flat surface of the stretch apparatus which could restrict cellular deformations and result in variable stresses across the entire mesh. The dimensionality of the scaffold also affects cellular responses. Kuo and Tuan showed an upregulation in mRNA expression of scleraxis but a downregulation of collagen type XII in human MSCs cultured in 3D collagen gels compared to 2D TCPS plates. They also showed that cyclic loading (1%, 1Hz, 30min/day) of the 3D collagen gels, which had more

histologically pronounced matrix deposition, maintained levels of scleraxis expression while cells in planar culture exhibited diminished levels of expression over one week [134].

Overview of Dissertation

Tissue engineering is a promising alternative for the repair of ACL disruptions. A tissue engineering strategy incorporates three critical components to generate a functional tissue replacement: a cell population capable of producing the appropriate extracellular matrix (ECM) proteins, a scaffold on which cells may adhere and deposit ECM proteins, and cues to direct cell differentiation and gene expression. The overall goal of this work is to develop methods to induce stem cell differentiation into mature ligament/tendon fibroblasts. The present work describes efforts using three complementary approaches to promote differentiation of MSCs: architecture of the scaffold (Chapter 2, 3 and 4), mechanical stretch (Chapter 4) and over-expression of the transcription factor, scleraxis (Chapter 5).

In the first approach, the effect of electrospun fiber diameter and fiber orientation on progenitor stem cell growth, morphology and differentiation was studied. Using electrospinning methods, fibrous scaffolds with discrete fiber diameters and orientation were prepared. Primary rat mesenchymal stem cells (Chapter 2) and murine multipotent C3H10T1/2 cells (Chapter 3) were chosen to investigate fiber architecture effects on cellular responses. DNA content, cell morphology and expression of tendon/ligament related genes were measured.

In the second approach, the effect of biomaterial architecture, specifically fiber diameter, under cyclic stretch on cellular differentiation was evaluated (Chapter 4). Using a custom bioreactor with imaging capabilities, MSCs on electrospun scaffolds were

cyclically stimulated. Cell attachment and morphology was monitored before and after tensile stretch. Gene expression was measured following three days of mechanical stress.

In the third approach, mesenchymal stem cells were transiently transfected with a plasmid encoding the transcription factor scleraxis (Chapter 5). Cellular viability following scleraxis transfection was evaluated. Nuclear compartmentalization of scleraxis was observed using image analysis. Temporal ECM gene expression in a response to an upregulation in scleraxis activity was also measured.

Finally, conclusions from the described studies and future recommendations to improve tissue engineered ligaments are then discussed in Chapter 6.

Chapter 2: Effect of fiber diameter and alignment of electrospun polyurethane meshes on mesenchymal progenitor cells.

[2]Chris A Bashur[#], [1]Robyn D Shaffer[#], [3]Linda A Dahlgren, [4]Scott A Guelcher, and [1,2]Aaron S Goldstein

[1]School of Biomedical Engineering and Sciences and
[2]Department of Chemical Engineering,
Virginia Polytechnic Institute and State University,
Blacksburg, VA 24061

[3]Department of Large Animal Clinical Sciences,
Virginia-Maryland Regional College of Veterinary Medicine,
Blacksburg, VA 24061

[4]Department of Chemical Engineering, Vanderbilt University
Nashville, TN 37235

 # authors contributed equally to this work

RDS was responsible for cell culture and Figures 2.7, 2.8, 2.9, 2.10, and 2.11

CAB is responsible for fabrication of meshes and Figures 2.1, 2.2, 2.3, 2.4, 2.5, and 2.6

Abstract

Effective strategies to guide cell alignment and the deposition of an oriented extracellular matrix are critical for the development of anisotropic engineered tissues suitable for the repair of ligament defects. Electrospinning is a promising means to create meshes that can align adherent cells, but the effect of fiber mesh architecture on differentiation has not been examined closely. Therefore, the goal of this study was to determine the effect of fiber diameter and the degree of fiber alignment on mesenchymal progenitor cell morphology, proliferation and ligament gene expression. Specifically, a poly(esterurethane)urea elastomer was electrospun onto rigid supports under conditions designed to independently vary the mean fiber diameter (from 0.28 to 2.3 μm) and the degree of fiber alignment. Bone marrow stromal cells – seeded onto supported meshes – adhered to and proliferated on all surfaces. Cells assumed a more spindle-shaped

morphology with increasing fiber diameter and degree of fiber alignment, and oriented parallel to fibers on aligned meshes. Expression of the ligament markers collagen 1α1, decorin, and tenomodulin appeared to be sensitive to fiber diameter and greatest on the smallest fibers. Concurrently, expression of the transcription factor scleraxis appeared to decrease with increasing fiber alignment. These results suggest that the formation of a ligament-like tissue on electrospun scaffolds is enhanced when the scaffolds consist of aligned submicron fibers.

Introduction

Approximately 150,000 surgical procedures are performed annually in the United States to treat injured anterior cruciate ligament (ACL) tissue [58], and current materials for ACL replacement include autologous and allogeneic grafts. Both options, however, have intrinsic limitations. Autologous tissue – the preferred material for ACL replacement – exists in limited quantities, requires a secondary surgery to obtain donor tissue, and risks morbidity at the donor site [204]. Allogenic tissue – typically from cadaveric sources [246] – avoids donor site complications, but risks disease transmission and host inflammatory response [117]. Given these limitations, ligament tissue engineering holds promise as a method to create new materials for ACL reconstruction.

In its most generic form, ligament tissue engineering involves the combination of biomaterial, biologic, and pharmaceutic ingredients to form a composite material that is capable of integrating with the host bone and ligament tissues, stimulating normal tissue remodeling, and providing mechanical stability to the joint [7, 153]. Within this general paradigm, an approach for achieving an engineered ACL tissue involves *in vitro* culture of mesenchymal progenitor cells on a biomaterial scaffold under the appropriate conditions

to stimulate cell differentiation toward the ligament phenotype. Two complementary *in vitro* strategies to accomplish this are the use of growth factors (e.g., EGF, IGF-II, FGF-2, TGF-β1 [170, 171]) and mechanical stimulation [7]. However both strategies require a biomaterial scaffold that is capable of deforming elastically under physiologically relevant strains, controlling the alignment of the adherent cells, and supporting cell differentiation into the ligament phenotype.

For tissue engineering applications the biomaterial must be both degradable and elastomeric, which limits the number of suitable candidate materials. In particular, many degradable polyesters that are commonly employed in tissue engineering applications (e.g., poly(lactic acid), poly(glycolic acid), polycaprolactone (PCL)) are not sufficiently elastic (yield strains < 10% [207]). However, a number of segmented polyurethanes have been described in the literature that are biocompatible, elastomeric, and degradable [100, 102, 125, 223, 227, 228]. These materials are formed by end-capping low molecular weight polyesters (e.g., PCL) with a diisocyanate and then chain-extending them to produce a high molecular weight linear polymers with ester, urethane, and urea linkages (i.e., poly(esterurethane) ureas (PEUURs)). Further, some of these polymers can be processed into micron-scale fiber meshes by electrospinning [228, 232].

Electrospinning is an attractive method for producing fiber meshes with anisotropic properties suitable for musculoskeletal [143], cardiac [59, 270], and nerve regeneration [263] applications. In particular, the alignment of electrospun fibers produces topographic cues that orient adherent cells [22, 27, 139] through the phenomenon of contact guidance [61]. However, analysis of cell morphology on electrospun meshes has indicated that projected cell area and aspect ratio are sensitive to the diameter and degree of fiber

alignment of underlying mesh [27]. Because cell shape and cell function are interdependent [147], the architecture of electrospun meshes may affect cell phenotype.

The primary goal of this study was to determine the effect of electrospun mesh architectures on mesenchymal progenitor cell differentiation into the ligament phenotype. Morphologically, ligament fibroblasts exhibit an elongated cell body – that is oriented parallel to collagen bundles *in vivo* – and a network of cytoplasmic extensions that mediate cell-cell and cell-ECM interactions. Ligament fibroblasts express of variety of ECM proteins, including collagen types I and III, biglycan, decorin, elastin, and tenascin-C [246]. Although these proteins are common to many soft tissues, scleraxis and tenomodulin have been recently identified as selective markers of ligament fibroblasts. Scleraxis is a transcription factor – expressed during the early stages of musculoskeletal development [212] – that is necessary for development of mature tendon tissue [175], and may be considered an early marker of the ligament phenotype. Tenomodulin is a transmembrane glycoprotein [216] that is induced by scleraxis [218], and is thought to aid in the organization of collagen into fibrils [66] and the suppression of ligament tissue vascularization [190].

In this study an elastomeric PEUUR was electrospun onto rigid substrates with mean fiber diameters of 0.28 to 2.3 μm and varying degrees of fiber alignment. To determine how fiber diameter and the degree of fiber alignment affect development of the ligament phenotype, bone marrow stromal cells (BMSCs) were cultured under static conditions on the resultant meshes, and cell morphology, cell density, and expression of the ligament proteins collagen 1α1 (Col1α1), decorin, tenomodulin, and scleraxis were measured.

Materials and Methods

Polyurethane synthesis

A linear segmented degradable PEUUR elastomer, consisting of alternating poly(ε-caprolactone) (PCL) soft segment and a urethane- and urea-containing hard segment, was synthesized using a standard two-step technique in a three-neck, round-bottom flask equipped with argon inlet and outlet, condenser, and stirrer [102]. In the first step, the flask was charged with anhydrous dimethyl sulfoxide (DMSO, < 50 ppm water; Acros Organics, Morris Plains, NJ) and 1,6-diisocyanatohexane (HDI, Sigma-Aldrich, St. Louis, MO), immersed in a 75°C oil bath, purged with argon, and stirred with a Teflon blade stirrer turned by an electric motor. Next, PCL diol (average molecular weight 1250 Da, PCL1250, Sigma, St Louis, MO) – that had been dried for 24 h at 80°C under vacuum (10 mm Hg) and dissolved in DMSO – was charged into the reactor by means of an addition funnel. The prepolymer content in the reactor was controlled at 14 wt%, and the relative masses of HDI and PCL1250 were selected to achieve a prepolymer NCO:OH equivalent ratio of 2.0:1.0. Dibutyltin dilaurate (DBTDL, Sigma) was added to the flask at 1000 ppm and the reaction was allowed to proceed for 3 h to produce a HDI.PCL1250.HDI prepolymer. In the second step, a solution of 1,3-propanediol bis(4-aminobenzoate) (PDAB, Sigma-Aldrich) in DMSO was prepared at 50°C and added to the resultant prepolymer in the reaction vessel. The NCO:OH equivalent ratio of the polyurethane was controlled at 1.03:1.0 and the polymer concentration was 12 wt%. DBTDL was added to a concentration of 1000 ppm. The reaction was allowed to proceed at 80°C for 20 h. The final polymer was then precipitated in diethyl ether (Sigma) and dried in a vacuum oven for 24 h at 80°C under 10 mm Hg vacuum.

Electrospinning

The PEUUR was electrospun onto rigid glass supports to form fused-fiber meshes with controlled fiber diameters and degrees of fiber alignment as described previously [27]. Briefly, 18 mm glass coverslips (Fisher Scientific, Pittsburgh, PA) were sonicated in ethanol and allowed to air dry. To facilitate adhesion of electrospun fibers a thin film of PEUUR was deposited onto coverslips. For each coverslip, 0.30 mL of a 2.75 wt% solution of PEUUR in 50:50 isopropanol:1,1,1,3,3,3-hexaflouro-2-propanol (HFIP, Sigma) was placed in the center, and the coverslip was spun at 2,500 rpm for 30 s using a Model 1-EC101D-R485 spincoater (Headway Research, Garland, TX). Coverslips were allowed to dry under vacuum for two days. Two sets of electrospun meshes were prepared concurrently. First, to study the effect of fiber diameter, unaligned fiber meshes were prepared by electrospinning PEUUR onto spincoated coverslips that were mounted onto a stationary target. Electrospinning was performed on three different occasions and PEUUR concentrations of 7.5 to 8.0 wt%, 12.0 to13.5 wt%, and 20.0 wt% in HFIP were used to achieve three ranges of fiber diameters. These concentrations were selected using a trial-and-error approach with the objective of producing meshes consisting of regularly shaped fibers with the smallest and largest possible diameters, and one intermediate fiber diameter. Second, to study the effect of fiber alignment, spincoated coverslips were mounted onto a 6 cm diameter drum that was rotated at linear velocities of 2.6 ± 0.29 and 4.6 ± 0.26 m/s. For this study, only the intermediate PEUUR concentration (12.0 to 13.5 wt% PEUUR in HFIP) was used. All electrospinning was performed under ambient conditions using a 22 gauge Teflon tipped needle, a 15 kV potential, a throw distance of 15 cm, and a syringe flow rate of 5 mL/h. Because HFIP is toxic, meshes were soaked in

ethanol for 7 days followed by deionized water for 2 days to remove residual HFIP. The meshes were then dried and stored in a desiccator – to minimize degradation – until use.

Prior to cell culture studies electrospun PEUUR meshes and spincoated PEUUR films (the control group) were placed into 12-well tissue culture plates (Fisher Scientific) and sterilized by overnight exposure to UV light. To facilitate cell adhesion, substrates were incubated for 1 h with 2 mL of a 2 μg/mL solution of fibronectin (Fisher Scientific) in phosphate buffered saline (PBS, Fisher Scientific) at room temperature. Substrates were kept wet in PBS until cell seeding.

Scanning Electron Microscopy (SEM) Analysis

For SEM analysis of fiber diameter and alignment electrospun meshes were mounted onto studs and sputtercoated with a 20 nm layer of palladium (Model 208HR, Cressington Scientific Instruments, Cranberry, PA). These surfaces were then imaged with a LEO 1550 Field Emission SEM (Carl Zeiss SMT, Thornwood, NY) operating at 5kV with a 16 mm working distance. Resultant images were imported into ImagePro Plus software (ICube, Crofton, MD) and the orientation and diameter of individual fibers was measured manually using the interactive measurement tools. (At least 100 fibers were analyzed per sample and care was taken to measure only fibers that had clearly defined edges.) Mean angle of orientation relative to the direction of rotation, μ, and average angular standard deviation, σ, were calculated from a wrapped normal distribution [27]. Briefly, μ and mean resultant length, ρ, were determined using the following equations.

$$\mu = \tan^{-1}\left(\frac{\sum \sin 2\theta_i}{\sum \cos 2\theta_i}\right) \qquad \text{- 1 -}$$

$$\rho = \frac{\sqrt{\left(\sum \cos 2\theta_i\right)^2 + \left(\sum \sin 2\theta_i\right)^2}}{n} \qquad \text{- 2 -}$$

Here θ_i is the angle of orientation for an individual fiber. Finally, angular standard deviation was calculated from mean resultant length by the following equation.

$$\sigma = \frac{1}{2}\sqrt{-2\ln \rho} \qquad \text{- 3 -}$$

Cell Culture and Cell Seeding

Cell studies were performed using rat bone marrow stromal cells (BMSC) isolated from male 125-150 g Sprague-Dawley rats (Harlan, Dublin, VA) in accordance with the Institutional Animal Care and Use Committee at Virginia Tech [125]. Dispersed whole marrow extracts were grown on 100 mm tissue culture polystyrene Petri dishes (Fisher Scientific) for 10 days in growth medium consisting of Minimal Essential Medium α modification (α-MEM, Invitrogen, Bethesda, MD) with 10% fetal bovine serum (FBS, Gemini, Calabasas, CA) and 1% antibiotic/antimycotic (Invitrogen). Cells were then enzymatically lifted using trypsin/ ethylenediamine tetraacetic acid (EDTA) (Invitrogen), split 1:2 and seeded into fresh 100 mm Petri dishes. (This process selectively increases the concentration of the proliferative, marrow-adherent fraction, which includes a population of mesenchymal progenitor cells. However, it does not select for specific antigen markers nor achieve a homogeneous cell population.)

After four days of expansion, first passage cells were enzymatically lifted, and seeded onto PEUUR meshes and PEUUR films in 12 well plates. Cells were added as a suspension of 1.9×10^4 cells in 2 mL of growth medium to achieve a uniform distribution of cells across the well bottom of 5.0×10^3 cells/cm^2. After 24 h, medium was replaced with

growth medium supplemented with 2 mM ascorbate-2-phosphate (Sigma). Thereafter, medium was replaced twice weekly. Samples were then collected and analyzed for cell morphology, cell density, and mRNA expression of ligament proteins decorin, Col1α1, tenomodulin, and scleraxis.

Cell Morphology

After 3 days of culture on fibers, cell morphology was determined by imaging fluorescently labeled cells. Briefly, medium was replaced with 2 mL fresh medium containing 15 μL of 1 mg/mL calcein-AM (Molecular Probes, Eugene, OR) in DMSO and incubated for 30 min at 37 °C in the dark. Next, cell-seeded substrates were washed two times with 2 mL/well PBS, and 2 mL α-MEM without phenol red was added to each well. Fluorescent images were obtained at 20× magnification with a wide blue filter using an Olympus IX50 microscope (Opelco, Sterling, VA) equipped with a cooled CCD camera (Hamamatsu C4742-98-12NRB). Phase contrast images of each field were also collected. Sixteen pairs of images per substrate were then imported into ImagePro Plus software and length of the long axis, aspect ratio, projected area, and angle of orientation of each cell were measured from fluorescent images using ImagePro algorithms. These algorithms calculate long axis, aspect ratio, and angle of orientation by approximating the cell as an ellipse. On average, 100 cells were analyzed per substrate, although the smallest sample size was n = 18 cells. Concurrently, the angle of fiber orientation was measured for at least 100 fibers per substrate from phase contrast images. Mean values for projected cell area, aspect ratio, length of the long axis, and angle for both fibers and cells were calculated per substrate. Angular standard deviations for both cell and fiber orientation were calculated

for each substrate using Equations 1 - 3. Statistical analyses were performed using the mean properties of each substrate.

Cell Number

Cell number was calculated from fluorescence measurements of DNA as described in detail elsewhere [19]. Briefly, meshes were mechanically disrupted using cell scrapers and collected in 10 mM EDTA (pH 12.3). Samples were sonicated for 10 min on ice, neutralized with the addition of KH_2PO_4, and combined with a solution of Hoechst 33258 (Sigma) in 100 mM NaCl and 10 mM Tris (pH 7.0, Sigma). Fluorescence was measured with a DyNAQuant 200 fluorimeter (Hoefer, San Francisco, CA)and cell number was calculated from measurements of fluorescence intensity using a set of DNA standards and a conversion factor of 10.4 pg DNA/cell [97].

mRNA Expression

Expression of collagen 1α1, decorin, scleraxis and tenomodulin was determined quantitatively by real-time polymerase chain reaction (PCR). Briefly, total RNA was isolated from the cells on days 7 and 14 using the RNeasy Mini Kit (Qiagen, Valencia, CA) according to the manufacturer's instructions. Lysates were first homogenized with QIAShredder columns (Qiagen) and then were subjected to on-column DNase digestion using DNase I (Qiagen). RNA was quantified using Quant-It RiboGreen kit (Molecular Probes) and a fluorescent plate reader (SpectraMax M2, Molecular Devices, Sunnyvale, CA). Equal masses of RNA – approximately 0.5 μg – were reverse-transcribed to cDNA using SuperScript® First-Strand Synthesis kit (Invitrogen) with random hexamers as primers according to manufacturer's protocol. Real-time PCR was performed in the ABI 7300 Real Time PCR System (Applied Biosystems, Foster, CA) using 50 ng cDNA, Power Sybr®Green

Master Mix (Applied Biosystems), and specific primers for collagen 1α1, decorin, scleraxis, tenomodulin and β-actin (the internal reference). Primer sequences were designed in Primer Express® software (Applied Biosystems) using the NCBI database accession numbers as shown in Table 2.1 and purchased from Integrated DNA Technologies (Coralville, IA). Primers for the reference gene, β-actin, were developed as described previously [131]. Quantification of target gene expression, relative to spincoated substrates on day 7, was performed using the comparative threshold cycle (ΔΔCt) method [151]. Relative gene expression was reported as $2^{-\Delta\Delta C_t}$. Control reactions (e.g., amplification without cDNA template, amplification of isolated RNA) were performed to verify the fidelity of the amplification process.

Table 2.1: Rat primer sequences for real-time polymerase chain reaction amplification

Gene	Forward Primer	Reverse Primer	Product Size
Col1a1 NM_053304	5′ GAGGGCGAGTGCTGTCCTT 3′	5′ GGTCCCTCGACTCCTATGACTTC 3′	74 bp
Decorin NM_024129	5′ CATCTCCGAGTGGTGCAGTGT 3′	5′ GCAATGTTGTGTCAGGTGGAA 3′	76 bp
Scleraxis NM_001130508	5′ TCTGCCTCAGCAACCAGAGAAAGT 3′	5′ ACTCTTCAGTGGCTTCCACCTTCA 3′	130 bp
Tenomodulin NM_022290	5′ CCCACAAGTGAAGGTGGAGAA 3′	5′ AACAGTAACCTCTCTCATCCAGCAT 3′	125 bp
β actin NM_031144	5′ CGTGAAAAGATGACCCAGATCA 3′	5′ CACAGCCTGGATGGCTACGT 3′	72 bp

Statistical Analysis

All studies were performed two or three times using separate batches of PEUUR meshes and BMSCs. Results are presented as the mean ± standard deviation for n = 2 or 3

substrates for SEM analysis of fiber diameter and orientation, n = 6 or 9 coverslips per condition for cell morphology, n = 8 or 12 coverslips per condition for cell number. Results are presented as the mean ± standard error of the mean, with n = 6, 9, or 12, for mRNA expression of collagen 1α1 and decorin, and with n = 4, 6, or 8, for scleraxis and tenomodulin. Statistical significance was determined in SAS 9.1.3 (SAS Institute Inc. Cary NC) and mixed model analysis of variance (ANOVA) was used with post-hoc comparisons using the Tukey-Kramer method with a significance criterion of $p \leq 0.05$.

Results

Electrospun Meshes

SEM images were analyzed to determine fiber diameter and degree of alignment for each electrospinning condition. When electrospun onto a stationary target, PEUUR solution concentrations of 7.5-8.0, 12.0-13.5, and 20.0 wt%, resulted in mean fiber diameters of 0.28, 0.82, and 2.3 μm, respectively (Table 2.2, Figure 2.1). When electrospun from a 12.0-13.5 wt% solution onto a rotating drum, the angular standard deviation decreased from 49.5° to 27.8° and the mean fiber diameter decreased from 0.72 to 0.46 μm (Table 2.2, Figure 2.2) as the drum speed was increased from 0 to 4.6 m/s.

Table 2.2: Fiber diameter and angular standard deviation for meshes electrospun from PEUUR solutions of different concentrations and at different rotation rates. Mean ± standard deviation for n=2 or 3 replicates with greater than 150 fibers per sample.

Concentration (%)	Rotational Speed (m/s)	Fiber Angular Deviation (°)	Fiber Diameter (μm)
7.8 ± 0.2	Stationary	61.9 ± 4.4	0.28 ± 0.07
12 ± 0.7	Stationary	49.9 ± 3.7	0.82 ± 0.14
20 ± 0.0	Stationary	60.3 ± 5.2	2.3 ± 0.15
12 ± 0.7	Stationary	49.5 ± 3.2	0.72 ± 0.21
11 ± 1	2.6 ± 0.3	33.7 ± 0.99	0.53 ± 0.15
12 ± 0.9	4.6 ± 0.3	27.8 ± 2.5	0.46 ± 0.12

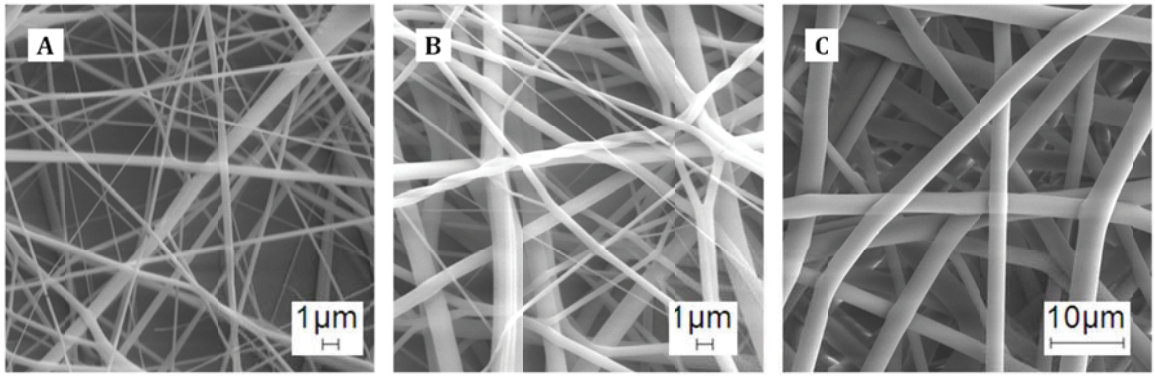

Figure 2.1: SEM images of PEUUR fibers electrospun from different solution concentrations: a) 8 wt%, b) 12 wt%, and c) 20 wt%.

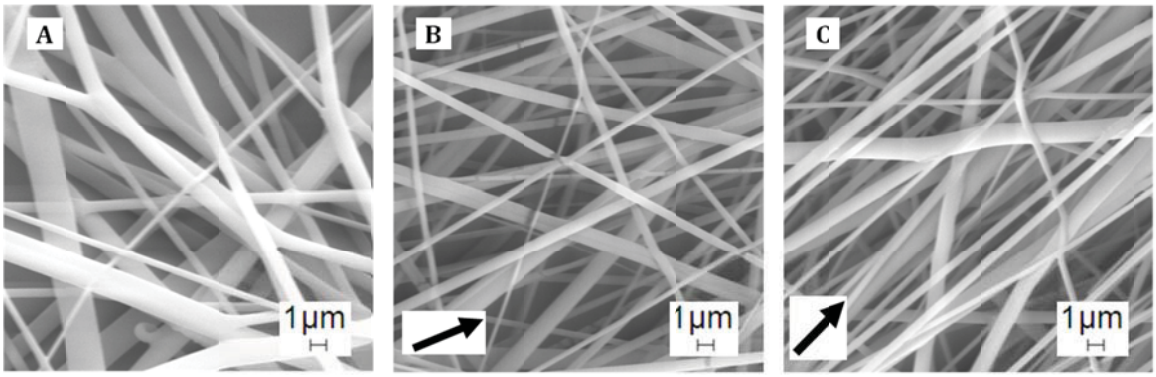

Figure 2.2: SEM images of PEUUR fibers electrospun from 12 wt% solutions onto moving target: a) stationary target, b) 2.4 m/s, and c) 4.4 m/s. Arrows corresponds to the average orientation of fibers.

Cell orientation and morphology on meshes

BMSCs were cultured on electrospun meshes for three days, and then fluorescent images were collected to characterize cell morphology. Representative images of cells (green) on meshes (red) showed that cells were rounder and exhibited random orientations on unaligned fiber meshes (Figure 2.3A) compared to cells on more aligned fiber meshes (Figure 2.3B). Quantitative image analysis was performed to characterize the projected cell area, aspect ratio, and length of the long axis as a function of fiber diameter (Figure 2.4) and degree of fiber alignment (Figure 2.5). Projected cell area was diminished on fibers relative to spincoated films (Figure 2.4A and Figure 2.5A), and this difference was

significant for the 0.28 and 2.3 μm fibers (p = 0.008 and 0.046, respectively). However, projected cell area did not appear to vary systematically with either fiber diameter (Figure 2.4A) or degree of fiber alignment (Figure 2.5). In contrast, cell aspect ratio was increased on all fibers relative to spincoated films (Figure 2.4B and Figure 2.5B), and differences were statistically significant for diameters of 0.82 and 2.3 μm, (p = 0.003 and 0.006, respectively, Figure 2.4B) and all degrees of fiber alignment (p= 0.005, <0.001, and <0.001 for σ = 49.5°, 33.7°, and 27.8°, respectively, Figure 2.5B). Further, cells on the more aligned fiber meshes (σ = 33.7° and 27.8°) had significantly greater aspect ratios than cells on the unaligned fiber meshes (p= 0.002 and <0.001, respectively, Figure 2.5B). Finally, the length of the long axis was unaffected by fiber diameter and angular standard deviation (Figure 2.4C and Figure 2.5C, respectively).

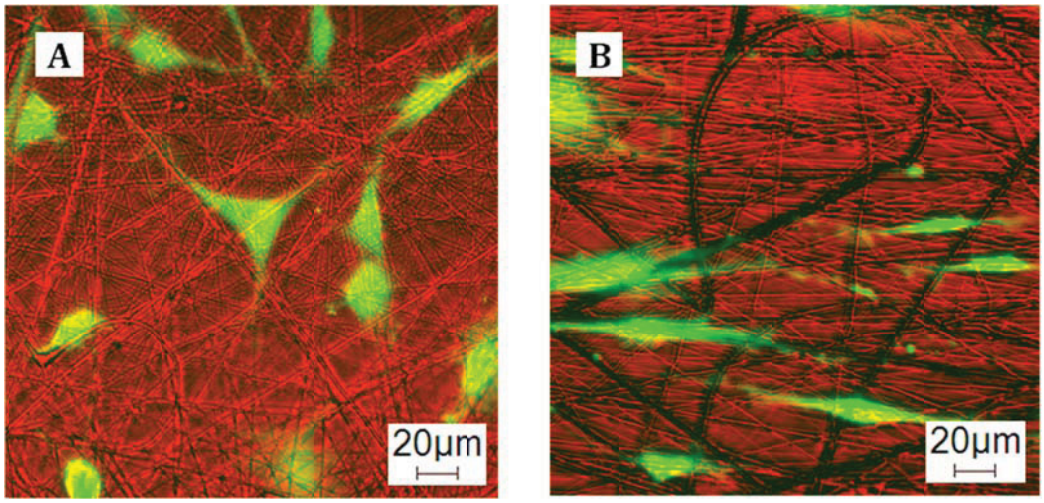

Figure 2.3: BMSC morphology on fiber meshes electrospun onto a) a stationary target and b) a drum rotating at 4.4 m/s. Images were constructed by merging phase contrast (red) and fluorescence (green) images of calcein-loaded cells attached to fibers.

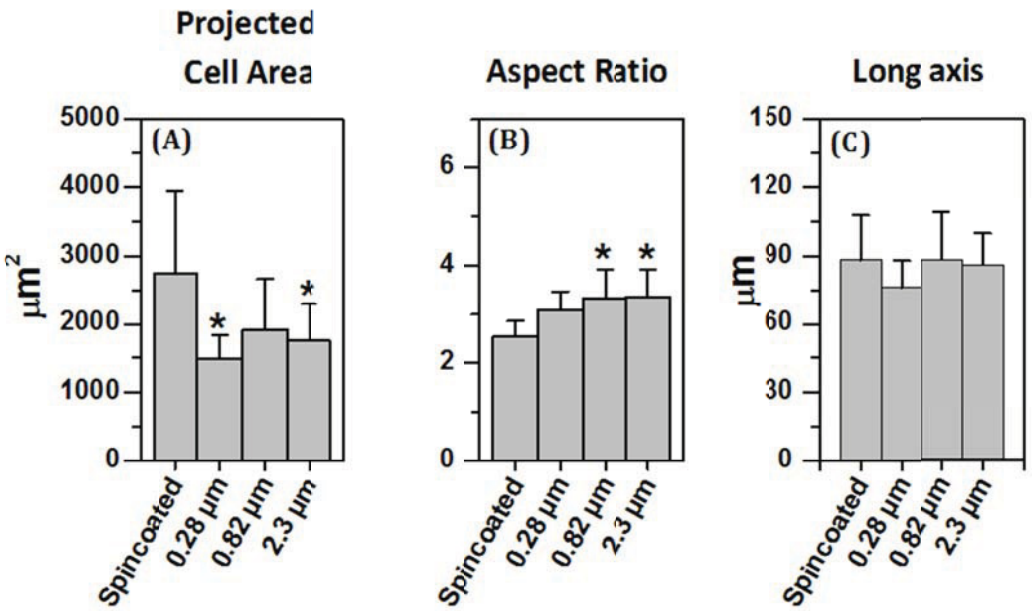

Figure 2.4: Effect of PEUUR fiber diameters [of 0.28 ± 0.07, 0.82 ± 0.14, and 2.3 ± 0.15 μm] on a) projected cell area, b) aspect ratio, and c) length of long axis. Mean fiber diameter controls were spincoated PEUUR films. An asterisk indicates statistical difference relative to control for n=6 or 9 coverslips.

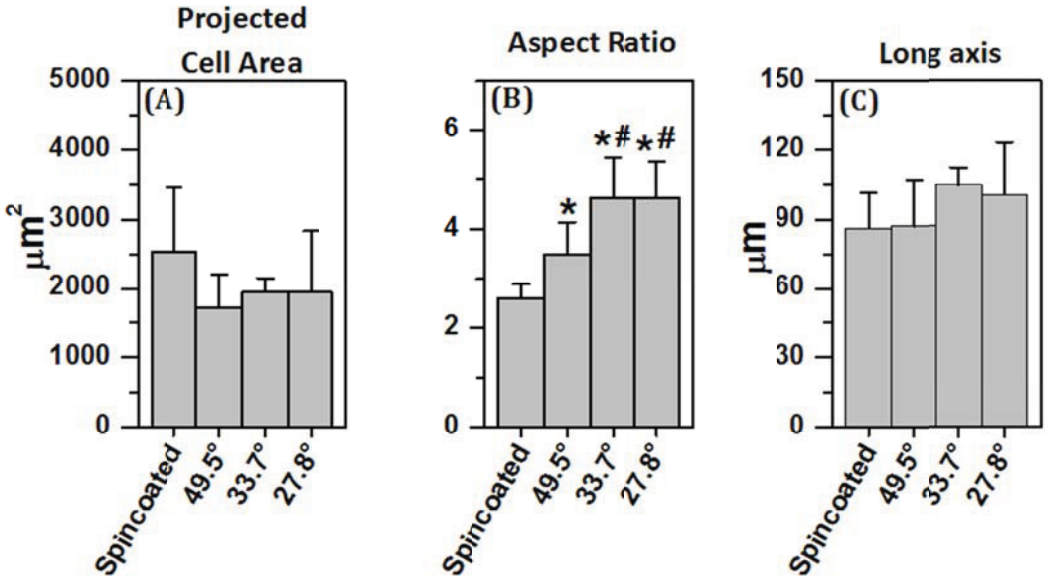

Figure 2.5: Effect range of PEUUR fiber orientation [of 49.5 ± 3.2°, 33.7 ± 0.99°, and 27.8 ± 2.5°] on a) projected cell area, b) aspect ratio, and c) length of long axis. Angular standard deviation controls were spincoated PEUUR films. An asterisk indicates statistical difference relative to control, and a pound symbol indicates statistical difference relative to the randomly oriented fibers (i.e., angular deviation = 49.5°) for n=6 or 9 coverslips.

Fluorescent images (e.g., Figure 2.3) were analyzed quantitatively to compare the orientation of BMSCs to that of the underlying fibers. Cells seeded onto spincoated surfaces and unaligned fiber meshes were unoriented, as indicated by angular standard deviations of σ = 50° and 38°, respectively (Table 2.2). In contrast, cells cultured on aligned fiber meshes oriented parallel to the fibers. Specifically, the mean angle of cell orientation differed from that of the fibers by 7° and the angular standard deviations for the cells were σ = 22° and 15° for linear velocities of 2.6 and 4.6 m/s, respectively (Table 2.2).

Table 2.3: Cell alignment on oriented meshes. Angular standard deviation of cells (averaged for n=2 or 3 replicates) and cell orientation relative to fibers on electrospun surfaces with different degrees of orientation for n=6 or 9 coverslips.

Fiber Angular Deviation (º)	Cell Angular Deviation (º)	Difference in Mean Angle (º)
Spincoated	52.3	–
52.1	39.6	34.9 ± 27.2
43.7	22.5	6.4 ± 6.9
33.6	15.0	7.1 ± 6.5

Cell Density on Meshes

Cell density was measured at days 3, 7, and 14 to characterize BMSC attachment and proliferation on the electrospun meshes. On day 3 the cell densities on the 0.28 and 0.82 μm fiber meshes were similar to those on the spincoated films (Figure 2.6A). In contrast cell density on the 2.3 μm fiber meshes was significantly lower than on the 0.28 and 0.82 μm fibers (p = 0.035 and 0.001, respectively). Between days 3 and 7 similar increases in cell density were noted on 0.28 and 0.82 μm fiber meshes and spincoated films, while no change in cell density was noted between 7 and 14 days. Cell density on the 2.3 μm fiber meshes was significantly lower than on the 0.28 μm fiber meshes at day 7 (p = 0.035). However, by day 14 cell density on the 2.3 μm fiber meshes was comparable to that on the other surfaces. On meshes with similar fiber diameters (0.46 to 0.82 μm) but with different

degrees of fiber alignment, cell densities were comparable to the spincoated films at all time points (Figure 2.6 A, B).

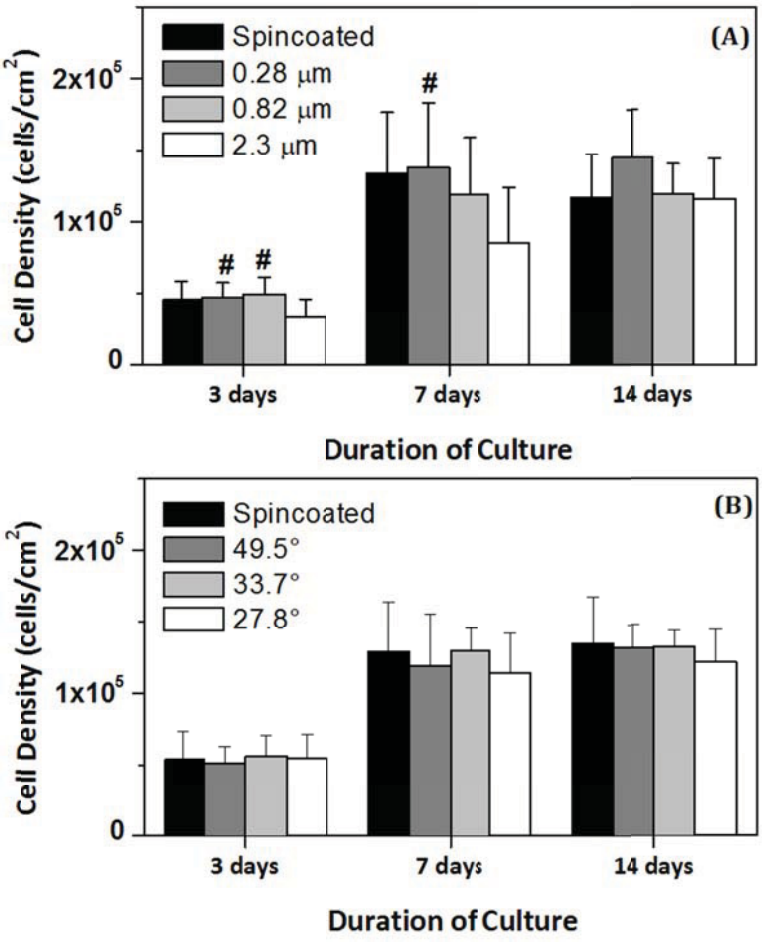

Figure 2.6: Cell density on PEUUR fibers as a function of culture duration: a) effect of fiber diameter, and b) effect of fiber orientation. A pound symbol indicates statistical significance from the largest diameter fibers for n=8 or 12 substrates.

Ligament protein expression

Real-time PCR was performed to determine the effect of fiber architecture on the expression of ligament proteins Col1α1, decorin, tenomodulin, and scleraxis. At day 7 BMSCs cultured on 0.82 and 2.3 μm fiber meshes exhibited lower expressions of Col1α1, decorin, and tenomodulin relative to BMSCs cultured on 0.28 μm fiber meshes and spincoated films (Figure 2.7). In particular, Col1α1 expression by BMSCs on both 0.82 and

2.3 μm fibers was significantly lower than by BMSCs on spincoated films ($p = 0.008$ and 0.028, respectively) and the expression of decorin on 2.3 μm fibers was significantly lower than on both spincoated films and 0.28 μm fibers ($p = 0.039$ and 0.047, respectively). When BMSCs were cultured on meshes with similar fiber diameters but with different degrees of fiber alignment, expression of Col1α1, decorin, and tenomodulin were lowest for BMSCs on the randomly oriented fibers ($\sigma = 49.5°$, Figure 2.8). Although the differences were not statistically significant, these lower levels of mRNA expression for $\sigma = 49.5°$ relative to spincoated surfaces are consistent with Figure 2.7, while the lower levels for $\sigma = 49.5°$ relative to the more aligned fibers ($\sigma = 33.7°$ and 27.8°) may be related to differences in both fiber alignment and fiber diameter. Scleraxis expression at day 7 was not significantly affected by either fiber diameter or degree of fiber alignment; however scleraxis expression increased with increasing fiber diameter (Figure 2.7) and decreasing degree of fiber alignment (Figure 2.8). Finally, expression of these four genes was also measured on day 14 (Figure 2.9 - Figure 2.11). Although no differences between groups were significant, expression of Col1α1 and tenomodulin were lower on all surfaces at day 14 relative to day 7, and tenomodulin expression was slightly higher on fiber meshes than on the spincoated films.

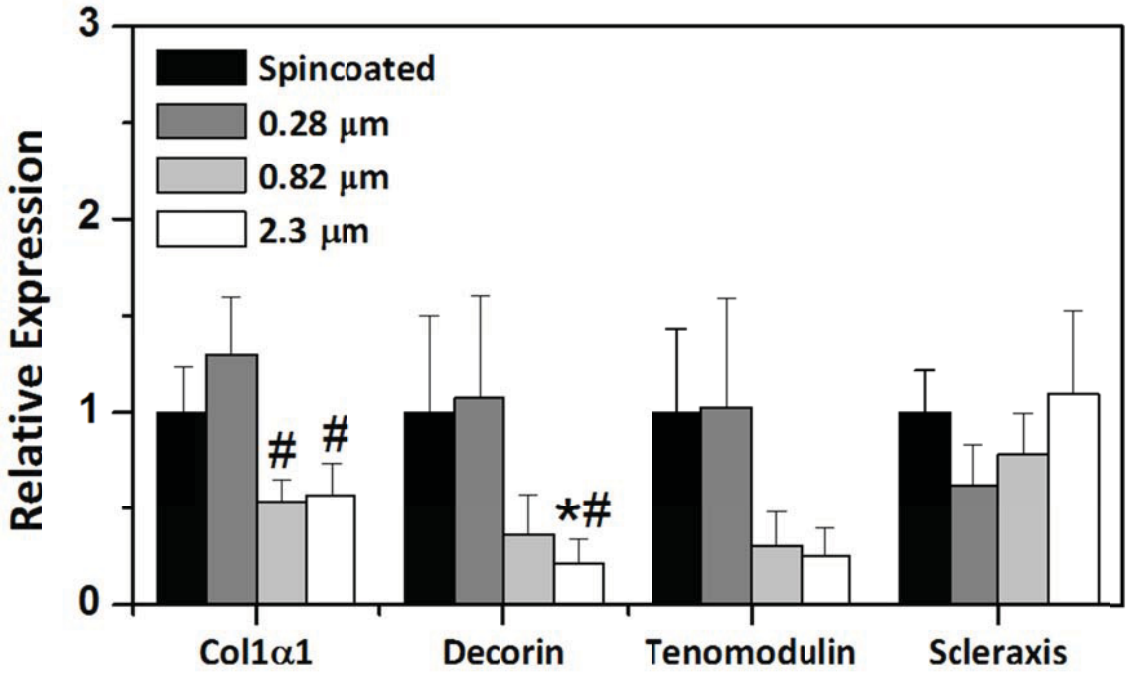

Figure 2.7: PCR results for collagen 1α1 and decorin normalized by the β-actin housekeeping gene for different fiber diameters. An asterisk indicates statistically significant difference from the spincoated control group and a pound symbol indicates significant difference from the smallest diameter fibers for n=6 or 9 substrates.

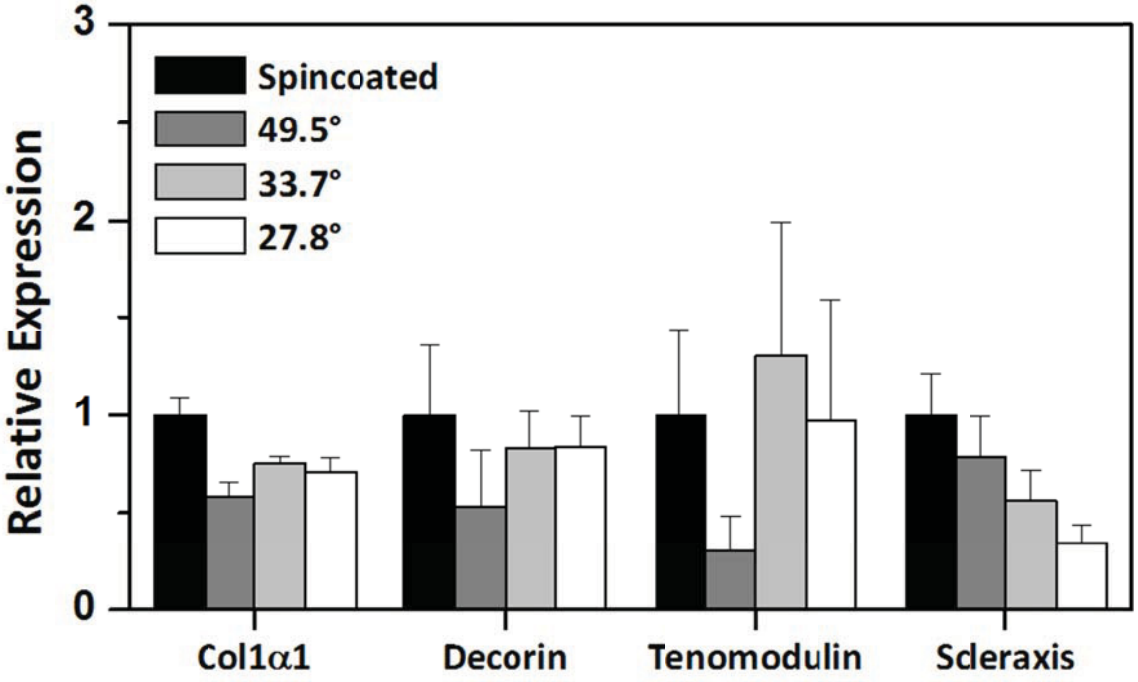

Figure 2.8: PCR results for collagen 1α1 and decorin normalized by the β-actin housekeeping gene for different fiber orientations. An asterisk indicates statistically significant difference from the spincoated control group for n=6 or 9 substrates.

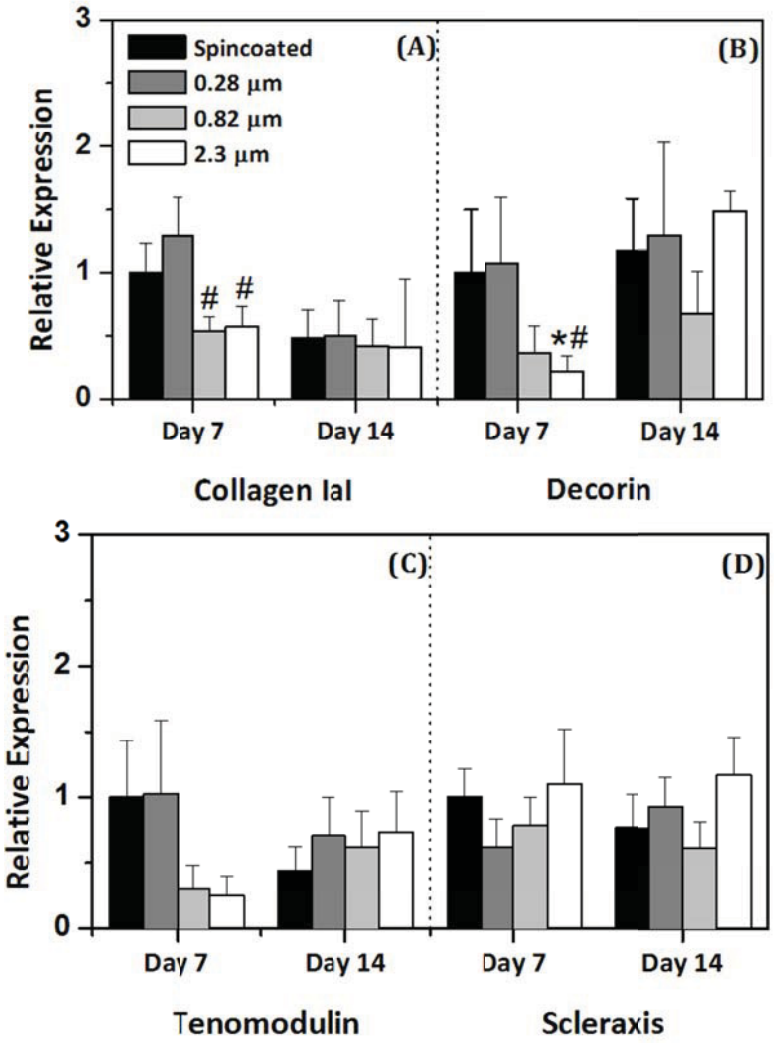

Figure 2.9: Effect of fiber diameter on mRNA expression of a) collagen 1α1, b) decorin, c) tenomodulin, and d) scleraxis after 7 and 14 days of culture.

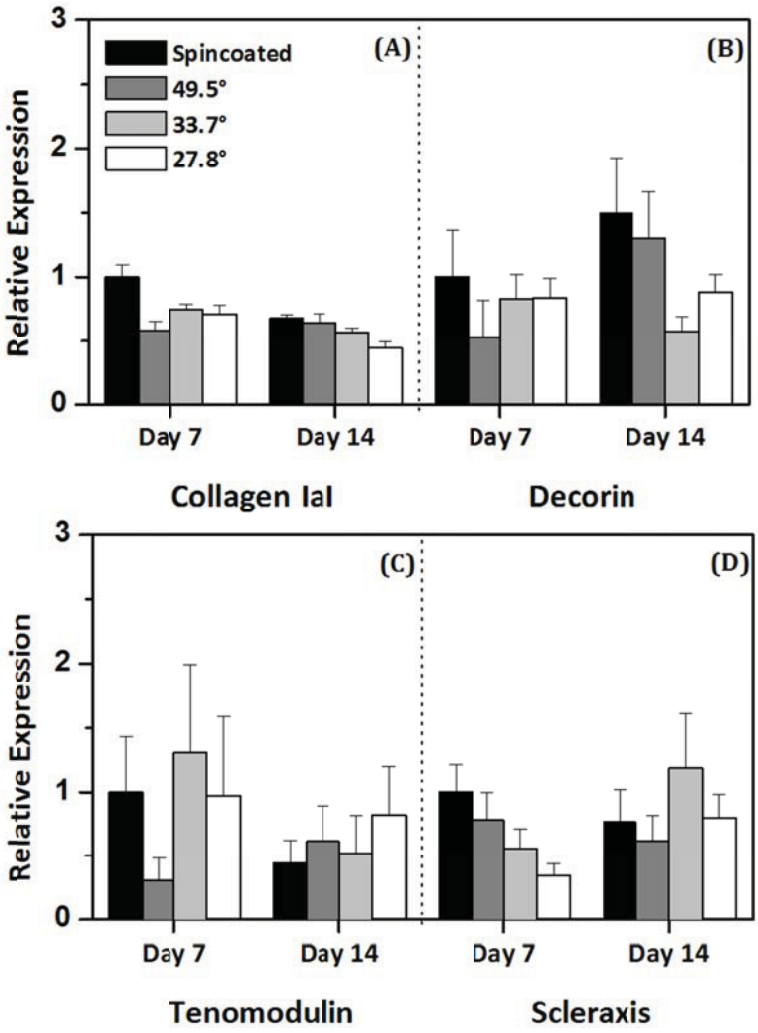

Figure 2.10: Effect of fiber orientation on mRNA expression of a) collagen 1α1, b) decorin, c) tenomodulin, and d) scleraxis after 7 and 14 days of culture.

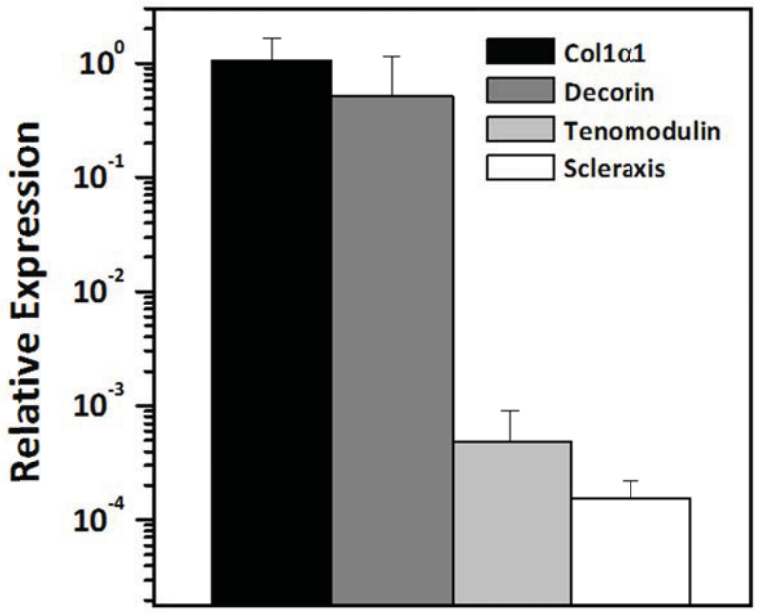

Figure 2.11: Comparison of mRNA expression on spincoated PEUUR films for collagen1α1, decorin, tenomodulin, and scleraxis after 7 days of culture.

Discussion

In this study BMSCs were cultured on electrospun PEUUR meshes to determine the effect of fiber diameter and alignment on cell morphology, proliferation, and ligament gene expression. Meshes with mean fiber diameters of 0.28 to 2.3 μm were achieved by using PEUUR solution concentrations of 7.5 to 20 wt%, while differing degrees of fiber alignment– characterized angular standard deviation of 27.8° to 49.5° – were achieved by varying the velocity of the target from 0 to 4.6 m/s. When BMSCs were cultured on resultant meshes, the projected cell areas were smaller than on spincoated PEUUR films; however cell aspect ratios were significantly greater on larger (0.82 and 2.3 μm diameter) unaligned fiber meshes and were further increased when the fibers were aligned (σ = 33.7 and 27.8°). In addition, cells oriented parallel to fibers on aligned fiber meshes. Cells proliferated on all surfaces, but expression of proteins Col1α1, decorin, and tenomodulin

were diminished at day 7 on the larger (0.82 and 2.3 μm diameter) unaligned fiber meshes relative to the smallest (0.28 μm diameter) unaligned fiber meshes and spincoated films.

The primary goal of this study was to determine the effects of electrospun mesh architecture on the expression of ligament genes, and a body of evidence is emerging to indicate that fiber diameter and alignment have pronounced effects on cell phenotype. For example, recent work by Kumbar et al. showed that the expression of Col1α1 is suppressed when human dermal fibroblasts are grown on larger fibers but that expression of collagen type III and elastin are enhanced when cells are grown on fibers with intermediate diameters (0.35 to 1.1 μm) [133]. The study presented here shows a decrease in the expression of Col1α1 with increasing fiber diameter (Figure 2.7), consistent with Kumbar et al., but it also demonstrates decreases in expression of decorin and tenomodulin, which have not been examined previously. In particular, the expressions of these three proteins as a function of substrate properties are remarkably similar, suggesting a common mechanism of gene regulation. In another study, Lee et al. examined the effect of fiber alignment and showed that collagen deposition is increased when ligament fibroblasts are grown on aligned fibers [139]. Although the study presented here does not demonstrate a change in Col1α1 (Figure 2.8), which is consistent with Baker et al. [22]) it does show increases in expression of decorin and tenomodulin (both involved in collagen bundle formation) and a decrease in scleraxis (an early marker of the ligament phenotype) with increasing fiber alignment. These data, while not statistically significant, suggest that fiber alignment promotes phenotypic maturation. Importantly, a similar observation was reported by Chew et al. for Schwann cells on aligned fiber meshes [52].

The ability to control electrospun mesh architecture has been described extensively and fiber diameters from as small as 0.03 μm to greater that 6 μm [233] have been achieved by changing spinning conditions such as electric potential, throw distance, flow rate of the metering pump, diameter of the syringe tip, and solution concentration [84, 103, 166, 180, 233]. Variation of the solution concentration is an effective means to control mean fiber diameter, but the range of achievable diameters is limited by bead formation [27, 166] and electrospraying [233] at low concentrations and viscous resistance to flow at high concentrations [233]. Because the goal of this study was to evaluate the biological effects of fiber diameter and degree of alignment, PEUUR solutions of 7.5 to 20 wt% in HFIP were selected to ensure that meshes were comprised of regularly shaped fibers. However, future examination of a broader range of fiber diameters may be both prudent and feasible. In this study, the expression of Col1α1, decorin, and tenomodulin were maximal on the smallest (0.28 μm) diameter fiber meshes (Figure 2.7), suggesting further increases in expression of these ligament proteins can be achieved by decreasing the fiber diameter. This may be testable as the addition of salts and the reduction of the throw potential have been reported to reduce bead formation at low solution concentrations. Concurrently, the limited penetration of cells into electrospun meshes that has been noted in the literature (e.g., [22]) may be overcome by the use of larger fibers, which provide larger interfiber spaces for cell migration.. Such larger fibers may be achieved by shortening of the throw distance [233].

Methods to align electrospun fibers also have been described extensively in the literature, and include depositing fibers on a rotating drum [27, 209], rotating disc [228, 263], between two grounded targets [142], and by stretching the resultant mesh [270]. In

this study, partial alignment – marked by angular standard deviations of 33.7° and 27.8°– was achieved using a rotating drum. Better alignment of electrospun fibers has been reported previously (e.g., [139, 263]), but the partial alignment demonstrated in this study was sufficient to achieve aspect ratios in excess of 4 (Figure 2.5) and to induce alignment of adherent BMSCs (Table 2.3). Further, the achievement of highly aligned electrospun fibers may not be beneficial for development of engineered ligament tissues because fiber packing density increases with fiber alignment, reducing interfiber pore size and the ability for cells to infiltrate [21].

A caveat of these studies is that the measured cell properties may reflect the mechanical properties of the PEUUR meshes. The rationale for electrospinning PEUUR meshes onto rigid glass supports was to isolate the effects of the mesh architecture. However, mechanical testing of the PEUUR meshes indicates that the modulus is approximately 1 MPa [232]. This relatively low modulus may contribute to the diminished projected cell areas, as previous studies have shown that cell spreading decreases with increasing substratum compliance [235]. Indeed, fibroblastic cells on rigid microgrooved titanium substrates are well-spread [64], in contrast to the BMSCs on PEUUR meshes in this study (Figure 2.3-Figure 2.5). In addition, when electrospun fibers are deposited on a rotating drum the resultant mesh can be as much as five times stiffer in the direction of fiber orientation than in the direction perpendicular [232]. This mechanical anisotropy may contribute to BMSC alignment as cells have been shown to align their actin cytoskeleton parallel the axis of greatest substratum stiffness [143, 211].

Previous work has shown that differentiation of progenitor cells and the achievement of a target phenotype is sensitive to the compliance of the underlying

biomaterial [76]. Although an optimal modulus for stimulating BMSCs to differentiate into tendon/ligament fibroblasts has not been identified, the PEUUR used in this study has a Young's modulus of 2.7 MPa [232], which is nearly two orders of magnitude lower than human adult ACL tissue (111-144 MPa [124, 188]). This suggests that new elastomers with higher Young's moduli may need to be identified in order to fabricate clinically useful engineered ligaments. However, processing conditions remain important, as the modulus of PEUUR meshes is sensitive to both fiber diameter and the degree of fiber alignment [232].

Finally, the results of this study suggest that electrospun fiber meshes consisting of smaller and more aligned fibers are attractive over larger unaligned fiber for ligament tissue engineering applications. The smaller fibers achieve higher expression of ligament proteins Col1α1, decorin, and tenomodulin, and the more aligned fibers stimulate alignment and elongation of adherent cells. However, differences in gene expression among the different electrospun meshes were modest, which suggests that additional stimuli (e.g. mechanical stretch [7] and growth factors [170, 171]) are required to achieve clinically effective engineered ligament tissues. Therefore, future studies, will concern the effect of uniaxial mechanical strain, which has been shown to induce expression of several ECM proteins, including collagen types I and III, decorin, and tenascin-C [49, 95, 139].

Conclusions

This study demonstrates that electrospun PEUUR meshes with fibers diameters of 0.28 to 2.3 μm and angular standard deviation of 27.8 to 49.5° support attachment and spreading of BMSCs. In addition, cell morphology was sensitive to fiber diameter and alignment, and adherent cells oriented parallel to fibers on aligned fiber meshes.

Expression of collagen 1α1, decorin, and tenomodulin was suppressed on the larger fibers. Together, these results suggest that aligned electrospun meshes consisting of submicron fibers may be preferable for ligament tissue engineering.

Acknowledgments

This research was funded by the ASPIRES grant program and through the Institute for Critical Technologies and Sciences at Virginia Tech.

Chapter 3: Effect of fiber diameter and alignment of electrospun polyurethane meshes on C3H10T1/2 cells

Robyn D Cardwell[1], Linda A Dahlgren[3], and Aaron S Goldstein[1,2]

[1]School of Biomedical Engineering and Sciences and
[2]Department of Chemical Engineering,
Virginia Polytechnic Institute and State University,
Blacksburg, VA 24061

[3]Department of Large Animal Clinical Sciences,
Virginia-Maryland Regional College of Veterinary Medicine,
Blacksburg, VA 24061

Abstract

Efforts to develop tissue engineered tendon and ligament replacements are numerous and focus on the use of a biomaterial scaffold and cell source to create a neotissue. However, providing the ideal milieu to promote the differentiation of stem cells and development of organized extracellular matrix (ECM) remains a challenge. Through electrospinning, scaffolds can be designed with tailorable architectures to mimic the intended tissue. In this study, an elastomeric poly(esterurethane urea) (PEUUR) is electrospun into fibrous scaffolds with a defined mean fiber diameter and orientation. Mesenchymal stem cell (MSC) morphology, growth and gene expression was evaluated on randomly oriented or semi-aligned scaffolds of varying mean fiber diameter, as evidence differentiation towards a tendon/ligament phenotype. Results demonstrated that the diameter of the fibers in the scaffold affects cellular responses more significantly than the alignment of the fibers within the scaffold. Initially, MSC cell density was greater on the smallest mean fiber diameter (≤ 1 μm) scaffolds but similar cell densities were found on all scaffolds after an additional week in culture. After two weeks, relative gene expression of

collagen type I and decorin was increased on all electrospun scaffolds compared to planar surfaces. A systematic increase in matrix gene expression was found as the scaffold mean fiber diameter increased at 14 days. Expression of the tendon/ligament transcription factor, scleraxis, was decreased on electrospun scaffolds at one week but semi-aligned, large mean diameter scaffolds appeared to have the greatest expression at two weeks. These results suggest that large diameter fibers (≥ 2 μm) may be more suitable for a tendon/ligament scaffold as gene expression was increased over smaller fiber diameter scaffolds.

Introduction

Repetitive and acute injuries of tendons and ligaments are a common musculoskeletal pathology, often necessitating surgical intervention to restore biomechanical integrity [32, 37, 70, 86]. For example, acute rupture of the anterior cruciate ligament (ACL) has been estimated to occur in one in 3,000 Americans, leading to approximately 100,000 ACL reconstructions each year [37, 86]. Despite a relatively high success rate using autologous tissue grafts, many patients do not return to pre-injury activity levels, which may be attributed to structural differences between the graft and native ACL tissue [1, 83, 240]. In addition, the efficacy of current reconstruction techniques in preventing long-term degenerative changes within the knee has been debated within the literature [83, 152].

Tissue engineering has emerged as a potential alternative to current surgical intervention practices for functional repair of these load-bearing, highly-collagenous tissues. Efforts to develop tissue engineered tendon and ligament replacements include growth factor augmentation [176], gene therapeutic approaches [110] and the use of a

biomaterial scaffold for directed differentiation of stem cells to create a neotissue [6, 138]. In the third approach, tissue engineers are challenged to provide the ideal microenvironment to promote the differentiation of stem cells and development of organized extracellular matrix (ECM). In particular, a cell source capable of ECM production and a scaffold designed with adequate composition and structure to support tissue formation is needed.

Biomaterial scaffold topographies have been shown to alter cellular behavior, including stem cell differentiation. The topography of the substrates can direct cellular activity through the phenomenon of contact guidance. As such, micropatterned substrates have been extensively used as a 2D surface for which to control cell alignment and shape for many cell types [48, 93, 123, 163]. In the absence of osteoinductive supplements, disordered topographical roughness, as compared to ordered features, has been shown increase osteoblastic differentiation of human mesenchymal stem cells (hMSCs) [62]. Neuronal differentiation of hMSCs was also enhanced on nanopatterned surfaces over standard induction media as evidenced by increased neuronal marker expression [265]. For successful *in vivo* tendon/ligament regeneration, a biomaterial scaffold with topographical features that facilitate cell alignment and differentiation towards tendon/ligament fibroblast phenotype would be ideal.

Electrospinning is an attractive method for fabrication of biomaterial scaffolds with tunable architectures, namely fiber size and orientation. Using an electrical potential to create fiber jets, this versatile method draws a polymer solution across a short distance to a grounded target where the fibers are collected. Electrospun fiber diameters can range in size from tens of nanometers to a few microns to mimic native extracellular matrix, and can

be aligned within the deposited matrix by rotation of the collector or parallel plates [178]. Collagen molecules are arranged in a hierarchal structure composed of fibrils (less than 100 nm diameter), fibers formed from bundles of fibrils (1-20 μm in diameter), and then groups of fibers packed into larger fascicles (100-250 μm in diameter) [25, 220]. In native tendon/ligament, spindle-shaped fibroblasts are arranged parallel to collagen fibrils and produce additional proteins to assist in regulation of collagen fibril size and organization [219].

The individual fibers within the electrospun matrix provide a 3D micropattern for cell attachment and growth. In addition, electrospun fibrous scaffolds fabricated from polymers, such as PCL, produce a unique non-linear mechanical behavior better suited for replacement of collagen-reinforced tissues, such as tendons and ligaments [157]. However, commonly used polyesters, such as PCL and PLGA, exhibit plastic deformations above 10% elongation and are too stiff to recapitulate native tissue mechanics [207]. Electrospinning of elastomeric materials, such as segmented polyurethanes, resist time-dependent changes under low strain conditions, allowing recovery during repeated cyclic loading as experienced in the tendon/ligament milieu.

Mesenchymal stem cells (MSCs) are an attractive cell source for cell-based tissue engineering strategies. While the use of mature fibroblasts may ensure expression of the target proteins, potential morbidity associated with the donor site, the limited capacity of the mature cells to proliferate *in vitro*, and rapid loss of phenotypic markers are significant drawbacks [11, 242]. Mesenchymal stem cells are adult stem cells residing primarily in the bone marrow but can also be found in other mesenchyne tissues such as skin and fat [3]. As multipotent cells, MSCs are capable of differentiating into mesenchymal tissue lineages

including bone, cartilage, fat, tendon, muscle and marrow stroma [197]. The process of mesenchymal stem cells differentiation to tendon or ligament fibroblasts is poorly understood. Since ligaments and tendons do not have unique extracellular matrix protein markers to define the tissue, expression of extracellular matrix proteins (e.g. collagen types 1 and 3, decorin) and cell morphology is often used to determine cell phenotype. More recently, scleraxis, the transcription factor present in developing ligaments and tendons, has been considered a selective, but not specific, marker of tendon and ligament tissue [119, 212]. Scleraxis levels are very low in undifferentiated mesenchymal progenitor cells but can be induced in three-dimensional culture [134].

In the current study, a mesenchymal stem cell line, C3H10T1/2, were cultured on electrospun scaffolds with small (≤ 1 μm,), medium (1-2 μm) or large fiber diameters (≥ 2 μm), chosen based on their similarity to developing tendon collagen fibril bundles [220, 230], with either random or semi-aligned mesh orientation to determine the effect of the scaffold on MSC morphology, proliferation and phenotype. Scaffolds were prepared from a segmented poly(esterurethane urea) (PEUUR) that is elastomeric, biocompatible and degradable [28, 101]. After static culture on the prepared scaffolds, preliminary MSC differentiation towards a tendon or ligament fibroblast was assessed by morphological analysis using cytoskeletal staining, quantification of tendon/ligament gene expression and visualization collagen type I deposition.

Materials and Methods

Fabrication and characterization of electrospun PEUUR scaffolds

All chemicals for the synthesis of PEUUR and reagents for biochemical assays were obtained from Sigma-Aldrich (St Louis, MO) unless otherwise specified. A segmented poly

(esterurethane urea) (PEUUR) was synthesized and characterized as previously described using poly (ε-caprolactone) diol (average molecular weight 2000 Daltons, PCL) [28]. The segmented polyurethane had bulk material properties similar to those previously reported with glass transition and melting point temperatures of -55.5°C and 32.7°C, respectively [99]. Polymer molecular weight (Mw) was 146 kDa with a polydispersity index of 1.77 as measured by GPC (not shown). Solutions of PEUUR in 1,1,1,3,3,3-hexaflouro-2-propanol (HFIP) at concentrations (wt%) of 7%, 12% and 20% were used to form scaffolds with fibers with small (≤ 1 μm), medium (1-2 μm) and large fiber (≥ 2 μm) diameters, respectively. Electrospun meshes were produced with either a random or a semi-aligned fiber orientation, resulting in six separate scaffolds (Table 3.2). The PEUUR solution was loaded into a syringe equipped with a 22 gauge steel flat-tip needle and positioned 15 cm from a stationary target or a mandrel rotating at a linear speed of 9.5 m/s. A potential of 15 kV between the needle and target was applied and a syringe flow rate of 3 mL/h was set to create fibers that were drawn across the gap and deposited onto the target. The electrospun fibers were collected onto pre-cleaned 18 mm diameter circular glass coverslips, which were previously spincoated using a 3.5 wt% PEUUR solution in 50:50 HFIP:isopropanol solution to ensure attachment of the fibers to the substrate. Glass coverslips spincoated with PEUUR were used as a smooth surface control.

The electrospun mats were allowed to dry overnight in the laminar flow hood and then leeched in 70% ethanol for 2 days followed by distilled water for an additional 2 days with daily changes of fluid to remove residual HFIP. Scaffolds were dried in a dessicator and then sterilized by gamma irradiation. Scanning electron microscopy (LEO 1550 Field Emission SEM, Carl Zeiss SMT, Thornwood, NY) was used to verify fiber diameter size and

alignment, measured manually from the SEM images using ImageJ v1.40 (National Institutes of Health, Betheseda, MD). The relative frequency of fiber diameter was plotted from 0.1 to 5.5 μm for scaffolds collected on the stationary target and from 0.1 to 4.0 μm on the rotating mandrel with a bin size of 0.2 μm. The degree of fiber alignment was determined by calculating the angular standard deviation (ASD), as previously described [28]. For fiber orientation histogram, approximately n=200 fibers were analyzed per scaffold group. The mean angle subtracted from the population to center the distribution about 0° and normalized. Histograms of the normalized data were plotted between -90° to +90° with a 10° bin size for each scaffold group.

Cell culture and seeding

Prior to cell seeding, scaffolds were placed in individual wells of standard 12-well plates and immersed in 1mL of a 2 μg/mL fibronectin solution in phosphate buffered saline (PBS) for 1 hour at 37°C. C3H10T1/2 Clone 8 mouse embryonic fibroblasts were obtained from the American Type Culture Collection (ATCC, Manassas, VA) and maintained in Dulbecco's modified Eagle's medium (DMEM, Invitrogen, Carlsbad, CA) with high glucose (4,500 mg/L) supplemented with 10% fetal bovine serum (FBS, Gemini Bio-Products, W Sacramento, CA) and 1% antibiotic/antimycotic (Invitrogen). For all experiments, DMEM growth medium was supplemented with 50 μg/mL ascorbate-2-phosphate. C3H10T1/2 cells were seeded at a density of 10,000 cells/cm^2 onto electrospun scaffolds placed into wells and media was replaced every 3 days.

Cell number

After three and ten days of culture, cell density on electrospun scaffolds was determined by analysis of total DNA content. Scaffolds were rinsed twice with phosphate

buffered saline (PBS) and then transferred to a new well of a 12-well plate. Cells were lysed in 300 μL per scaffold digestion buffer (100mM NaCl, 10mM Tris-Cl, 25mM EDTA, 0.5% SDS, 0.1 mg/mL proteinase k) and mechanically removed from the glass coverslip using a cell scraper. Samples was allowed to digest overnight at 50°C and then extracted using an equal volume of phenol/chloroform/isoamyl alcohol (25v:24v:1v) [231]. DNA was precipitated by adding 1/2 volume of 7.5 ammonium acetate and 2 volumes of 100% ethanol. Following recovery and wash, sample DNA was resuspended in 1X Tris-EDTA (TE) buffer. Total DNA content was measured using Quant-iT PicoGreen® kit (Invitrogen) according to manufacturer's instructions using a fluorescent plate reader (SpectraMax M2, Molecular Devices, Sunnyvale CA). DNA content was determined from a serial dilution of lambda DNA standard, provided in the kit.

Cell Morphology

After 3 days of culture (prior to confluency), cell-seeded scaffolds were fixed and stained to qualitatively determine cell morphology. Scaffolds were rinsed twice with 1X PBS and fixed in 3.7% methanol-free formaldehyde (Polysciences Inc, Warrington PA) for 10 minutes followed by incubation with 0.1% Triton X-100 in PBS for 5 minutes at room temperature. Next, cells were incubated with rhodamine phalloidin (Invitrogen), diluted 1:40 in PBS for 20 minutes at room temperature. Scaffolds were mounted with semi-permanent mounting medium containing DAPI (Vector Laboratories, Burlingame CA) and visualized under a fluorescent microscope (Leica Microsystems, Wetzlar Germany). Average cell area was calculated using ImageJ after thresholding individual images.

Gene expression

Scaffolds were rinsed twice with 1X PBS, transferred to a new well of a 12-well plate and then collected using Buffer RLT, provided in the RNeasy Mini Kit (Qiagen, Germantown, MD) Cells and scaffolds were manually crushed using a microtube pellet pestle before homogenization in QIAshredder columns (Qiagen). Following homogenization, an equal volume of 70% ethanol was added and the lysate was loaded onto the RNeasy silica spin columns and total RNA isolated according to the kit instructions. Samples were subjected to on-column DNase digestion using DNase I (Qiagen) prior to elution. Total RNA was quantified using Quant-iT RiboGreen® kit (Invitrogen) using a fluorescent plate reader (SpectraMax M2, Molecular Devices). Equal amounts of total RNA, approximately 500 ng, were then reverse transcribed to cDNA using High Capacity cDNA Reverse Transcription kit (Applied Biosystems, Carlsbad CA) with random hexamers as primers, according to manufacturer's protocol.

Real time PCR was performed in the ABI 7300 Real Time PCR System (Applied Biosystems) using Power Sybr® Green Master Mix (Applied Biosystems). For PCR amplification, approximately 100 ng of sample cDNA was used. Specific primers for mouse collagen type 1α1, decorin, and scleraxis were designed using Primer Express software v2.0 (Applied Biosystems), shown in Table 3.1: Primer sets for real-time polymerase chain reaction. β-actin was used as the reference gene [130]. Isolated total RNA – to test for genomic DNA contamination – and no template (nuclease-free H_20 in place of cDNA) were used as negative controls. Quantification of target relative gene expression (e.g. collagen type 1α1) is referenced to the reference/housekeeping gene (β-actin) using the comparative threshold cycle (ΔΔCt) method using the spincoated surface as the calibrator

[151]. Gene expression data for day 14 is also referenced to day 7 the spincoated surface to analyze temporal expression changes.

Table 3.1: Primer sets for real-time polymerase chain reaction

Gene *Accession No.*	Significance	Primer Set	Amplicon Size
Beta Actin *NM_007393*	housekeeping/ reference	Forward: 5' TGCTCCCCGGGCTGTATT 3' Reverse: 5' ACATAGGAGTCCTTCTGACCCATT 3'	87 bp
Collagen Type 1α1 *NM_007742*	Primary structural protein of tendon/ligament ECM	Forward: 5' ATGTTCAGCTTTGTGGACCT 3' Reverse: 5' CAGCTGACTTCAGGGATGT 3'	92 bp
Decorin *NM_007833*	Proteoglycan mediator in collagen fibrillogenesis	Forward: 5' TCGAGTGGTGCAGTGTTCTGA 3' Reverse: 5' TTGCAGGTCTAGCAAGGTTGTGTC 3'	82 bp
Scleraxis *NM_198885*	Selective tendon/ligament transcription factor	Forward: 5' TCTGCCTCAGCAACCAGAGAAAGT 3' Reverse: 5' ACTCTTCAGTGGCATCCACCTTCA 3'	130 bp

Immunohistochemistry

After two weeks of culture, samples for immunohistochemistry were fixed in AFA fixative (74% alcohol, 2% formalin, 5% acetic acid, 19% DI H_20) overnight at 4°C. This fixative prevents disruption the collagen three-dimensional structure. For immunostaining of collagen type I, 5 μm paraffin sections were heated at 56°C for 2 hours and deparaffinized by submersion twice in xylene for 5 minutes each. Sections were then rehydrated using a graded ethanol series consisting of: 2X in 100% ethanol for 3 minutes each, 2X in 90% ethanol for 1 minute each and 2X in 80% ethanol for 1 minute each. Next, sections were washed in deionized water and PBS for 5 minutes each. Sections were then pretreated with 100 mM glycine-HCl + 50 mM ammonium chloride in PBS for 30 minutes at room temperature followed by enzymatic treatment with 0.2% hyaluronidase in 20 mM sodium acetate for 15 minutes at 37°C. After 3 washes in PBS, sections were blocked using diluted normal goat serum from the VectaShield ABC kit (Vector Laboratories, Burlingame,

CA) according to kit instructions for 20 minutes at room temperature. Excess liquid was blotted prior to incubation with rabbit anti-mouse collagen type I antibody (1:500, Meridian Life Sciences, Saco, ME) in a humidified chamber overnight at 4°C. Incubation with diluted normal goat serum and Rabbit IgG antibody served as the negative and isotype controls, respectively. Next, sections were washed three times with PBS and incubated with biotinylated secondary antibody from the VectaShield ABC kit for 30 minutes at room temperature followed by incubation with the ABC reagent for 30 minutes at room temperature. Brown color was developed using Immpact DAB substrate (Vector Laboratories) for 2-5 minutes. Sections were counterstained with hematoxylin QS (Vector Laboratories).

Statistical analysis

Results are presented as mean ± standard deviation for n=3 samples per experimental condition unless otherwise noted. Statistical significance was determined using one-way ANOVA, followed by post-hoc comparisons using the Fisher least significance difference method with a significance criterion of $p \leq 0.05$ (OriginPro 8.1, Northhampton, MA). The full experiment was completed twice; however, due to variation between batches of polymer, only one experiment is presented in the results section. Similar results were obtained in both experiments.

Results

To test the effect of scaffold fiber diameter and alignment on cell morphology and phenotype, six distinct electrospun scaffolds were fabricated using differing concentrations of PEUUR electrospinning solutions collected on either a stationary platform or a rotating mandrel. Electrospinning of the PEUUR elastomer resulted in long, smooth fibers covering

the glass coverslip as shown in the representative SEM micrographs in Figure 3.1. As illustrated in Table 3.2, a 7wt% PEUUR solution, henceforth known as the "small" group, resulted in fiber diameters of 0.39 ± 0.11 μm with an angular standard deviation (ASD) of 62.5° for a stationary target Figure 3.1a) and 0.50 ± 0.11 μm with an ASD of 42.6° for a mandrel rotating at 9.5 m/s (Figure 3.1d). Similarly, the 12 wt% PEUUR solution, designated as the "medium" group, created scaffolds with fiber diameters of 1.53 ± 0.43 μm with an ASD of 42.7° on stationary target (Figure 3.1b) and 1.08 ± 0.22 μm with an ASD of 27.2° on the rotating target (Figure 3.1e). Prepared from a 17wt% PEUUR solution, the final scaffold group of "large" diameter contained fiber diameters of 3.56 ± 0.51 μm with an ASD of 63.0° collected on the stationary target (Figure 3.1c) and 2.08 ± 0.57 μm with an ASD of 61.5° (Figure 3.1f).

Table 3.2: Physical characteristics of electrospun PEUUR2000 scaffolds

Designation		Solution conc.	Mandrel Speed	Fiber Diameter (μm)	Fiber Alignment (ASD)
Random	Small (≤ *1 μm*)	7 wt %	Stationary	0.39 ± 0.11	62.5°
	Medium (*1-2 μm*)	12 wt %		1.53 ± 0.43	42.7°
	Large (≥ *2 μm*)	17 wt %		3.56 ± 0.51	63.0°
Semi-aligned	Small (≤ *1 μm*)	7 wt %	9.5 m/s	0.50 ± 0.11	42.6°
	Medium (*1-2 μm*)	12 wt %		1.08 ± 0.22	27.2°
	Large (≥ *2 μm*)	17 wt %		2.08 ± 0.57	56.3°

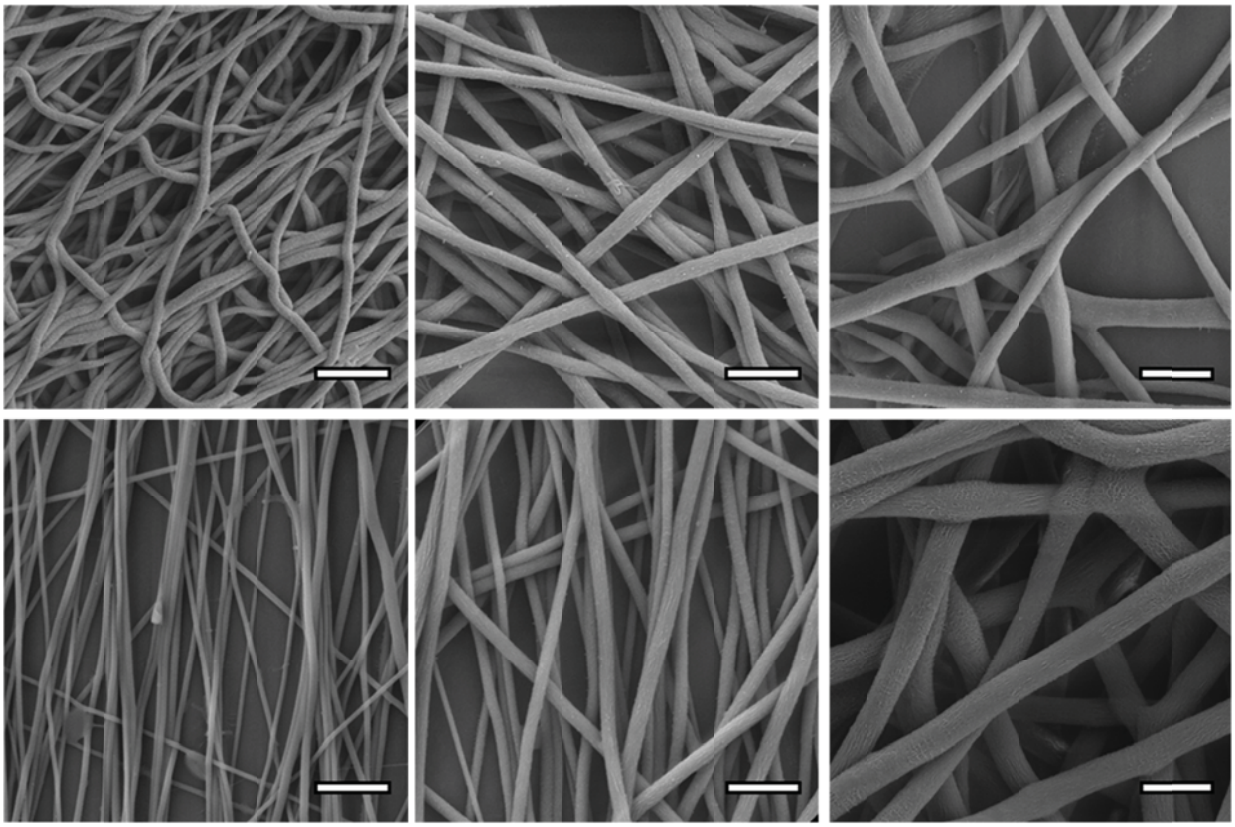

Figure 3.1: Representative scanning electron micrographs of PEUUR electrospun scaffolds with random (a, b, c) or semi-aligned (d, e, f) fibers with small (a,d) , medium (b, e) or large (c, f) average fiber diameters. Scale: 10 μm

Deposition of the electrospun fibers on the rotating target tended to decrease the mean fiber diameter slightly, as compared to a non-moving collector. As shown in Figure 3.2, the distribution of fiber diameters for small, medium and large scaffold groups displayed uni-modal peaks for collection on both the stationary target and the rotating mandrel, with the sharpest peaks occurring in the small diameter scaffold group.

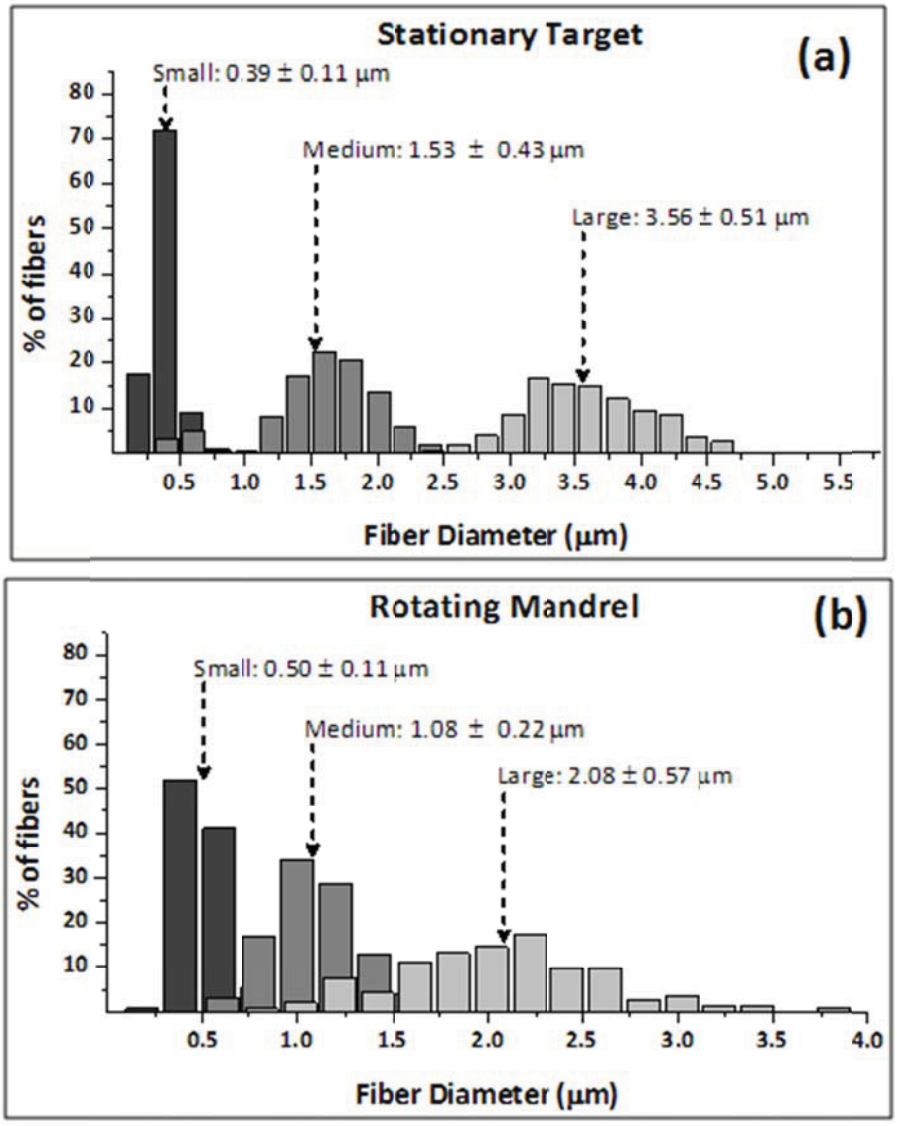

Figure 3.2: Distribution fiber diameter within small, medium or large scaffolds collected on a stationary target (a) or rotating mandrel (b) to create random or semi-aligned fiber orientation, respectively. Fiber diameters were measured manually from SEM images. Diameters are plotted in bins (0.2 µm/bin), > 200 measurements per group.

Collection of the electrospun fibers on a mandrel rotating at 9.5 m/s induced semi-alignment of the fibers within the scaffold relative to the more random orientation of fibers within the scaffolds collected on a stationary target. The distribution of fiber orientation within the random and semi-aligned scaffolds is shown in Figure 3.3. Distinct peaks of fiber orientation were observed on a rotating mandrel whereas fibers collected on a

stationary target were dispersed across all orientations in the small and medium fiber diameter scaffolds. However, similar distributions of the fiber orientation were observed for the random and semi-aligned large fiber scaffolds.

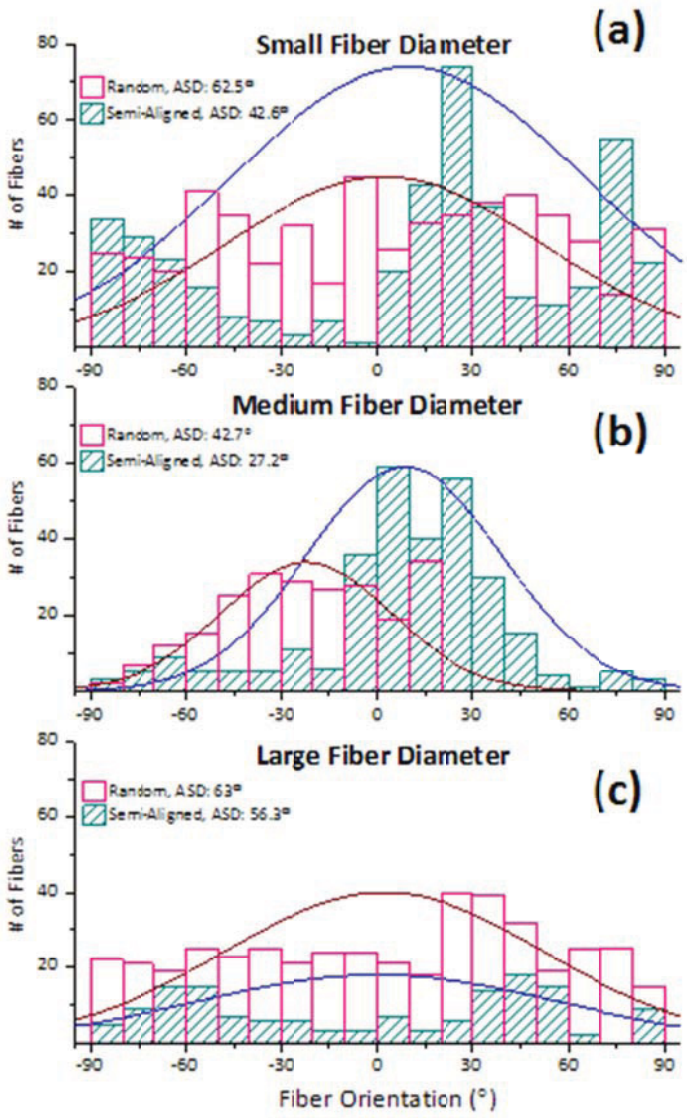

Figure 3.3: Histograms of fiber orientation for small, medium and large fiber diameter scaffolds are shown in (a), (b) and (c), respectively.

Cell density was measured on all electrospun scaffold types including a smooth, spincoated control surface following three days of culture. Shown in Figure 3.4a, cell density decreased as the mean fiber diameter increased on both the randomly oriented and

semi-aligned scaffolds. Cell density was significantly less on the scaffolds with a large fiber diameter compared to the small diameter fibers on both random ($p=0.005$) and semi-aligned ($p=0.004$) scaffolds. Semi-aligned large fiber diameter scaffolds also had significantly less cell density than semi-aligned medium fiber diameter scaffolds ($p=0.049$). Small fiber diameter scaffolds (≤ 1 μm) had significantly greater cell density than the medium (1-2 μm) fiber diameter for randomly oriented scaffolds ($p=0.033$). No difference in cell density was found between random or semi-aligned scaffolds of paired fiber diameter size. After nine days of culture, cell density was less than cell density after three days of culture on the electrospun scaffolds (Figure 3.4b). The cell line used in this study is known to be highly contact inhibited and overconfluence could cause regulated cell death on the scaffolds [208]. No indication of decreasing cell density with increasing fiber diameter was observed at this later time point. In fact, randomly oriented small and large diameter scaffolds had significantly fewer cells as compared to the spincoated control scaffold ($p=0.040$ and $p=0.025$, respectively).

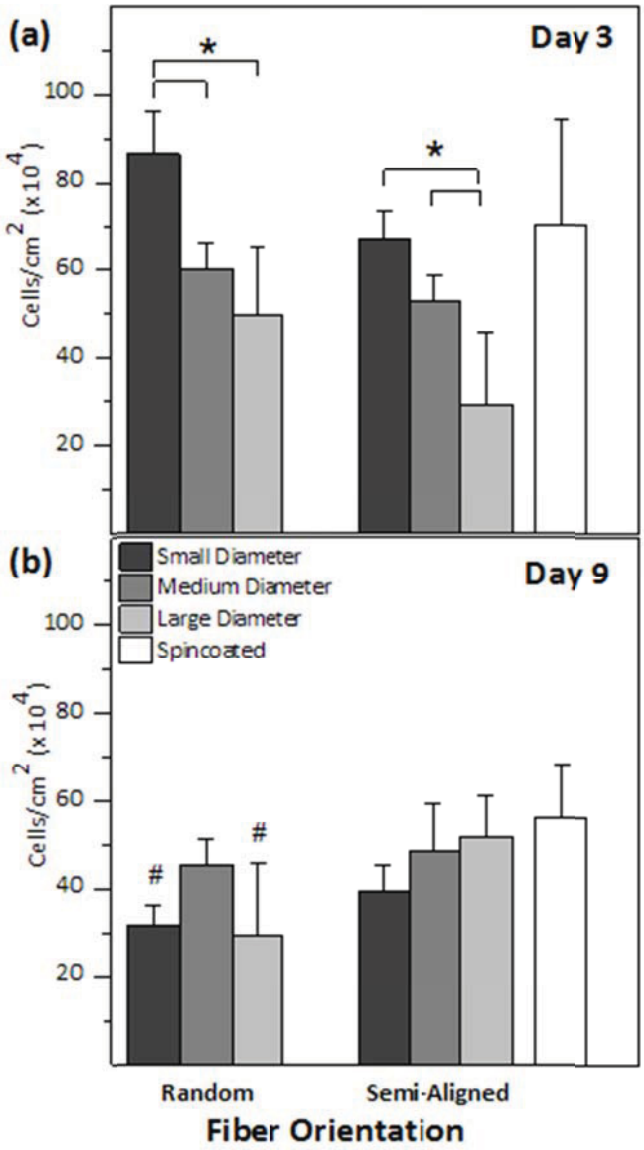

Figure 3.4: Cell density on PEUUR electrospun scaffolds after 3 (a) or 9 (b) days of culture (n=3, mean ± SD). An asterisk indicates statistical significance ($p \leq 0.05$) between electrospun groups and a pound sign indicates statistical significance relative to spincoated control.

Prior to confluency, cell morphology was qualitatively and quantitatively assessed by visualizing the actin cytoskeleton with rhodomine phalloidin. In Figure 3.5, cell shape is depicted on (a) spincoated PEUUR surface, (b) random or (c) semi-aligned electrospun scaffolds with medium fiber diameters of 1-2 μm. Cell bodies on the smooth spincoated surface are well-spread, large and contain diffuse bands of actin filaments interspersed with radial filaments in the lamellipodium of each cell. In contrast, cells on electrospun

scaffolds have more projecting filopodia containing bundled actin filaments, possibly clustering integrins and other proteins that make up the focal adhesion complex [156]. These projections coincide with the underlying electrospun fibers, detailed in Figure 3.5d. Semi-aligned fiber scaffolds oriented the cells in an ordered configuration (Figure 3.5c) as opposed to the random fiber scaffolds where no directionality of the cells is apparent (Figure 3.5b). Projected cell area was also quantified by measuring thresholded fluorescence images of the actin cytoskeleton. On random scaffolds with large fiber diameters, projected cell area was significantly greater than for cells on all other fiber sizes or on the spincoated control surfaces ($p < 0.05$) (Figure 3.5e). Cell area on semi aligned scaffolds with medium diameter fibers also were significantly increased compared to cells on the smallest fiber size scaffold ($p=0.017$).

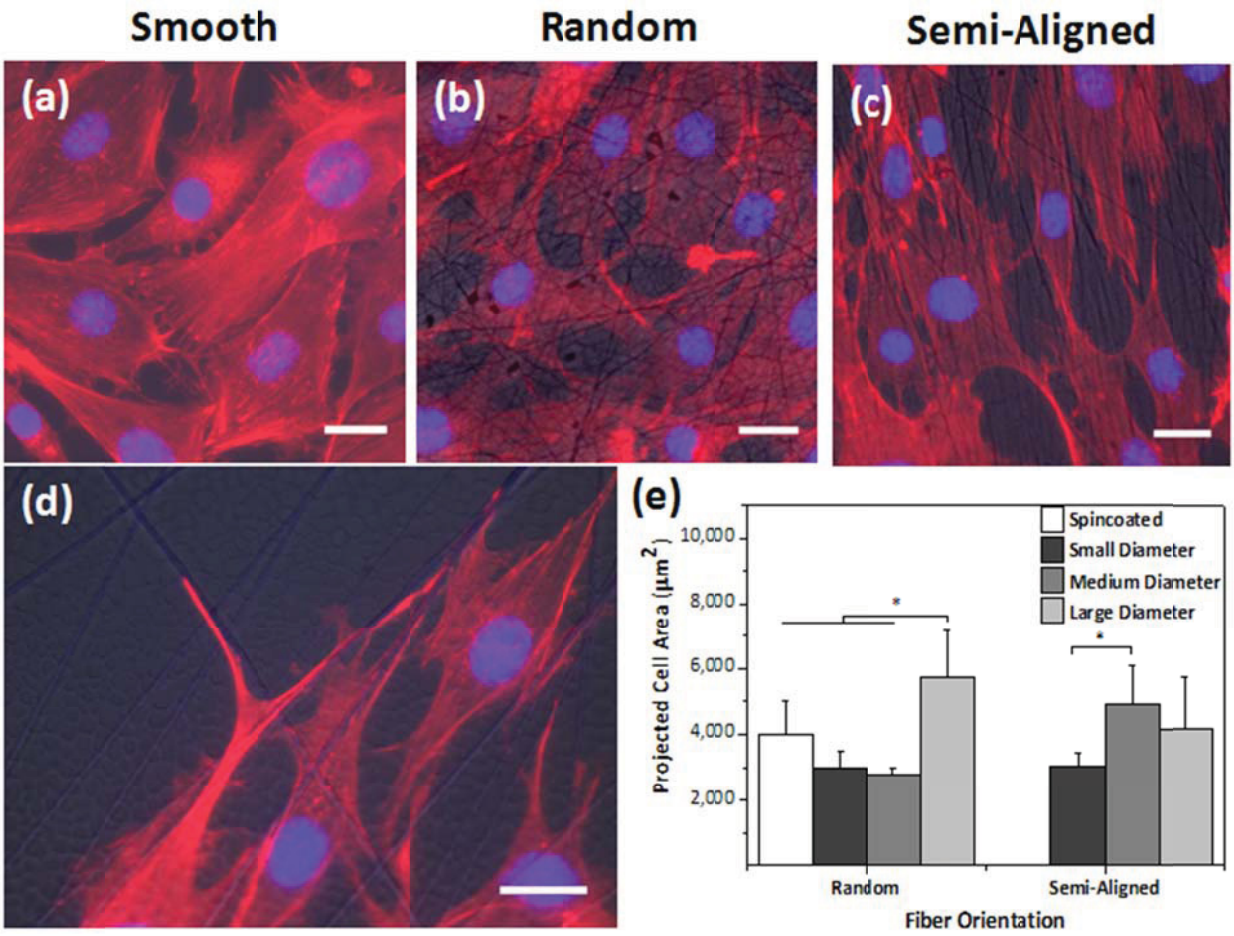

Figure 3.5: F-actin filaments (red) of C3H10T1/2 cells stained with rhodamine phalloidin on (a) spincoated, (b) randomly oriented or (c) semi-aligned electrospun PEUUR scaffolds with a mean fiber diameter of 1-2 μm (medium) after three days of static culture. In (d), a cell process extends along a large PEUUR electrospun fiber with mean diameter ≥ 2 μm. Cell nuclei are counterstained with DAPI (blue). (Scale bars: 25 μm). The projected area (μm²) of cells on electrospun scaffolds varies with scaffold fiber size in (e). (n=3, mean ± SD). Statistical significance at $p \leq 0.05$ is denoted with an asterisk.

To assess the effect of scaffold architecture on cell phenotype, relative gene expression of major ligament proteins collagen type I, decorin and scleraxis was quantified following one and two weeks of culture. For cells cultured on scaffolds with random fiber orientation, expression of collagen type I and decorin was significantly decreased on the largest fiber diameter (≥ 2 μm) scaffolds , compared to the smallest fiber diameter (≤ 1 μm) scaffolds after one week ($p < 0.05$) (Figure 3.6). However, these effects were not observed

for semi-aligned scaffolds, which indicated little effect from the fiber diameter at day 7. Scleraxis gene expression was significantly reduced on all electrospun scaffolds compared to the spincoated control ($p < 0.05$). In addition, scleraxis gene expression systematically increased with increasing fiber diameter on semi-aligned scaffolds but this was not significant.

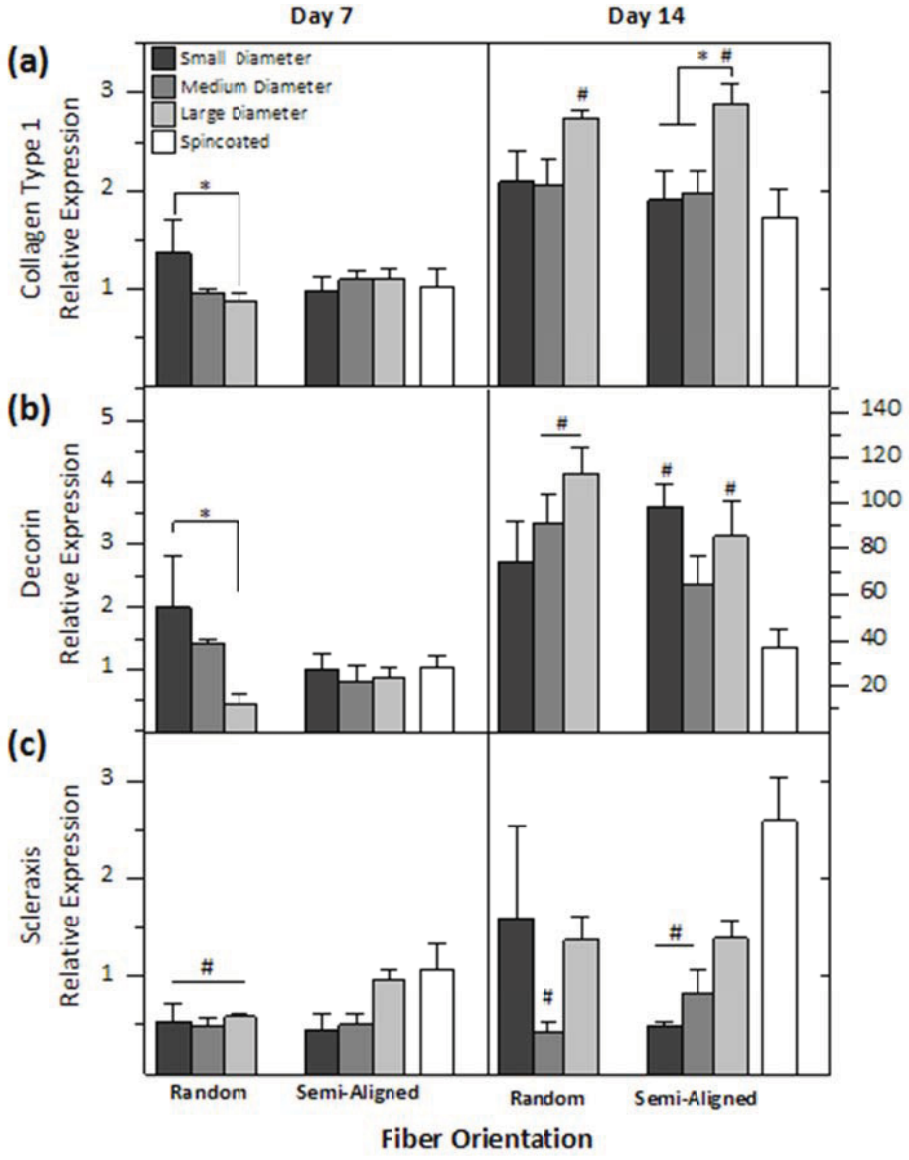

Figure 3.6: Relative gene expression of (a) collagen type I, (b) decorin and (c) scleraxis on randomly oriented or semi-aligned electrospun scaffolds of small, medium and large fiber diameters. An asterisk indicates statistical significance ($p \leq 0.05$) between electrospun groups and a pound sign indicates statistical significance relative to spincoated control. n=3, mean ± SEM

After two weeks of culture, opposite trends to one week expression were found for collagen type I and decorin. Gene expression of collagen type I and decorin on the largest diameter fibers (≥ 2 μm) was significantly increased ($p < 0.05$) over spincoated control for both random and semi-aligned scaffold types Figure 3.6). In semi-aligned scaffolds, the largest diameter fibers (≥ 2 μm) also significantly increased ($p < 0.05$) MSC collagen type I gene expression versus cells on the two smaller fiber sizes (Figure 3.6a). In addition, decorin gene expression increased with increasing fiber diameter for randomly aligned scaffolds, with the medium and large fiber diameter scaffolds having significantly greater gene expression than the smooth, spincoated surface ($p < 0.05$). On semi-aligned scaffolds, decorin gene expression on small and large diameter fibers was significantly increased ($p < 0.05$) as compared to the spincoated control (Figure 3.6b). It should also be noted that a greater temporal increase, from week one to week two, in collagen type I and decorin gene expression was found on all electrospun scaffolds, especially large fibers, than on the spincoated control surface. After two weeks of culture, scleraxis gene expression was less on all electrospun scaffolds compared to the spincoated control surface (Figure 3.6c), with significantly less expression on the medium fiber diameter scaffolds of both orientations ($p < 0.05$). For semi-aligned scaffolds, scleraxis gene expression was significantly less on the smallest diameter fibers compared to control surfaces ($p < 0.05$). However, on the semi-aligned scaffolds, a notable increase in scleraxis gene expression with increasing fiber diameter was observed.

Using immunohistochemistry, collagen type I protein deposition on the scaffolds was examined. As shown in Figure 3.7, the smaller cells on the electrospun scaffolds with small fiber diameters of ≤ 1 μm produced dense areas of protein immediately adjacent to

individual cells. In contrast, cells on the smooth spincoated surfaces produced diffuse areas of collagen that covered only a small portion of the large cell.

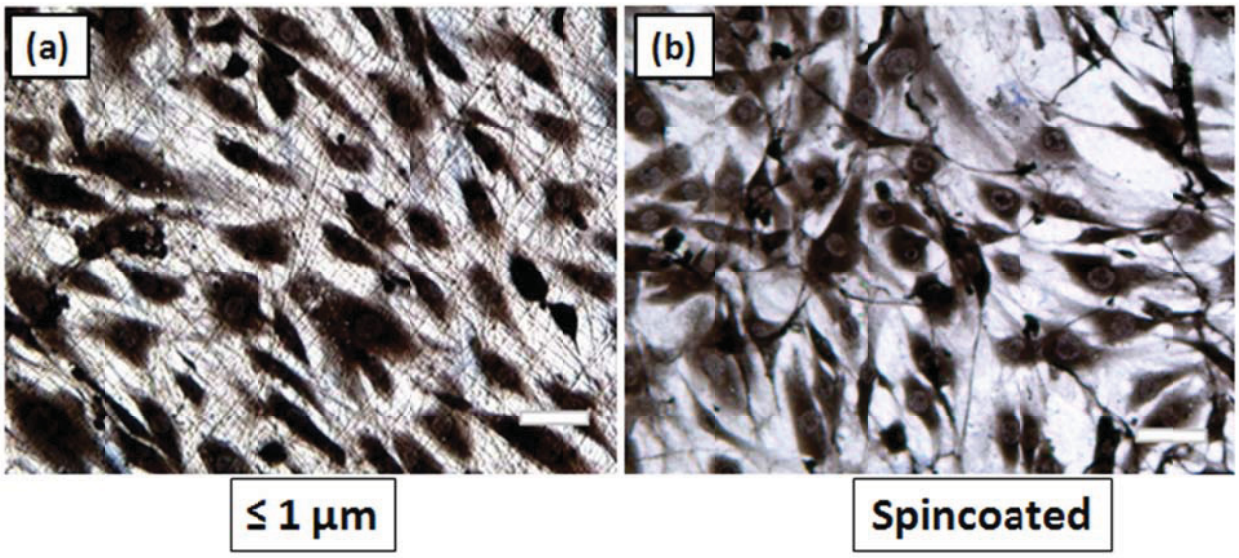

Figure 3.7: Immunohistochemistry for collagen type I. Scale bar: 50 µm

Discussion

The current study evaluated cellular morphology, growth and gene expression as evidence of mesenchymal stem cell differentiation towards a tendon/ligament phenotype on fibrous scaffolds that were designed to mimic the intended native tissue. As shown in a recent review, the mechanics of electrospun fibrous scaffolds are better suited to the repair of musculoskeletal tissues of complex architecture and function such as tendons and ligaments [157]. Here, electrospun scaffolds were fabricated using an elastomeric segmented poly (esterurethane urea) to determine the effect of average fiber diameter in a randomly oriented or semi-aligned matrix on cell behavior. The mesenchymal stem cell line, C3H10T1/2, utilized individual fibers as guides to direct cellular morphology and growth over a two week period. On randomly oriented but not semi-aligned scaffolds, total cell area was greatest on the largest diameter fibers (≥ 2 µm). At the earliest timepoint, cell

density on the electrospun scaffolds systematically increased as the average fiber diameter decreased, regardless of fiber orientation. After the first week of culture, gene expression of tendon/ligament ECM proteins was greatest on the random, smallest diameter fibers (≤1 μm). This result was diminished if the fibers were semi-aligned within the matrix. After two weeks, the largest diameter fiber scaffolds produced the greatest relative expression of collagen type 1α1 and decorin after two weeks, suggesting an alteration in cell phenotype over time. Finally, expression of the tendon/ligament selective transcription factor, scleraxis, increased as fiber diameter increased on the semi-aligned scaffolds at both one and two weeks of culture.

As a method of biomaterial scaffold fabrication, the versatility of electrospinning allows creation of matrices with well-defined fiber architectures. In the optimal configuration, the resultant scaffolds can stimulate tissue formation. To determine the role of fiber architecture on lineage differentiation to a tendon or ligament fibroblast, representative mesenchymal stem cells were cultured on electrospun scaffolds supported by a rigid substrate. Rigid substrates were used as the platform of collecting electrospun fibers in order to eliminate any effects from surface modulus, a known parameter for directed differentiation [76]. For this study, matrices were created with average fiber diameters on the order of native collagen fibers within the ECM [230] and divided into three groups: small, medium, and large. The fiber matrix was either randomly dispersed or semi-aligned for each fiber size for a total of six groups, as previous investigators have shown dependence on fiber orientation for a number of cell processes [28, 52, 139, 266]. Because collagen fiber alignment in musculoskeletal tissues is not necessarily organized along the line of action and can change within the tissue, such as in the anterior cruciate

ligament, a highly aligned scaffold may not be ideal. Despite the use of identical polymer solution concentrations during electrospinning, slight differences in average fiber diameters were found between paired random or semi-aligned matrices. For example, a 12wt% PEUUR produced random, medium fiber diameter scaffolds containing fibers with a mean of 1.53 μm while the mean fiber diameter of the semi-oriented scaffolds was 1.08 μm. The rotation of the mandrel imparts a greater elongation force on the fiber jet exiting the charged syringe, resulting in a slight decrease in mean diameter [52, 263]. This effect was also seen in large diameter scaffolds fabricated from a 17wt% PEUUR solution, but not observed in the small diameter scaffolds.

Topographic cues provided by electrospun fibers produce a microenvironment for influencing cell behavior, especially morphology. As shown in Figure 4, cells on electrospun matrices have a distinctly different actin cytoskeleton as compared to cells on smooth surfaces. Cells on fibrous matrices had a greater number of projections, or filopodia, which correlated with the underlying fiber, as compared to smooth surfaces where cells were more spread and generally contained only two large lamellipodium. For this study, cell area was greatest on the large, randomly aligned scaffolds. Increased cell area with increased fiber diameter is in agreement with other studies of primary bone marrow stromal cells and fibroblasts, but is in contrast with a study involving osteoprogenitor cells where the opposite effect was observed [19, 27, 28, 149]. A modest increase in cell area was observed on semi-aligned, medium fiber scaffold compared to the random, matched diameter scaffold in this study, consistent with modest changes in cell morphology as a result of orientation reported previously[27, 28]. Visually, cells aligned along the prevailing orientation of the semi-aligned fibrous scaffolds. While not quantified

in this study, previous investigations have shown increasing cell alignment with increasing fiber alignment as well as a greater cell aspect ratio on oriented scaffolds [27, 28].

The model mesenchymal stem cells used in these experiments demonstrated increased cell number on the smallest fiber diameter (≤ 1 μm) electrospun matrices, regardless of the fiber orientation. After 3 days of culture, cell density systematically decreased as the average fiber diameter of the matrix was increased to greater than 2 μm. These results are in agreement with previously published studies using primary rat bone marrow stromal cells where the lowest cell numbers were found on scaffolds with a fiber diameter of 2.3 μm after 3 and 7 days of culture [28]. However, human mesenchymal stem cells on electrospun PEOT/PBT scaffolds exhibited the greatest cell number on matrices with 10 μm average fiber diameter as compared to smaller (1 and 4 μm) and larger (21 μm) fiber diameter [172]. The dissimilar results between that study and the current study may be attributed to the formation of beads within the 1 and 4 μm PEOT/PBT scaffolds, an often encountered phenomenon produced by electrospinning. Rat neural stem cell proliferation also decreased as the fiber diameter increased from 0.26 to 1.452 μm, an effect that was further enhanced with the addition of FGF-2 to the media [55]. When PCL electrospun fiber diameter increased from 0.428 to 1.051 μm, the cell proliferation rate of NIH 3T3 fibroblasts decreased, an effect most pronounced during the first 5 days of culture [50]. In contrast, Bashur et al. reported NIH3T3 cell density had little dependence on PLGA fiber diameters of 0.14, 0.76 and 3.6 μm except at the final 14 day time point where the largest fiber diameter had the greatest cell density [27]. Over a two week culture period, MC3T3-E1 osteoprogenitor cells had greater cell numbers on the largest electrospun PDLLA fiber (2.1 μm) compared to fibers with a mean diameter of 0.25 μm, while MG63 osteosarcoma

cells preferred the largest (0.60 μm) gelatin fiber scaffolds over 0.11 μm fibers at 5 and 7 day time points [19, 222]. The current study also examined the effect of fiber orientation on cell growth and showed that fiber alignment did not affect cell proliferation (Figure 4) as also reported by others [27, 28, 105, 154].

The effects of fibrous matrix architecture on cell phenotype, assessed by increased gene expression and deposition of characteristic proteins, are likely to influence successful clinical repair. As the main constituent of tendon, ligament and other fibrous musculoskeletal tissues, collagen type I is an important structural protein [30]. The induction of collagen fibril formation would both facilitate mechanical integrity as well as provide a template for addition ECM deposition through integrin-mediated cell signaling in biomaterial scaffolds [107]. Decorin is an abundant proteoglycan in tendon and ligament that assists in collagen fibrillogenesis but the exact role in regulating fibril size is not known [81]. After seven days in this study, gene expression of collagen type I and decorin was significantly greater on electrospun matrices with the smallest average fiber diameter compared to the largest fibers (Figure 6a, b). Conversely, this response was diminished on semi-aligned scaffolds of paired diameters. After fourteen days, no difference was observed between random or semi-aligned matrices, as the largest fiber diameters (≥ 2 μm) showed the greatest collagen type I and decorin expression among all treatment groups. Similar results were reported in primary bone marrow stromal cells [28]. While relative expression of both collagen type I and decorin increased on all electrospun scaffolds from day 7 to day 14, the largest diameter scaffolds (≥ 2 μm) showed the greatest temporal fold change in gene expression. Ma et al. reported no difference between random or aligned

electrospun PLLA fibers on expression of osteogenic genes but few studies have measured gene expression as a function of electrospun fiber diameter [154].

Gene expression of scleraxis, considered a tendon and ligament 'selective' marker [119], followed the opposite expression pattern of the ECM genes with the greatest expression occurring on the smooth, spincoated surface. Semi-aligned scaffolds suggested increased scleraxis expression with increasing fiber diameter but this was not seen with randomly oriented scaffolds (Figure 3.6c). This effect was also found in primary bone marrow stromal cells seeded on random electrospun matrices of comparable fiber size [28]. Scleraxis is transcription factor present during embryogenesis of tendon and ligament that has been reported to bind the collagen type I promoter [60, 141]. Therefore, upregulation of scleraxis could indicate early fibroblastic differentiation with a subsequent increase in matrix production. The surveying of earlier time points during culture would determine if scleraxis is upregulated prior to increased collagen type I gene expression seen in the smallest diameter matrices.

In summary, the data presented herein suggest small diameter electrospun fibers, regardless of orientation, support initial development of proliferative, fibroblastic-like cells, but the larger diameter fibers scaffolds promote greater ECM gene expression in extended culture. While scaffolds made of small, 200-400 nm fibers could promote increased growth, scaffolds composed of microfibers would permit greater cellular infiltration [196]. The fiber diameters examined in this study suggest decreased initial cell growth and larger cell areas with the larger (≥ 2 μm) electrospun fibers. However, these drawbacks are likely less significant, as they are diminished after one week of culture, than the benefits of increased ECM gene expression which is necessary for the development of a

neotissue. By tailoring the architecture of the electrospun scaffold to enhance desired cellular responses, a suitable tissue engineered tendon or ligament replacement can be developed. Additional studies examining the effects of fiber diameter under mechanical stimulation on tendon/ligament fibroblastic differentiation and ECM deposition may provide further insights to the ideal fiber size for enhancing tendon/ligament regeneration.

Conclusions

In developing a strategy for a tissue engineered tendons and ligaments, the ideal scaffold will have fiber morphology that maximizes ECM gene expression and protein deposition while supporting cellular growth. In these studies, the diameter of the fibers within the scaffold affected cellular responses, including lineage differentiation, more substantially than the alignment of the fibers within the scaffold. Variation of the average fiber diameter within the matrix had pronounced effects on cellular morphology, growth and gene expression. These results suggest that large diameter fibers (≥ 2 μm) may be more suitable for a tendon/ligament scaffold as gene expression was increased over smaller fiber scaffolds.

Acknowledgements

This work was supported by fellowship grant number F31AR055872 to RDC from the National Institutes of Health. The authors gratefully acknowledge Dr. Scott Guelcher for providing the synthesized PEUUR.

Chapter 4: Cyclic mechanical loading of mesenchymal stem cells on elastomeric, electrospun polyurethane scaffolds

[1]Robyn D Cardwell, [3]Jonathan A Kluge, [4]Linda A Dahlgren, [3]David L Kaplan, and [1,2]Aaron S Goldstein

[1]School of Biomedical Engineering and Sciences and
[2]Department of Chemical Engineering,
Virginia Polytechnic Institute and State University,
Blacksburg, VA 24061

[3]Department of Biomedical Engineering,
Tufts University
Medford, MA 02155

[4]Department of Large Animal Clinical Sciences,
Virginia-Maryland Regional College of Veterinary Medicine,
Blacksburg, VA 24061

JAK was responsible for design and operation of bioreactor

Abstract

Electrospun scaffolds are attractive substrates for tissue engineering of fibrous musculoskeletal tissues, mimicking the nanostructure of a collagenous matrix and providing a 3D micropattern to align adherent cells. However, few studies have successfully combined a suitable fibrous biomaterial with cyclic strain to enhance stem cell differentiation and matrix production. Here, we report the mechanical stimulation of model mesenchymal stem cells (MSCs) on a biodegradable, elastomeric scaffold capable of maintaining integrity during cyclic strain. Using a degradable poly(esterurethane urea) elastomer, electrospun scaffolds were fabricated with small (0.60 μm) or large (1.74 μm) mean fiber diameters and seeded with C3H10T1/2 cells, a multipotent MSC line. A custom bioreactor was used to apply cyclic stretch at 4% strain for 30 minutes per day for 3 days. Cells proliferated, remained attached to the biomaterial under cyclic loading, and were visualized *in situ* using confocal microscopy. Following three days of stimulation,

observations of cell morphology revealed highly elongated cells with principal alignment in the direction of tensile stress under cyclic strain. Analysis of mRNA expression of ligament-related genes collagen 1α1, collagen 3a1, decorin, scleraxis and tenomodulin revealed expression of these proteins, but no statistical difference between cyclic load, static load and no load. Nevertheless, these results demonstrate MSC behavior on elastic, fibrous scaffolds before and after cyclic mechanical strain thereby setting a precedent for future studies aimed at enhancing matrix production.

Introduction

Tissue engineering of oriented fibrous tissues, such as tendons, ligaments, menisci and annulus fibrosus, requires a robust scaffold that can deform elastically under physiological loading conditions and direct neotissue formation *in vivo*. Disease and injuries to these highly collagenous, intrasynovial tissues present numerous challenges in reproducing the unique structure and mechanical anisotropy with replacement grafts. Current surgical procedures are dominated by the use of autografts and decellularized allografts, which are limited in availability and may lack sufficient mechanical strength. Fabrication of reparative tissue engineered constructs, consisting of a biomaterial scaffold and appropriate cell source, is a promising alternative to the current repair strategies. *In vitro* maturation of tissue engineered constructs could be accelerated and functional outcomes may be improved by the application of mechanical stimulation.

Numerous bioreactors have been developed to mechanically stimulate cell-seeded scaffolds. For musculoskeletal soft tissues, uniaxial tensile loading is the most physiologically relevant; however, bioreactors for shear, compressive or biaxial tensile mechanical stimulation have also been developed [23, 112, 130, 131, 159, 214]. Tendons

and ligaments transfer loading from muscle-to-bone or bone-to-bone along their longitudinal axis, respectively, and this tensile loading is required to maintain homeostasis of these tissues [13, 259]. For application of tensile loading *in vitro*, bioreactor systems elongate cell-seeded substrates via computer-driven controls. Custom-designed bioreactor systems apply linear substrate translation; examples include integrated cam systems [183, 205], pneumatic actuators [24, 39, 90, 121, 253], and motor-driven linear actuators [8, 41, 56, 67, 192, 243, 254]. In comparing these designs, the accuracy and precision of resulting linear translations varies. The addition of load and displacement monitoring to the bioreactor design can ensure repeatable mechanical stimulation as well as feedback to the user on evolving construct material properties. To this end, load cells, linear variable differential transformers (LVDT), optical encoders and strain gauges have been added to improve performance and accuracy of bioreactor systems [38, 41, 95, 192]. Commercial biodynamic testing stations for application of mechanical stimulation are currently available; however many of these systems cannot be accommodated inside a climate-controlled incubator [38, 160]. In addition, many bioreactors behave as black boxes, and the assessment of cellular responses, such as cell growth and matrix deposition, require the removal of samples from their sterile environment and the application of a destructive assay. The ability to monitor construct viability and extracellular matrix development via imaging modalities during mechanical stimulation would therefore represent a substantial improvement to current bioreactor designs.

The variety of scaffold types used successfully in bioreactor systems is limited. To this end, mechanical stimulation studies have used collagen type I gels and sponges as a three-dimensional environment in which to apply cyclic stretch to cells [7, 92, 134, 187].

While these scaffolds can support cell growth and organization when tensioned, their poor inherent mechanical strength make them unsuitable for fibrous tissue regeneration. Decellularized native extracellular matrix (ECM) scaffolds from donor small intestine submucosa (SIS) and tendon have been used as substrates for applying cyclic stretch to seeded cells [95, 210]. The processing techniques required to remove cellular debris from these tissues can cause profound alterations in mechanical integrity. Common polyesters such as poly(glycolic acid) and poly(lactide-co-glycolide acid)) (PLGA), known for their biocompatibility, degradation, and high tensile modulus, have also been studied as potential scaffolds for this application but lack elasticity, resulting in low elongation at yield [75, 157]. Elastic, open cell polyurethane foams have successfully been used in a custom tensile bioreactor by Webb et al. [254]. Braided scaffolds composed of silk fibroin recapitulate the mechanical strength necessary for fiber-reinforced tissues and have been successfully used in both static and cyclically loaded tissue engineered constructs [6, 49]. However, in order to create the nano- to micro- fiber architecture produced via techniques such as electrospinning, silk matrices must undergo post-processing techniques to stabilize the scaffold in aqueous environments, resulting in a significant loss of elasticity of the scaffold [164]. Currently, no elastomeric polymer with appropriate mechanical properties has been reported for use as a scaffold to apply mechanical stimulation to cells. Herein, we utilize a segmented, poly (esterurethane urea) (PEUUR) as our elastomeric scaffold of choice for tissue engineering of fibrous tissues. This polymer is derived from 2000 Da polycaprolactone diol, conferring both biodegradability and biocompatibility. When chain extended, it displays a tensile modulus of 18 MPa and a strain-to-failure of more than 100% [26].

Concurrently, scaffold processing techniques impart additional microstructure mechanical behavior to the polymer's macroscale properties. Creation of non-fibrous synthetic polymer scaffolds is achieved through methods such as phase separation, particle leaching and gas foaming. Non-fibrous scaffolds must strike a balance between a highly porous structure facilitating cell ingress and mechanical strength, which declines as the porosity increases [230]. In addition, structural anisotropy — a requirement for recapitulating soft tissue mechanics — is difficult to achieve in non-fibrous scaffolds. The open cell polyurethane foams used by Webb et al. allowed cells to infiltrate to the center but this matrix fell short of recreating the native anisotropy in collagenous fiber-reinforced tissues [120, 254]. Hydrogels, produced from either natural (e.g. fibrin, collagen) or synthetic (e.g. polyethylene glycol) polymers, can be tuned to the required permeability and chemical stability through crosslinking parameters but remain rather weak in tensile loading [237]. For fibrous scaffolds, self-assembling scaffolds can produce nanofibers through spontaneous organization of peptides but this process is difficult to control [262]. Woven scaffolds composed of materials such as silk [5] and PLGA [58] possess the necessary mechanical strength for fibrous tissues and can incorporate cells into their open pore structure; however, nanoscale fibers are not possible using woven technology. Electrospinning of native or synthetic polymers has been used extensively owing to the inherent ability to construct controlled fiber morphologies for structural anisotropy and architectural features for organized matrix deposition.

Synthetic polymer scaffolds consisting of micro- or nano- fiber architectures present numerous advantages for engineering of fibrous tissues. Through the process of electrospinning, matrices can be tuned to incorporate fibers on the order of nanometers to

grossly mimic collagen fibers present in native ECM [230]. Electrospun fiber matrices also exhibit unique material properties, namely anisotropy, as compared to other non-fibrous biomaterial scaffolds. Electrospinning can produce scaffolds with mechanical behavior similar to collagen-reinforced native tissues [157]. In addition, individual fibers within the matrix have been shown to facilitate development of organized ECM [28, 139, 266]. Electrospinning of elastomeric materials, such as segmented polyurethanes, produces scaffolds with viscoelastic behavior [157]. Still, anisotropic electrospun scaffolds with soft-tissue fiber characteristics have not been applied as a substrate for cellular mechanical stimulation. PEUUR electrospun scaffolds are biodegradable, biocompatible, have tunable fiber architectures and exhibit bulk mechanical properties that mimic native tissue mechanics [101].

The present study utilizes a novel, uniaxial stretch bioreactor, capable of applying precise cyclic mechanical stretch and optically assessing stimulated constructs non-destructively [128]. Using electrospun PEUUR scaffolds, the effects of cyclic stretch on model mesenchymal stem cells (MSC) was investigated. The primary goal of this study was to monitor MSC attachment and morphology *in situ* on mechanically stimulated elastomeric scaffolds. MSC cell number and gene expression in mechanically-loaded constructs were also quantified.

Materials and Methods

Materials

All chemicals were purchased from Sigma-Aldrich (St Louis, MO). Unless otherwise noted, cell culture reagents were purchased from Life Technologies (Carlsbad, CA).

Electrospun scaffold preparation

A segmented poly (esterurethane urea) (PEUUR) was synthesized and characterized as previously described [102]. For the PEUUR polymer, 1,6 diisocyanatohexane (HDI) was first reacted with poly (ε-caprolactone) diol (average molecular weight 2000 Daltons, PCL 2000) in a three-neck, round-bottom flask at 75°C purged with argon. The NCO:OH equivalent ratio of was 2.0:1.0. Dibutyltin dilaurate (DBTDL) was added as a catalyst to the flask at 1,000 parts per million (ppm) and the reaction was allowed to proceed for 3 hours to produce an NCO-capped linear pre-polymer. For chain extension of the pre-polymer, a solution of 1,3-propanediol bis(4-aminobenzoate) in dimethyl sulfoxide (DMSO) was prepared at 50°C and added to the HDI.PCL2000.HDI prepolymer in the reaction vessel. The NCO:OH equivalent ratio of the polyurethane was 1.03:1.0. DBTDL was again added at a concentration of 1000 ppm and the reaction was allowed to proceed at 80°C for 20 hours. The polymer was then precipitated with diethyl ether and dried in a vacuum oven at 80°C for 24 hours at 10 mmHg. The PEUUR was characterized using differential scanning calorimetry (DSC) and gel permeation chromatography (GPC). A glass transition temperature (T_g) of -47.4 °C and a melting point (T_m) of 36.3°C was measured for this batch of synthesized polymer. The number average molecular weight (Mn) and weight average molecular weight (Mw) of the polymer was 86.6 kDA and 127.9 kDa, respectively, corresponding to a PDI of 1.48.

Electrospun meshes were produced in a fume hood using the following parameters. Solutions of PEUUR in 1,1,1,3,3,3-hexaflouro-2-propanol (HFIP) at concentrations (wt%) of 8% and 12% were used to form scaffolds with fibers with small (≤ 1 μm) and large fiber (≥ 1 μm) diameters, respectively. The PEUUR solutions were loaded into syringes equipped

with 22 gauge steel flat-tip needles and positioned 15 cm from a mandrel covered in aluminum foil. A potential of 15 kV (between the needle and the grounded mandrel) was applied and a syringe flow rate of 3 mL/hour was set to create fibers that were drawn across the gap and deposited onto the mandrel, rotating at 3.5 m/s, to produce a semi-aligned mat. The electrospun mat was allowed to dry overnight in a fume hood and then stored in a desiccator until use. Scanning electron microscopy (LEO 1550 Field Emission SEM, Carl Zeiss SMT, Thornwood, NY) was used to acquire images of mats, and fiber diameter size and alignment were measured manually from the images using ImageJ v1.40 (National Institutes of Health, Bethesda, MD).

Mechanical testing of electrospun scaffolds

Two tensile tests were performed on the scaffolds to characterize their mechanical properties. Both tests were performed on a tensile test frame equipped with a 10 kN capacity load cell and BioPuls™ testing system including submersible pneumatic grips and temperature-controlled bath (Instron 3366, Norwood, MA). Scaffolds (35mm *long* x 5mm *wide* x ~200μm *thick*) were cut from the aluminum foil collection surface before being clamped between custom-designed grips. The original cross-sectional area was determined by measuring the film thickness using microscope analysis and multiplying by the specimen gauge width (5 mm). While samples were clamped, they were leeched in 70% ethanol for 2 days, and then distilled water for an additional 2 days with daily changes of fluid to remove residual HFIP. Scaffolds were then soaked in 1X phosphate buffered saline (PBS) for 20 minutes prior to testing. Subsequently, samples were loaded into the tester and immersed in a fluid bath (0.1 M PBS at 22 ± 0.3°C) for 2 minutes before the test was initiated.

A tensile load-to-failure test was used to define the range of elastic vs. plastic deformation for each scaffold type. A strain control rate of 0.1% s^{-1} was specified on the basis of the initial clamp-to-clamp length (nominal length 35 mm, elongation rate 35 μm/sec). Load and elongation data were captured at 10 Hz. The nominal tensile stress and strain were graphed on the basis of the original cross-sectional area and length, respectively, and the stiffness determined. The stiffness, or elastic modulus, was calculated by using a least-squares (LS) fitting algorithm using the linear portion of the curve. At least n=4 samples were used for scaffolds of both fiber diameter sizes.

Cyclic fatigue testing of the scaffolds was used to simulate the bioreactor cyclic stretch regime. In a fluid bath, a strain control rate of 0.1% s^{-1} was used to elongate the samples until a 0.05N preload was reached. At this load, the specimen gauge length was automatically recalculated and the sample was subsequently stretched between 0 and 4% strain at 0.25Hz for 30 minutes. This was repeated twice more (calculating a new gauge length at the beginning of each repeat) to simulate 3 days of cumulative loading applied during the bioreactor study.

Cell culture on scaffolds

C3H10T1/2 Clone 8 mouse mesenchymal stem cells (ATCC, Manassas, VA) were cultured in Dulbecco's modified Eagles medium (DMEM, ATCC) with high glucose (4,500 mg/L) supplemented with 10% fetal bovine serum, 2 mM L-glutamine, 1% antibiotic/antimycotic and 50 µg/mL L-ascorbic acid, referred to as DMEM growth medium, and were used for all experiments at passage 15. Cells were cultured for 4 days on tissue culture polystyrene, then detached using 0.25% trypsin/EDTA and labeled using

DiI (2.5 mg/mL in DMSO) at a final concentration of 10 μg/mL in DMEM growth medium for 30 minutes at 37°C, 5% CO_2.

Electrospun scaffolds were cut to 4.5 cm long by 1 cm wide, with the primary orientation of the fibers along the long axis, and then secured in custom Ultem® clamps, fitted with silicone inserts (Figure 4.1). The aluminum foil backing was removed and the scaffolds were leeched in 70% ethanol for 2 days, then distilled water for an additional 2 days with daily changes of fluid to remove residual HFIP. Scaffolds were dried and then sterilized by ethylene oxide under tension. A custom platform was designed to hold pre-clamped, leeched scaffolds for sterilization and cell seeding. Prior to cell seeding, scaffolds were immersed in 5 μg/mL fibronectin (MP Biomedicals, Solon, OH) for 6 hours at 37°C.

Using the custom platform, the clamps for each scaffold fit into recessed wells with the scaffold itself supported in the center by a 3.5" smooth plate. This platform maintained tension on the fibrous scaffolds during cell seeding. Absorbent cotton fiber paper (Bio-Rad, Hercules, CA) was cut to 3.5 cm long by 1.5 cm wide and placed underneath each sterilized electrospun scaffold in the custom seeding device (Figure 4.1). The filter paper was pre-wet with 100 μL of 1X PBS and then 300 μL of DiI-labeled cells were seeded dropwise on prepared electrospun scaffolds to achieve a final density of 15,000 cells/cm^2. The filter paper drew the culture medium through the scaffold thus facilitating cell attachment to the fibers. Cell-seeded scaffolds were placed in an incubator at 37°C for 4 hours and then an additional 250 μL of DMEM growth media was added gently to each scaffold. Following another 3 hours in the incubator, the scaffolds were carefully transferred to Petri dishes and submerged in DMEM growth medium overnight. Next, cell-seeded scaffolds were gently placed in individual, custom-designed bioreactor chambers (Figure 4.1). The cell-

seeded scaffold surface was placed closet to the bottom side of the chamber, fitted with a glass coverslip to facilitate confocal microscopy imaging.

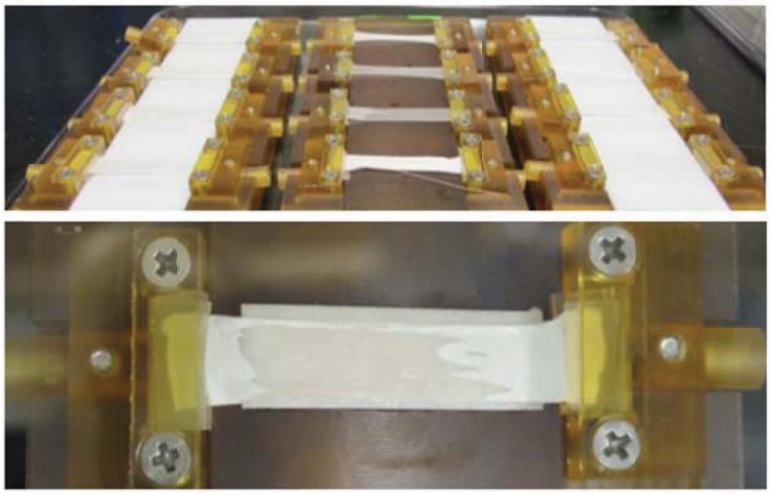

Figure 4.1: Custom platform for seeding scaffolds. Scaffolds were clamped at each end, stretched to initial cut length and a cotton pad was placed beneath the mat prior to cell seeding.

Bioreactor design

A custom bioreactor system – designed to impart uniaxial stretch and permit non-invasive cell monitoring – was used for mechanical stimulation of cell-seeded elastomeric electrospun scaffolds. The device consisted of four individual chambers that could be independently operated through a computer interface and fit within a standard incubator (Figure 4.2). The chambers were fabricated from autoclavable materials. Each chamber was machined from polyetherimide, was secured between a clear polycarbonate lid and a stainless steel baseplate using stainless steel screws, and accommodated approximately 10 mL of culture medium. Liquid-tight seals were maintained with a rubber gasket on the top surface of the culture well and a poured polydimethylsiloxane (PDMS) gasket between the culture well and baseplate. Each culture chamber was fitted with a standard glass coverslip integrated into a PDMS gasket at the base of chamber to allow unobstructed access to the construct for microscopy. Gas exchange was supported via two 0.2 μm filter ports placed at

the sides of the culture well above the fluid line. Clamps (which can be designed to accommodate a variety of biomaterials) were fully enclosed within the chamber and attached to the bioreactor mechanical stimulation system via universal adaptor rods.

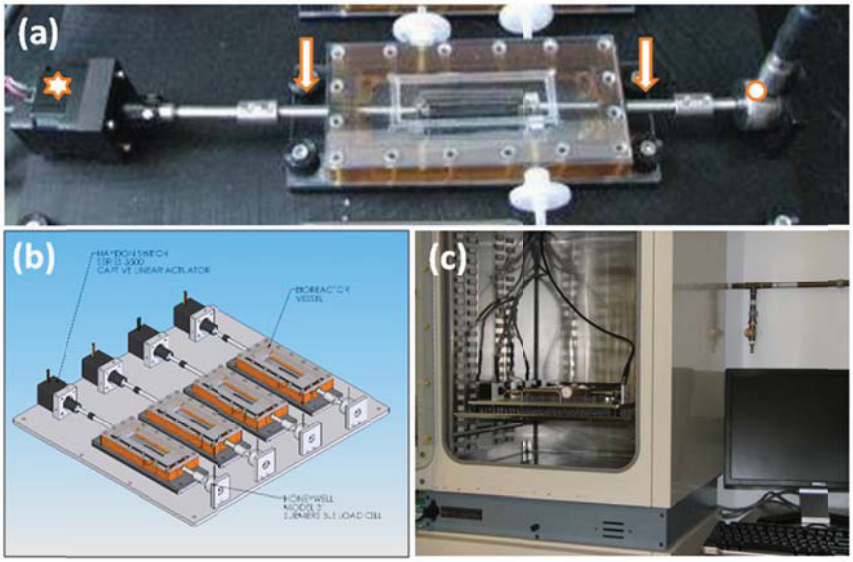

Figure 4.2: Custom bioreactor system for mechanical stimulation of electrospun scaffolds and *in situ* imaging. Preclamped electrospun scaffolds carefully loaded into an individual chamber (a) via adapter rods to the clamps (arrows). Each chamber is linked to a load cell (•) and a linear actuator (*) for precise control of loading regimens. Up to four chambers can be stimulated simultaneously on the platform (b), which is housed inside a standard incubator (c).

Mechanical stimulation of the constructs within assembled chambers was accomplished with a stepper motor (35000 Series Size 14, Haydon Kerk Motion Solutions, Waterbury, CT). User-defined motor commands, including displacement, frequency and speed, was entered into a custom LabVIEW software program (National Instruments, Austin, TX) and routed through a controller board (SS4D10USB, Peter Norberg Consulting, Inc. Ferguson, MO) to the motor. The opposite adaptor rod was mounted to a tensile load cell (Model 31, Honeywell, Morristown, NJ), that provided real-time load data to the LabVIEW software through an analog input module and CompactDAQ chassis (both National Instruments).

Mechanical stimulation of constructs

After 48 hours of undisturbed culture, the medium was changed and mechanical stimulation was applied to the scaffolds. Chambers were secured to the stretching platform and each chamber was linked to a linear actuator and a load cell via adapter rods (Figure 4.2). For the static load group, scaffolds were stretched to a preload of 0.05N only. The adapter rods were then locked in this position with set screw collars to prevent relaxation of the scaffold. For the cyclic load group, scaffolds were preloaded to 0.05N and then cyclically stretched 4% from the preload position at a rate of 0.5Hz for 30 minutes daily. After each 30 minute treatment, cyclically stretched scaffolds were locked in the 0.05N preload state as before. For the no load group, scaffolds were allowed to float freely (i.e., no tension) between the two clamped ends for the duration of the experiment.

Cellular imaging

The ability to image constructs *in situ* is an attractive feature of this bioreactor system. Each chamber was readied for imaging by releasing the adaptor rods from the stretching platform. The chamber was then placed between the objective and the condenser of an inverted microscope (Figure 4.3).

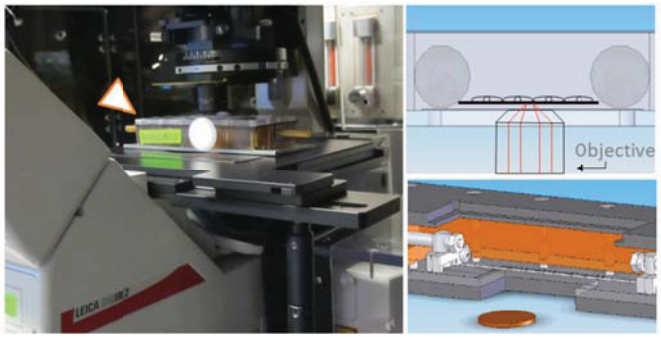

Figure 4.3: Direct imaging of bioreactor constructs on a confocal microscope. A chamber (arrowhead) can be detached from the stretching platform and placed on a standard microscope stage for imaging. The bottom portion of the chamber is fitted with a standard cover glass, recessed from the mainframe, allowing the objective to translate to a proper working distance.

To verify cell attachment to the electrospun scaffolds, DiI-labeled cells were imaged 24 hours after their transfer into the bioreactor chambers and following one round of cyclic stretch using a confocal microscope (Leica DM IRE2, Leica Microsystems, Wetzlar Germany). Following 3 days of mechanical stimulation, cells on scaffolds were stained with 2μM calcein-AM for 1 hour to visualize live cells. After which, the medium was replaced with 1X PBS and the entire bioreactor chamber was placed on the stage for confocal imaging of the cells on the scaffold. Z stacks (100-300 mm in thickness) were collected using 2 μm axial steps that were line averaged twice. Final images are shown as average projection across stacks.

Gene Expression

Six hours after the third cycle of mechanical stretch, scaffolds were washed twice with cold 1X PBS and split into two sections lengthwise using a scalpel to probe for mRNA expression and cell number. For mRNA expression, one half of each scaffold (2 per treatment group) was collected in 1mL TRIzol and then frozen at -80°C until further purification. Next, samples were thawed and total RNA was isolated from the cell-seeded scaffolds using TRIzol and column purification (RNeasy Mini Kit, Qiagen, Germantown, MD). Following homogenization in TRIzol and extraction of the aqueous layer using chloroform, an equal volume of 70% ethanol was added and the lysate was loaded onto the RNeasy silica spin columns and total RNA was isolated according to the manufacturer's instructions. Samples were subjected to on-column DNase digestion using DNase I (Qiagen) prior to elution. Total RNA was quantified using Quant-iT RiboGreen® kit using a fluorescent plate reader (SpectraMax M2, Molecular Devices, Sunnyvale, CA). Equal amounts of total RNA (approximately 500 ng) were then reverse transcribed to cDNA using

High Capacity cDNA Reverse Transcription kit with random hexamers as primers, according to manufacturer's protocol.

Real time PCR was performed in the ABI 7300 Real Time PCR System using Power Sybr® Green Master Mix. For PCR amplification, approximately 100 ng of sample cDNA was used. Specific primers for mouse collagen type Iα1, decorin, and other tendon/ligament ECM proteins were designed using Primer Express software v2.0 (Table 4.1). Equal quantities of isolated total RNA (to test for genomic DNA contamination) and no template (nuclease-free H_20 in place of cDNA) were used as negative controls for the reactions. Quantification of target gene expression was referenced to the housekeeping gene β-actin using the comparative threshold cycle (ΔΔCt) method [151]

Table 4.1: Murine primer sequences for quantitative polymerase chain reaction

Gene *Accession No.*	Significance	Primer Set	Amplicon Size
Collagen Type 1α1 *NM_007742*	Primary structural protein of tendon/ligament ECM	Forward: ATGTTCAGCTTTGTGGACCT Reverse: CAGCTGACTTCAGGGATGT	92 bp
Collagen Type 3α1 *NM_009930*	Secondary structural protein of tendon/ligament ECM	Forward: CACCCTTCTTCATCCCACTCTTA Reverse: TCTAGACTCATAGGACTGACCAAGGT	91 bp
Collagen Type 12α1 *NM_007730*	Fibril-associated collagen with a role in collagen fibrillogenesis	Forward: TCAAAGAGGTGGAGGTGGAC Reverse: 5' ATGTGCCCTCATCGTACACA	108 bp
Decorin *NM_007833*	Proteoglycan mediator in collagen fibrillogenesis	Forward: TCGAGTGGTGCAGTGTTCTGA Reverse: TTGCAGGTCTAGCAAGGTTGTGTC	82 bp
Tenascin-C *NM_011607*	Glycoprotein abundant in developing tendons	Forward: CCACCTAGTACTGATTTCATTGTCTACCT Reverse: CCGTCTGGAGTGGCATCTG	137 bp
Tenomodulin *NM_022322*	Late marker of tendon differentiation	Forward: GGCCTTAACTCTAATTGTCCTGTTTT Reverse: CTCGCCGTTGCTGTAGAAAGT	103 bp
Scleraxis *NM_198885*	Selective tendon/ligament transcription factor	Forward: TCTGCCTCAGCAACCAGAGAAAGT Reverse: ACTCTTCAGTGGCATCCACCTTCA	130 bp
Beta Actin *NM_007393*	housekeeping/ reference	Forward: TGCTCCCCGGGCTGTATT Reverse: ACATAGGAGTCCTTCTGACCCATT	87 bp

DNA content

For quantification of DNA, the second half of each divided scaffold was frozen at 80°C in 1X PBS until analysis. Samples were then digested with 0.5 mg/mL papain buffer

(MP Biomedicals) for 20 hours at 65°C. DNA content was measured using Quant-iT PicoGreen® kit (Invitrogen) according to manufacturer's instructions using a fluorescent plate reader (SpectraMax M2). DNA content was determined from a serial dilution of lambda DNA standard, provided in the kit.

SEM imaging

Prior to removal from the bioreactor chamber, scaffolds were immersed overnight in 2.5% glutaraldehyde in 0.1M sodium cacodylate buffer, pH 7.4, supplemented with 0.1 M sucrose and 4mM calcium chloride (Electron Microscopy Sciences, Hatfield, PA) at 4°C. Following two rinses in 1X PBS, scaffolds were dehydrated in a graded ethanol series and vacuum dried overnight. Samples were mounted using adhesive tape, sputter coated with a 10 nm layer of gold (Model 208HR, Cressington Scientific Instruments, Cranberry Township, PA), and observed with a LEO 1550 Field Emission SEM (Carl Zeiss SMT, Thornwood, NY) at 15 kV.

Statistical Analysis

The entire experiment was completed twice using the same batch of scaffolds and cells and data is combined. Unless otherwise noted, results are presented as mean ± standard deviation for n=4 in each treatment group. Results are presented as mean ± standard error of the mean for n=4 for relative gene expression data. Statistical significance was determined using one-way ANOVA, followed by Fisher post-hoc comparisons with a significance criterion of $p \leq 0.05$ (OriginPro 8.1, Northhampton, MA).

Results

Properties of electrospun scaffolds

For all scaffolds, electron micrographs revealed smooth, continuous polymer fibers without bead formation resulting in dense matrices. Scaffolds electrospun from 8 and 12 wt% PEUUR solutions had average thicknesses of 185 μm and 152 μm, respectively. Scaffolds electrospun from an 8 wt% PEUUR solution had an average fiber diameter of 0.60 ± 0.25 μm (Table 4.2, Figure 4.4a), while a 12 wt% PEUUR solution had an average fiber diameter of 1.74 ± 0.49 μm (Table 4.2, Figure 4.4b). Scaffolds were collected on a 3.5 m/s rotating mandrel and to induce a fiber principal alignment direction. Fiber alignments were estimated based on analysis of SEM images using an FFT algorithm developed by Ayers et al. [18] and were similar between both mean fiber diameter scaffolds (data not shown).

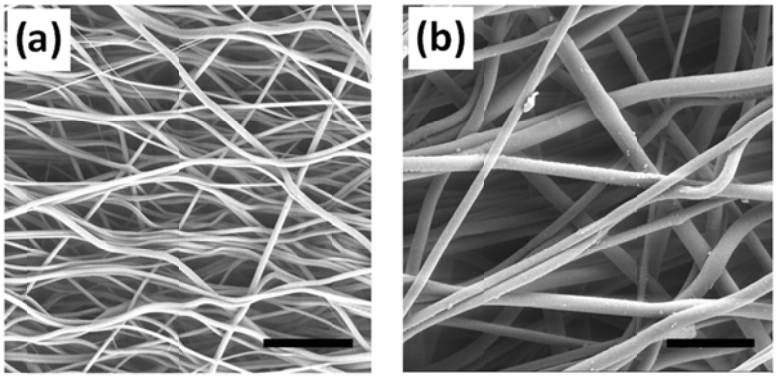

Figure 4.4: Electron micrographs of electrospun segmented polyurethane scaffolds. Scaffolds had a mean fiber diameter of (a) 0.60 μm or (b) 1.74 μm. Scale bar: 10 μm

To compare electrospun fiber matrices with different mean fiber diameters, mechanical properties of the matrices were determined by tensile loading to failure (Table 4.2, Figure 4.5). Both electrospun scaffolds displayed an S-shaped stress-strain curve composed of toe-in, linear, and yield regions (Figure 4.5). The transition between the

initial toe-in and the linear regions occurred at a stress of approximately 0.05N, corresponding to 2% strain. Electrospun PEUUR scaffolds were elongated to a strain of 30% without failure. The larger fiber scaffold, with a mean fiber diameter of 1.74 μm, exhibited an elastic modulus of 4.22 MPa with a linear region from 7.5 to 10% strain (Figure 4.5). For the smaller fiber scaffolds with mean fiber diameters of 0.60 μm, the elastic modulus was 9.24 MPa with a linear region from 5 to 10% strain.

Table 4.2: Physical properties of PEUUR electrospun scaffolds. Mean ± SD.

	PEUUR concentration (w/w)	
	8 wt %	12 wt %
Average Fiber Diameter	0.60 ± 0.25 μm	1.74 ± 0.49 μm
Elastic Modulus	9.24 ± 0.63 MPa	4.22 ± 0.25 MPa

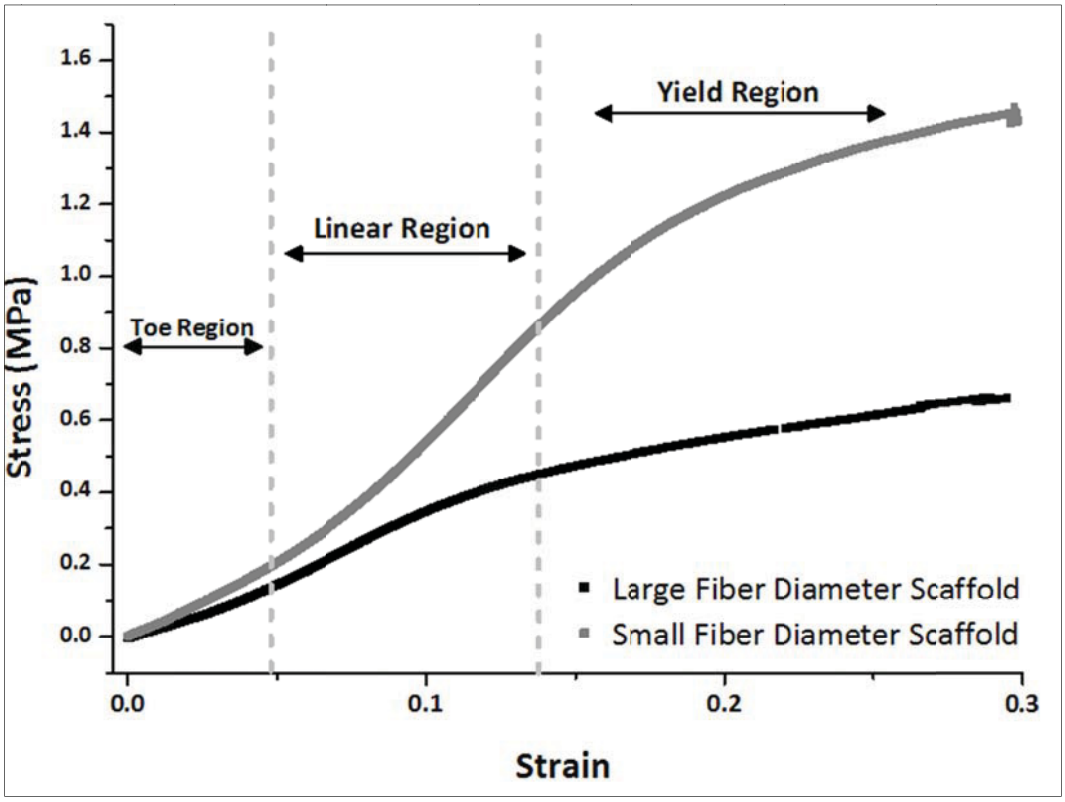

Figure 4.5: Stress-strain curves for PEUUR electrospun scaffolds. Electrospun scaffolds with a mean fiber diameter of 0.60 μm (small) and 1.74 μm (large) were tested. Prewetted scaffolds with a cross-sectional area of 1.85 (small) or 1.52 mm^2 (large) were elongated at a rate of 0.1% s^{-1} at room temperature. The average response of four of each scaffold type is shown

Cyclic fatigue mechanical testing was also performed to determine the viscoelastic and dynamic responses of the scaffolds under bioreactor loading conditions. Electrospun matrices were preloaded to 0.05N, to exit the toe-in region, and then cyclically stretched with a 4% grip-to-grip strain at a rate of 0.25 Hz for 30 minutes. As shown in Figure 4.6, the majority of energy loss in the scaffold occurred during the first load-unload cycle, after which the scaffold stabilized, as evidenced by the resultant small area of hysteresis. Scaffolds of both mean fiber diameters exhibited similar fatigue responses.

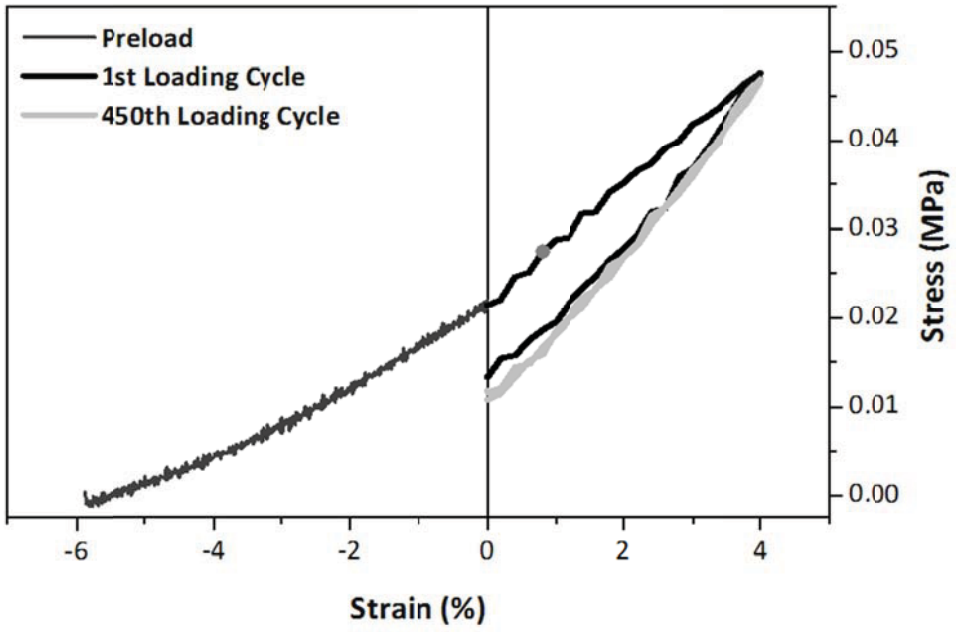

Figure 4.6: Cyclic mechanical testing of PEUUR electrospun scaffolds. Electrospun scaffolds with a mean fiber diameter of 0.60 µm (small) and 1.74 µm (large) were tested. Scaffolds were preloaded to 0.05N at a strain rate of 0.1% s-1 and then cyclically stretched between 0% and 4% elongation at 0.25 Hz for 30 minutes, simulating bioreactor conditions.

Cellular viability and morphology

Conventional dropwise seeding techniques were modified to facilitate cell attachment on the elastomeric scaffolds and permit transfer to the bioreactor chambers. Therefore, scaffolds were maintained in a tensioned configuration and a cotton pad was placed underneath the scaffold, which assisted in drawing the cell suspension into the

center of the mat by a wicking phenomenon. The entire clamp-scaffold-clamp assembly was transferred in sterile format from the seeding platform to the chamber to prevent the constructs from collapsing during handling, typical of thin (< 200 μm) nano-fibrous mats.

Following transfer to individual bioreactor chambers, cell adherence to the electrospun scaffold was verified prior the start of mechanical stimulation. Using the imaging modality of the bioreactor, cell membranes impregnated with a non-permanent tracer dye (DiI) were used to assure cell attachment to the scaffold. A dense population of DiI-labeled cells was apparent following transfer to the bioreactor chamber (Figure 4.7a). Cells were distributed equally across the scaffold. After one stretching cycle, cells were again visualized on the scaffold. Cell density decreased slightly after the initial cyclic stretch regime (Figure 4.7b). Finally, DiI-stained cells were imaged after three days of daily mechanical stimulation, confirming the presence of a dense population of cells on the scaffold (Figure 4.7c). Cells remained distributed throughout the length and width of the scaffold although cell density was diminished at the edges of the scaffold.

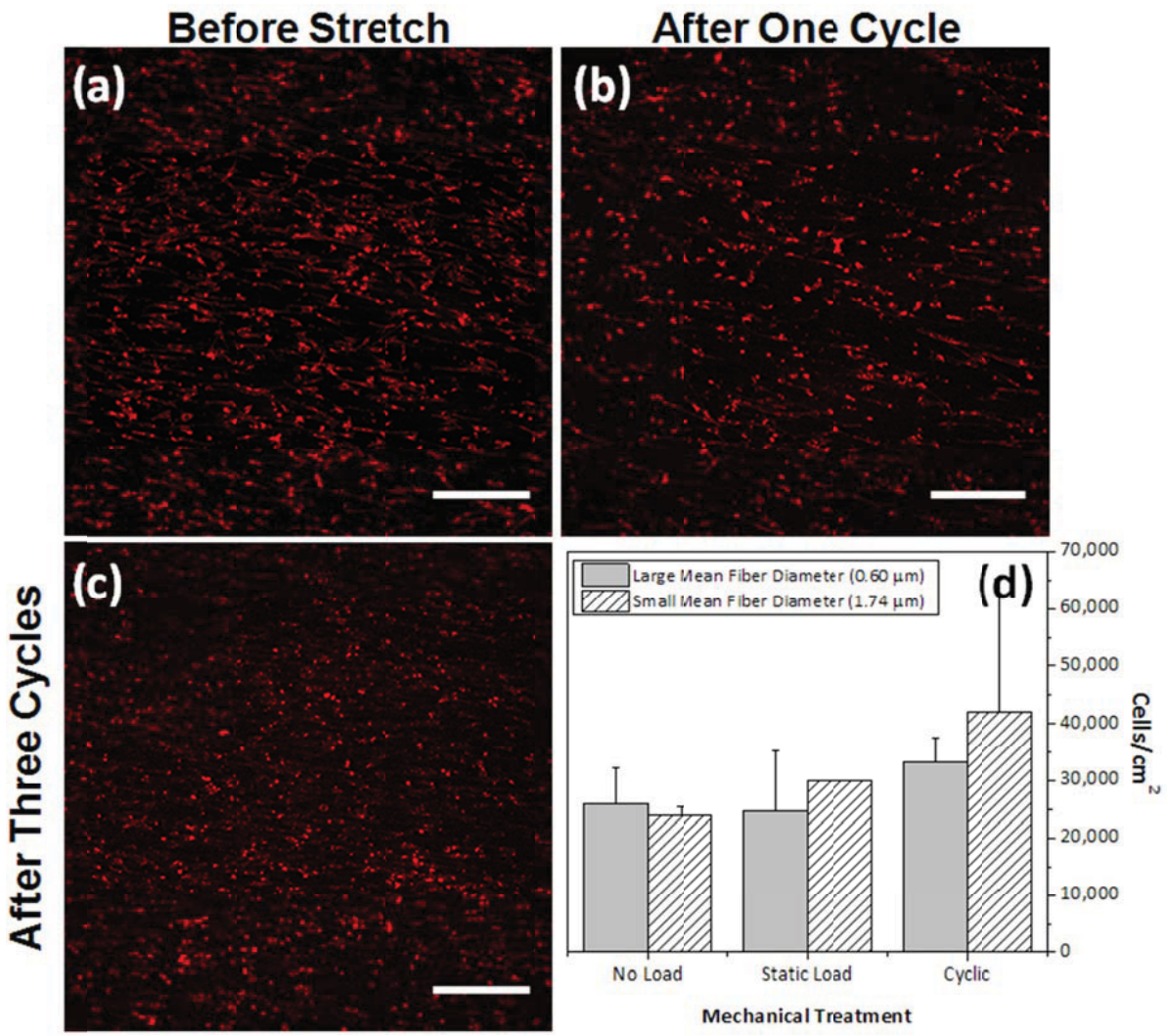

Figure 4.7: Confocal images of DiI-labeled C3H10T1/2 cells on scaffolds with mean fiber diameter of 1.74 µm following initial seeding (a), after one round of cyclic stretch (b) and three rounds of cyclic stretch (c). Total DNA content on electrospun PEUUR scaffolds after three days of mechanical treatment (d). Scale: 300 µm.

DNA content was measured at the end of three days to determine if cyclic stretch affected cell density. Measurements indicated differences in cell number density were not statistically significant; however, the cyclically strained scaffolds had a slightly higher total DNA content in both the small and larger fiber diameter scaffolds (Figure 4.7d). Cell density was comparable on scaffolds of both mean fiber diameters.

After three days of intermittent cyclic stretch, cells were stained with calcien-AM to visualize the entire cell membrane and subsequent orientation. Cells on cyclically stretched scaffolds were preferentially oriented parallel to the direction of stretch and had a highly elongated morphology (Figure 4.8a, b). Long cell processes can be seen extending along the direction of tensile force. Under no loading conditions, cells populated the surface of the scaffold with no preferential orientation and a cuboidal morphology (Figure 4.8c, f). A lack of orientation was observed for cells on both small and large fiber diameter scaffolds without loading. In Figure 4.8e, the small diameter scaffold appeared to buckle under static load, thereby creating waves or ridges within the scaffold where cells could not proliferate as evidenced by two sparsely populated areas. While the magnitude and duration of mechanical stimulation was not extreme, an alteration in cell shape between mechanically loaded and non-loaded scaffolds is apparent.

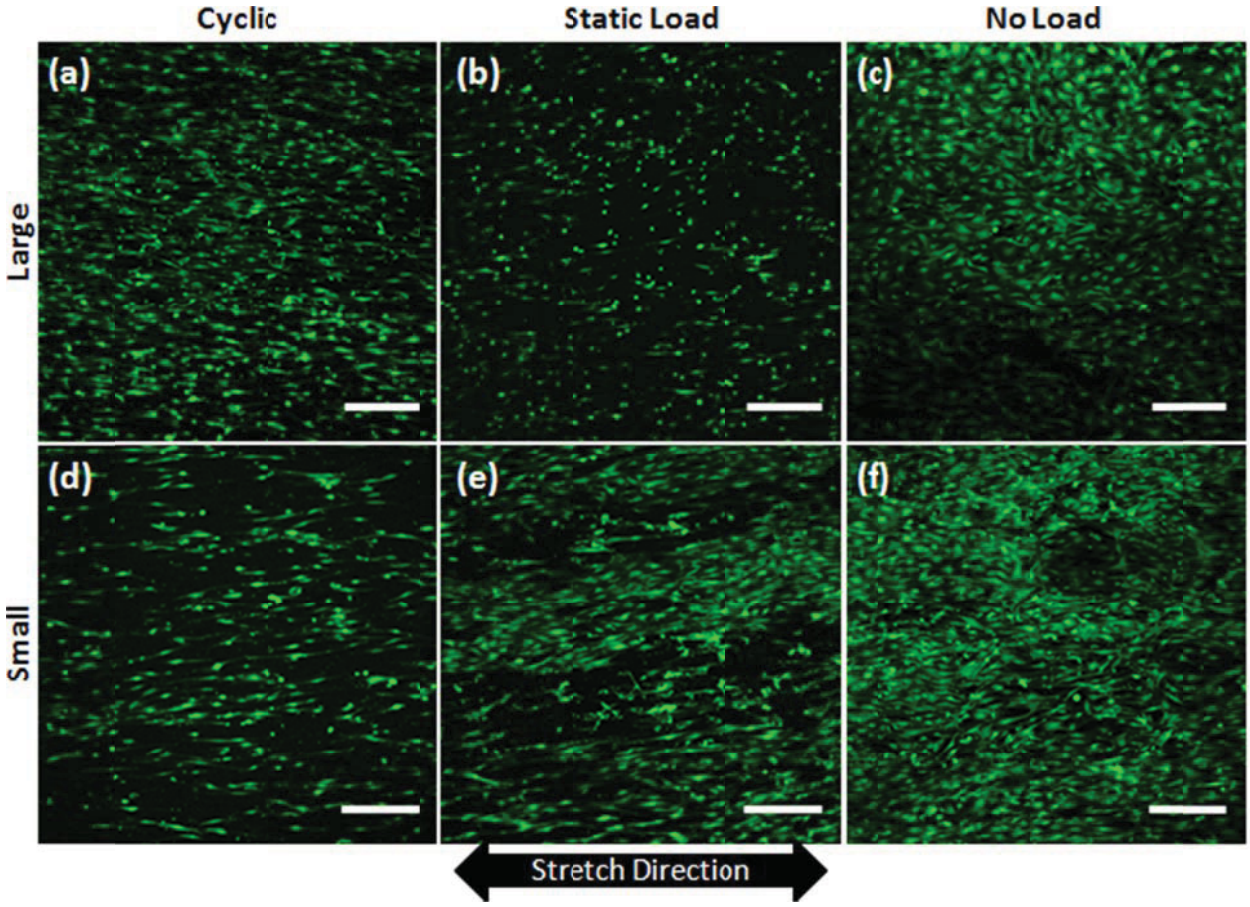

Figure 4.8: Confocal images of C3H10T1/2 cell morphology on scaffolds with large (a-c) or small (d-f) mean fiber diameter after three days of (a, d) cyclic stretch, (b, e) static load only or (c, f) static culture. Scale: 300 μm

Gene expression

After three days in the bioreactor, scaffolds were collected and analyzed for relative expression of the most abundant collagen types in tendon and ligament; collagen type 1α1 and collagen type 3α1 (Figure 4.9). Mechanical loading (cyclic or static) and electrospun fiber diameter did not alter MSC expression of collagen type 1α1 after three days. However, collagen type 1α1 expression was elevated in larger fiber scaffolds over the smaller scaffolds under static loading. Cellular mRNA expression on statically or cyclically-loaded large fiber scaffolds had greater collagen type 3α1 expression than the unloaded

control. In contrast, mechanically stimulated (cyclic or static) small fiber scaffolds decreased mRNA expression levels of collagen type 3α1 compared to control.

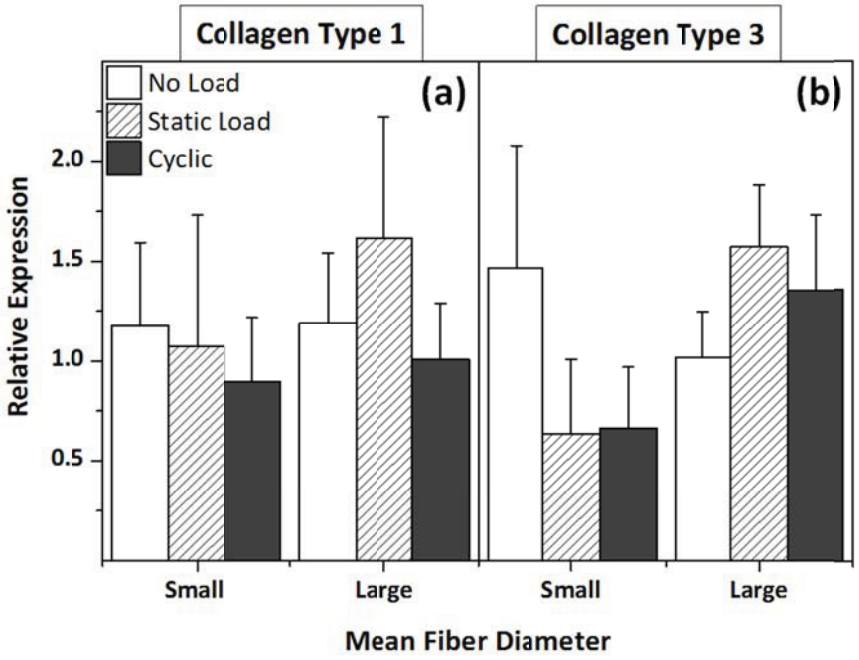

Figure 4.9: Relative gene expression of tendon/ligament primary collagens after three days of cyclic mechanical stretch, preload or static culture on electrospun PEUUR scaffolds with mean fiber diameter size of 0.6 μm (small) or 1.7 μm (large). n=4 for all except for small fiber diameter scaffolds at preload group, where n=2. Mean ± SEM

Expression of other extracellular matrix proteins decorin, tenascin c and collagen type 12α1 were also quantified (Figure 4.10). Static loading tended to decrease decorin and slightly increase tenascin-c mRNA expression for cells on both large and small fiber scaffolds but the differences were not statistically significant. Cyclic loading induced a slight decrease in tenascin-c but a slight increase in collagen type 12 expression for cells on large fiber scaffolds. Expression levels of tenascin-c and collagen type 12α1 was not appreciably altered in cells on cyclically loaded small diameter scaffolds from the no-load condition.

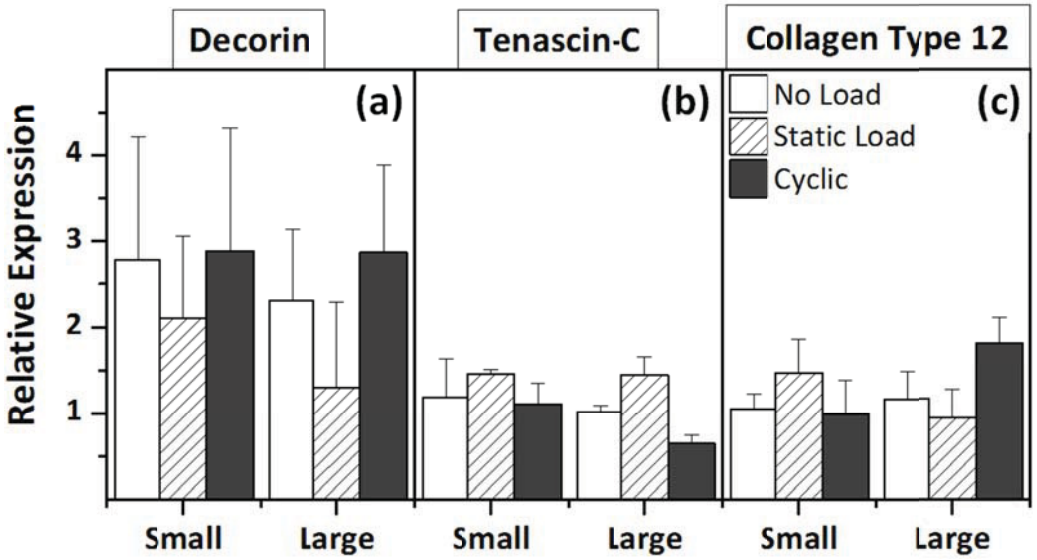

Figure 4.10: Relative gene expression of tendon/ligament ECM proteins after three days of cyclic mechanical stretch, preload or static culture on electrospun PEUUR scaffolds with mean fiber diameter size of 0.6 μm (small) or 1.7 μm (large). n=4 for all except for small fiber diameter scaffolds at preload group, where n=2. Mean ± SEM

Transcript levels were also determined for scleraxis and tenomodulin, known as tendon selective genes [119]. Scaffolds with a larger mean fiber diameter appeared to increase gene expression of both scleraxis and tenomodulin in cells under preloaded conditions, as compared to scaffolds with a smaller fiber diameter (0.6 μm) under the same conditions, but this was not statistically significant (Figure 4.11). Cyclic loading of cells did not alter scleraxis or tenomodulin expression on either scaffold type.

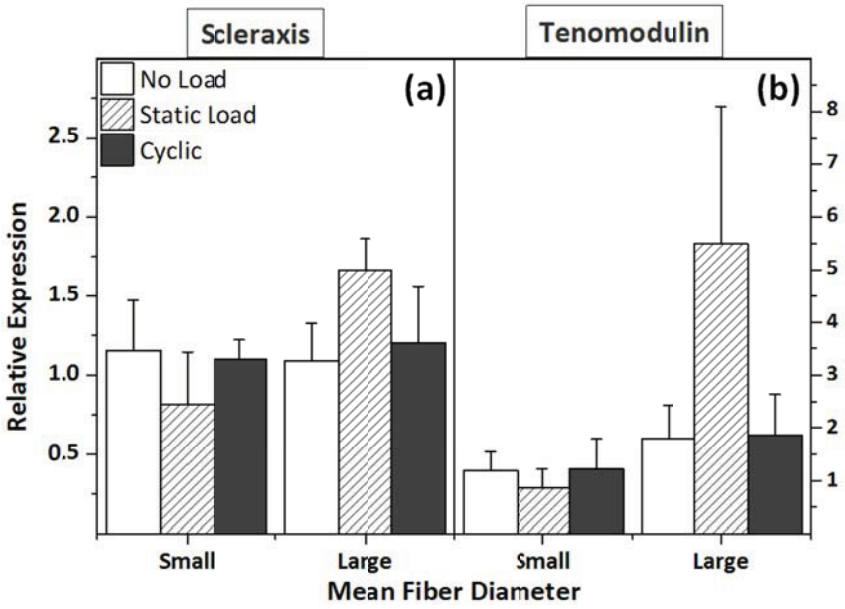

Figure 4.11: Relative gene expression of tendon/ligament selective genes after three days of cyclic mechanical stretch, preload or static culture on electrospun PEUUR scaffolds with mean fiber diameter size of 0.6 μm (small) or 1.7 μm (large). n=4 for all except for small fiber diameter scaffolds at preload group, where n=2 . Mean ± SEM

Scanning electron images of constructs

Cell morphology on electrospun constructs visualized using scanning electron microscopy was similar to that seen by the calcein-AM stain. Cells cultured statically on electrospun scaffolds appeared sheet-like, spanning many individual fibers (Figure 4.12c, f). Narrow cells were observed on statically-loaded constructs but some large spread cells were also observed (Figure 4.12b, e). Finally, cyclically stretched constructs contained highly elongated cells, parallel to the prevailing fiber orientation induced by the strain (Figure 4.12a, d). Long cell processes were noted in the small mean fiber diameter scaffolds; however, cell size does not appear affected by the scaffold's mean fiber diameter.

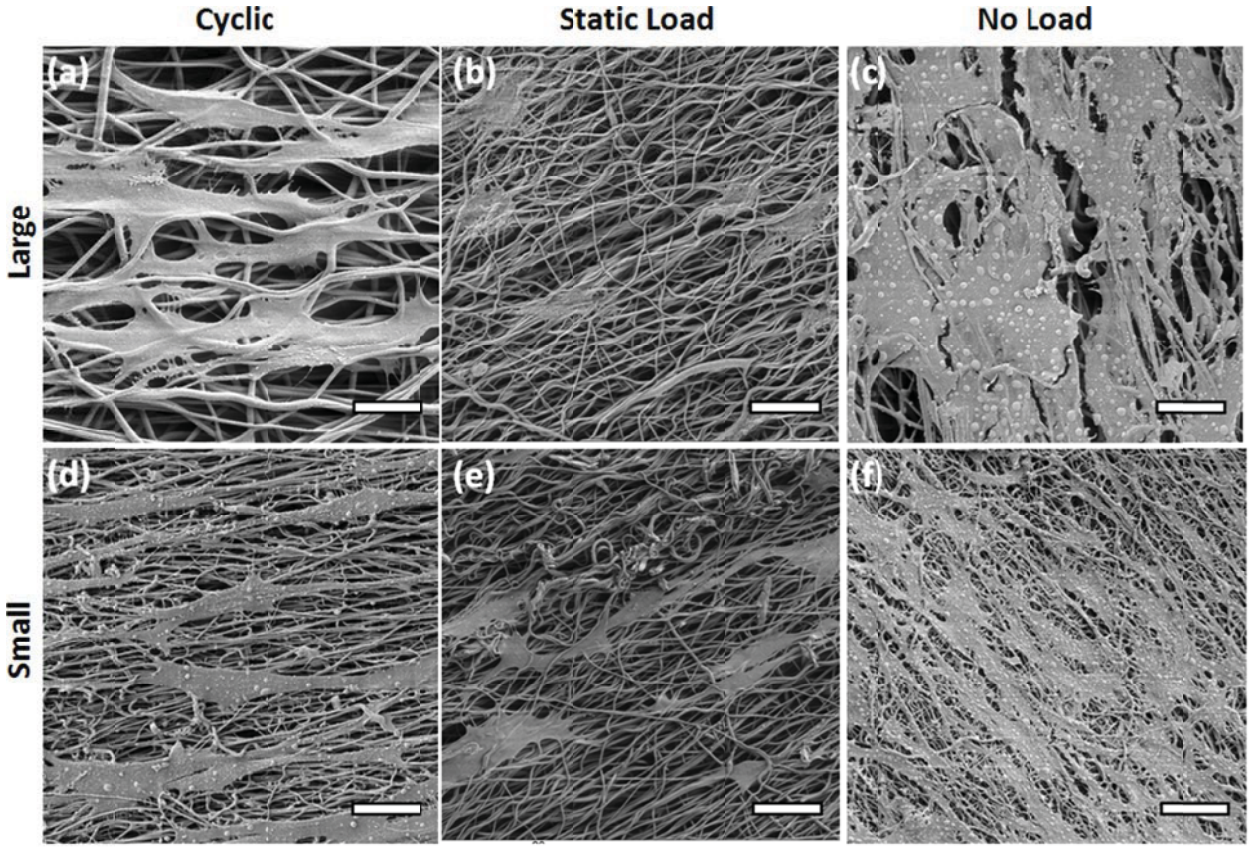

Figure 4.12: SEM images of C3H10T1/2 cells on electrospun PEUUR scaffolds after 3 days of cyclic mechanical stretch or static culture. Scale bars: 20 μm (a, c, d, e), 40 μm (b, f)

Discussion

In this study, model mesenchymal stem cells were stimulated on elastic fibrous scaffolds using a novel bioreactor system. This advanced bioreactor not only allowed precise mechanical control of the biomaterials but also permitted visual monitoring of cell presence on opaque substrates. Due to the elastomeric nature of the constructs and the importance of simulating the normal physiological niche of a tendon/ligament, the electrospun constructs were cyclically stretched with a low strain (4%). Cells proliferated and remained attached to the biomaterial, as determined *in situ* by confocal microscopy. Following three days of stimulation, observations of cell morphology revealed highly elongated cells with principal alignment in the direction of tensile stress under cyclic

strain. Differences in gene expression as a result of mechanical stress were moderate but results suggested that fiber diameter may affect cell behavior under dynamic culture.

Biomaterial scaffolds provide a critical template for controlling engineered tissue architecture and mechanical properties. Electrospinning facilitates development of controllable structures composed of many polymer types by a technically uncomplicated method [143, 230]. By variation of fabrication parameters, scaffolds can be produced with nano-to-micro fiber diameters and with fiber orientations ranging from fully aligned to random [27, 28, 143]. More importantly, electrospun scaffolds can be produced to mimic tissue-like mechanical behaviors such as structural anisotropy and non-linear stress-strain curves under tensile loading [59]. For tendons and ligaments, the stress-strain curve resulting from uniaxial tensile testing contains three distinct sections: (1) toe region (2) linear region and (3) yield and failure region [219]. The toe region results from straightening of crimped collagen fibers and alignment along the loading axis, typically occurring between 0 and 3% strain in tendons [185]. Segmented polyurethane electrospun scaffolds produced for this study displayed a non-linear mechanical behavior under tensile loading where distinct regions were present (Figure 4.5). Without direct observation of fiber kinematics during tensile loading, individual fibers within the semi-aligned scaffold are hypothesized to orient along the primary loading direction during the toe region followed by stretching of the fibers in the elastic region. An elastic modulus was calculated for each of the PEUUR scaffolds in the linear portion of the curve, generally between 5 and 10% strains. Scaffolds with mean fiber diameter of 0.60 μm had a significantly higher modulus (9.24 MPa) than the larger fiber diameter scaffolds (4.22 MPa). This behavior could be attributed to differences in packing density and inter-fiber behaviors of the two

distinct fiber populations. Small diameter fibers can pack closer together, and as a result will increase inter-fiber bonding sites and, due to increased surface area/volume ratio per fiber, exhibit greater inter-fiber friction during sliding contact. Finally, electrospun PEUUR scaffolds were distensible to greater than 20% strain before noticeable yielding. In contrast, the majority of synthetic electrospun polyester (e.g., PCL and PLGA) scaffolds yield before 10% strain [157].

PEUUR scaffolds were also tested for their ability to withstand cyclic loading. Cyclic strains are necessary to maintain homeostasis in many fibrous tissues; however stimulation at the extremes of physiological loading can induce degenerative changes [13, 116, 249]. Scaffolds were preloaded to exit the toe region and then cyclically stretched to 4% elongation for 30 minutes or 450 cycles. Here, the majority of the scaffold's strain energy was lost during the first loading cycle, possibly due to breakage of the smallest fibers (Figure 4.6). Thereafter, nearly all of the mechanical energy was stored in the scaffold as evidenced by the absence of creep between the first and last cycle. The results of cyclic loading at a physiologically relevant regimen suggest that the electrospun PEUUR scaffold behaved as viscoelastic material.

For cultivation of engineered tissues, bioreactor systems that apply tensile loading to cell-laden constructs have been shown to facilitate the composition and development of mature of extracellular matrix [132, 249]. One of the most commonly used commercially available systems is the FlexCell Tissue Train® system [90]. In this system, cell-seeded collagen gels are stretched by the applying a vacuum pull beneath a loading post. After a few weeks of stimulation, a tendon-like structure was formed. However, in this system, precise control over individual constructs is not possible. Individual control over

constructs allows for differences in scaffold size or errors in placing scaffolds. Another bioreactor developed by Atman et al. utilized a mechanical stimulation system to apply both rotational and tensile strains to silk scaffolds and collagen gels [7, 8]. Using this system, progenitor cell expression of collagen type I and decorin was stimulated. A limitation of this design was that it was too large to fit in an incubator, and therefore required environmental controls. A commercially available system from Tissue Growth Technologies offers precise mechanical control while fitting inside an incubator. This device has been used to improve the mechanical properties of decellularized tendons reseeded with tenocytes using cyclic loading [210]. A limitation of these systems, though, is that they are unable to monitor cell attachment and matrix production by microscopy during the high stress of mechanical stretch. However, one bioreactor system that was developed with imaging capabilities is that developed by the Humphrey group [113, 115]. This system can monitor collagen fiber alignment using nonlinear optical microscopy in collagen gels under stretch. The bioreactor used in the current study combines precise uniaxial loading and imaging modalities to stimulate individual scaffolds. Each cell-seeded scaffold can be preloaded and cycled separately thus compensating for scaffold size or position differences. The chamber can be placed on a confocal microscope stage without special equipment to non-destructively monitor cells or collagen fiber formation using multiphoton lasers. Thus, both cell and matrix organization can be monitored throughout the duration of the study.

Electrospun scaffolds with controllable architectures provide physical signals for cell orientation. Native fibrous tissues, such as tendons/ligaments, are composed of cells dispersed within the extracellular matrix along the primary axis of mechanical force. Many

current bioreactors utilize model surfaces, such as silicone membranes, as the substrate [112, 252]. However, cells on smooth surfaces, such as silicone membranes, will re-orient perpendicular to the direction of mechanical stress [248]. In this study, electrospun scaffolds – in which fibers were aligned along the loading axis – provided guidance cues to MSCs. Cell alignment parallel to the strain axis was more pronounced in cyclically stretched and statically loaded scaffolds relative to unloaded scaffolds, consistent with previous studies in tethered, but not cyclically stretched collagen gels and silk scaffolds [7, 49].

Mechanical stimulation may facilitate the maturity and extracellular matrix composition of engineered tissues. Through the process of mechanotransduction, mechanical signals are converted into cellular biological events, such as gene expression of ECM proteins. Limited to only uniaxial loading studies, tendon and ligament fibroblasts show increased mRNA expression of collagen types 1 and 3 in response to 10% or less cyclic stretch [127, 264]. Human bone marrow stromal cells seeded in collagen gels increased expression of collagen type I, collagen type III and tenascin-c following 14 days of mechanical stimulation at 10% elongation [7]. Previous investigators have also reported significant upregulation of decorin and bigylcan transcript levels in human MSCs under cyclic loading on silk scaffolds [49]. In the current study, relative transcript levels of abundant collagen types (type 1 and 3) in fibrous tissues were measured after three days of moderate stimulation, but no significant differences were found at this early time point. Static or cyclic-load large fiber scaffolds had greater collagen type 3 expression over no load controls whereas mechanically stimulated (cyclic or static) small fiber scaffolds decreased expression compared to no load controls – indicating effects from mean fiber

diameter under dynamic conditions. Other constituents of the extracellular matrix (e.g. tenascin-c, decorin, collagen type 12) were also measured following mechanical loading; however, no significant differences were found.

Finally, gene expression of scleraxis and tenomodulin was also investigated to determine if MSC differentiation along a tenogenic lineage is stimulated by cyclic stretch. As tendon/ligament selective genes, scleraxis and tenomodulin are considered early and late markers of tenogenesis, respectively [60, 66]. *In vivo* scleraxis and tenomodulin mRNA expression increased during the late stages of Achilles tendon healing during normal loading activities but not if the tendon was immobilized [73]. Scleraxis mRNA has also been shown to be increased following cyclic strains in either 3D collagen gels or PCL foam scaffolds [80, 134]. In our study, scaffolds with a larger mean fiber diameter appeared to increase gene expression of scleraxis under static loading conditions while cyclic loading did not alter scleraxis on either scaffold. Similar results were found for tenomodulin – large scaffolds had greater expression than small scaffolds under static load but no change during cyclic load.

Increased duration of mechanical stimulation in the current system could increase gene expression and matrix production. *In vitro* mechanical stimulation is known to increase extracellular matrix development when applied for multiple weeks [7, 67]. In this study, cyclic stretch was applied for only 3 days, resulting in only moderate changes in gene expression of tendon/ligament matrix constituents. Increasing the magnitude, elongation or duration of stretch has been shown to alter behavior in a number of cell types [65, 120]. Without alterations in the regimen (i.e. magnitude, frequency), simply increasing the number of days or weeks of stress application would potentially alter gene expression and

matrix deposition in our constructs. Also, monitoring each construct to ensure cell attachment and development of collagenous matrix throughout the experiment would further optimize the stretch regimen. In addition to use for accelerating cell differentiation and matrix development *in vitro*, the results of bioreactor studies might also be used for predicting constructs' physiologic responses to *in vivo* environments.

Conclusions

In this initial study, nanofibrous scaffolds were stimulated in a bioreactor and the response of model MSCs was evaluated. Under physiologic loading conditions, segmented polyurethane electrospun scaffolds displayed non-linear and viscoelastic mechanical behavior with tensile moduli ranging from 4 to 9 MPa. The bioreactor system used in this study not only allowed mechanical control of the biomaterials, but also permitted visual monitoring of cell morphology. Non-destructive imaging demonstrated that cells adhered to the scaffolds before and after mechanical stress. Cell morphology was altered following a short stimulation period. Gene expression differences between cyclically loaded, statically loaded, and unloaded cells were moderate. Preliminary results suggest that fiber diameter may also affect cellular behavior under dynamic conditions.

Acknowledgements

The authors thank the Tissue Engineering Resource Center at Tufts University for providing equipment and facilities to perform this work. The authors gratefully acknowledge Dr. Scott Guelcher for providing the synthesized PEUUR. This publication was made possible by Grant Number AR 055872 to RDC from the National Institutes of Health.

Chapter 5: Effects of constitutive overexpression of the basic helix-loop-helix transcription factor scleraxis on mesenchymal stem cells

[1]Robyn D Cardwell, [3]Christine S Jones, [1,2]Aaron S Goldstein and [4]Linda A Dahlgren

[1]School of Biomedical Engineering and Sciences and
[2]Department of Chemical Engineering,
[3]Department of Animal and Poultry Science,
Virginia Polytechnic Institute and State University,
Blacksburg, VA 24061

[4]Department of Large Animal Clinical Sciences,
Virginia-Maryland Regional College of Veterinary Medicine,
Blacksburg, VA 24061

CSJ performed cell culture and RNA isolation for temporal studies

Abstract

The need for novel grafting materials for anterior cruciate ligament (ACL) reconstructions has stimulated tissue engineering efforts to develop a functional tissue replacement. Generation of a signaling environment capable of directing progenitor cell differentiation along a tendon/ligament lineage remains a major challenge. In addition to extracellular signals, intracellular cues may also direct precursor cell differentiation into mature tendon or ligament fibroblasts. The transcription factor scleraxis is expressed during early embryological development and may play a crucial role in the development of these connective tissues. As initial steps in elucidating the role of scleraxis during tenogenic differentiation, temporal cellular responses to an upregulation in scleraxis activity was evaluated for evidence of tendon/ligament differentiation. Transient transfection resulted in scleraxis gene expression peaking at 6 hours but returning to basal levels by 48 hours. Moderate expression changes in tendon/ligament extracellular matrix genes were also observed following transfection. Using a second vector, forced expression

of GFP-tagged scleraxis indicated complete localization to the cell nucleus. This suggests that the constitutive expression of the gene product induced cell death; however, only minimal increases in apoptotic activity were observed. The combination of scleraxis-induced morphological changes and inability to detect scleraxis in cell lysates implies initiation of regulatory mechanisms within the cell.

Introduction

Approximately 45% of the 33 million musculoskeletal injuries occurring in the United States annually are associated with damage to tendons, ligaments, or joint capsule [199]. Because ruptures or tears of the anterior cruciate ligament (ACL) in the knee joint often require surgical reconstructions, there is growing need for alternatives to traditional choices of graft materials. Autologus tissue grafts can be associated with significant donor site morbidity, while allogeneic grafts are limited by the availability of suitable donors and the risk for disease transmission. The need for novel grafting materials has stimulated efforts to engineer a functional ligament replacement; however, providing a signaling environment capable of directing progenitor cell differentiation along a ligament lineage remains a major challenge. Ligament development is thought to require both intracellular (transcription factors and signaling proteins) and environmental (mechanical strain and three-dimensional environment surrounding the cells) signaling mechanisms. Therefore, strategies must be developed that activate one or more of these pathways and direct precursor cells to differentiate into mature ligament fibroblasts.

Multipotent mesenchymal stem cells (MSC) are a promising precursor cell type that offers many advantages as compared to terminally differentiated cell types. Mesenchymal stem cells are adult progenitor cells residing in numerous mesenchyme tissues such as bone

marrow, skin, muscle and fat [3]. MSCs are capable of forming a variety of musculoskeletal tissues including bone, cartilage, fat, tendon, and muscle [42]. Mesenchymal stem cells are an attractive cell source for cell-based tissue engineering strategies in which large numbers of cells are needed. MSCs can be readily harvested from bone marrow, are highly proliferative *in vitro* and are able to maintain a stable multipotent phenotype [197]. To date, lineage differentiation of uncommitted MSCs to bone, cartilage, and adipogenic cell types has been studied in depth [197] while the knowledge of the biological factors that promote MSC differentiation along a tenogenic lineage is limited. Often, model mesenchymal stem cell lines, such as murine C3H10T1/2, are utilized to further elucidate signaling pathways involved in specific differentiation cascades [43, 82, 91, 111].

Directed differentiation of MSCs along prescribed lineages can be induced by exogenous biochemical cues and mechanical signals. *In vitro* osteogenic differentiation of MSCs is induced by the addition of dexamethasone, β-glycerophosphate and ascorbic acid to standard medium [197] while indomethacin and 3-isobutyl-1-methylxanthine are needed for adipogenic differentiation [239]. Chondrogenesis not only requires supplementation with specific growth factors (e.g. TGF-β superfamily members) but also high-density pellet cultures, implying a role for the extracellular environment [213]. Application of shear [130], compressive [158] or tensile mechanical loading [184] has been shown to increase osteogenic, chondrogenic and myogenic differentiation, respectively [198]. Lineage specificity of MSCs is also highly sensitive to the elasticity, composition and structure of the underlying matrix [76, 206].

Differentiation of cells along specific phenotypic pathways can also be induced through activation of intracellular signaling pathways. Forced co-expression of BMP-2 (a

morphogen) and R-Smad8 (a transcription factor) in C3H10T1/2 cells generated tenocytes while blocking formation of osteoblasts and chondrocytes [111]. Overexpression of Runx2/Cbfa1 c, an osteoblast-specific transcription factor, has been shown to increase expression of bone specific proteins in a variety of cell types [40, 68]. The basic helix loop helix transcription factors (e.g., MyoD, NeuroD) have been suggested to play a key role in the differentiation of muscle and nerve cells and are considered tissue-specific transcription factors [168, 225]. Exogeneous expression of MyoD activates transcription of muscle-specific proteins in many cell types, including C3H10T1/2 cells [234, 256]. Transient overexpression of NeuroD2 and E12, a ubiquitous dimerization partner, induced neuronal differentiation in pluripotent P19 stem cells [79]. Therefore, it follows that over-expression of scleraxis – a ligament/tendon-related transcription factor – might enhance differentiation of MSCs into the tendon/ligament fibroblast phenotype.

Scleraxis is a basic helix-loop-helix transcription factor (bHLH) expressed in early embryological development and may assist in the differentiation of stem cells towards a tendon/ligament phenotype and the associated production of appropriate extracellular matrix proteins. Schweitzer et al. showed that the scleraxis gene is a marker for tendon development in chick and mouse and found that scleraxis was highly specific for connective tissues that mediate the attachment of muscle to bone and bone to bone [212]. Scleraxis transcripts have also been observed in the collateral and anterior cruciate ligaments in mouse embryos [15], and scleraxis has been shown to be continuously expressed during tendon and ligament development from the progenitor stage to that of mature tendons [36, 202]. Studies using knockout mice have demonstrated that scleraxis expression is essential for tendon differentiation, organization of tendon progenitor cells into functional tendons,

and production of a phenotypically mature tendon extracellular matrix [175]. Scleraxis has also been implicated as a positive regulator of tenomodulin, a glycoprotein that is expressed in tendon, nerve, and cartilage [218]. In addition, the collagen type 1α1 gene has been shown to be a downstream target of scleraxis in immortalized tendon fibroblasts [141]. Current literature supports a role for scleraxis in the induction of tendon and ligament formation; however, mechanistic studies demonstrating that scleraxis activation induces the differentiation of mesenchymal stem cells into tendon or ligament fibroblasts are lacking [14].

In this study, the tendon/ligament specific transcription factor, scleraxis, was over-expressed in a mesenchymal stem cell line to evaluate the potential of this signaling molecule to direct differentiation along a tendon/ligament lineage. Vectors encoding scleraxis cDNA and epitope tags were verified for sequence accuracy and protein production. Following transfection of scleraxis fusion proteins in C3H10T1/2 cells, transcript levels of scleraxis and constitutive tendon or ligament extracellular matrix (ECM) genes (tenomodulin, collagen type I, collagen type 3, collagen type 12, decorin and tenascin-c) were determined. C3H10T1/2 cell viability, cytotoxicity and caspase 3/7 activity was also measured following scleraxis expression. Using fluorescently labeled scleraxis, the intracellular fate of exogenous scleraxis protein was found.

Materials and Methods

Expression plasmids

Full length mouse scleraxis cDNA was amplified using PCR and inserted into the pcDNA3.1/HisC vector (Invitrogen, Carlsbad, CA). pcDNA3.1/HisC contains the cytomegalovirus (CMV) promoter region to direct expression of downstream sequence

(here, full length mouse scleraxis cDNA (NM_198885)) and conferring neomycin (analog to gentamicin) resistance for stable transfection. Scleraxis is constitutively expressed in this configuration. The vector also includes a label, the Xpress™ sequence (-DLYDDDDK-), upstream of scleraxis cDNA in order to track and quantify the protein as there are currently no commercially available antibodies to scleraxis. This entire scleraxis vector was a gift from Dr. Veronique Lejard (Paris-Descartes University) [141]. The vector will be referred to as pcDNA3.1/His/SCX and the gene product as Xpress-SCX hereafter (Figure 5.1a). A second plasmid, pCMV6-AC-GFP-SCX (OriGene, Rockville, MD) also contains scleraxis cDNA directed by the CMV promoter but includes a C-terminal GFP tag to create a fusion protein visible under fluorescent excitation (Figure 5.1b). The gene product of the pCMV6-AC-GFP-SCX vector will be referred to as SCX-GFP. Sequences of the expression plasmids were confirmed by DNA sequencing (Virginia Bioinformatics Institute Core Laboratory Facility, Blacksburg, VA). All plasmid DNA was replicated using chemically competent cells, screened using restriction enzyme digests and purified using a gravity-flow kit (EndoFree Plasmid Maxi Kit, Qiagen, Valencia, CA) (see details in Appendix C).

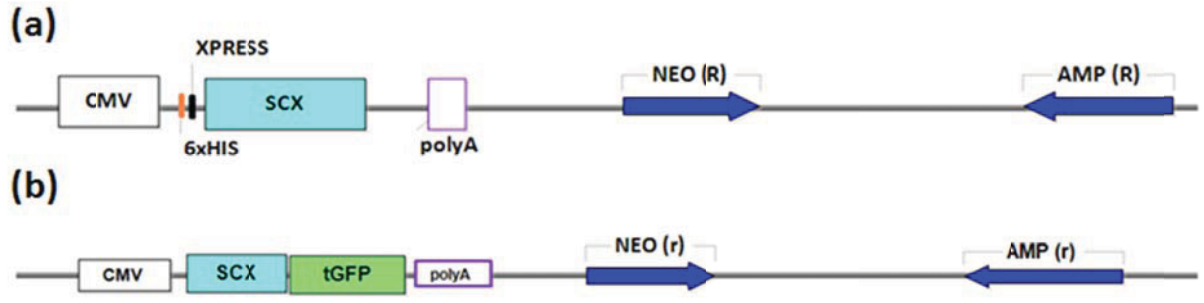

Figure 5.1: Linear representation of scleraxis expression plasmids. Constitutive transcription of the scleraxis murine cDNA is regulated by the CMV promoter. The pcDNA3.1/His/SCX plasmid (6753 bp) contains an Xpress epitope tag (a) while the pCMV-AC-GFP-SCX plasmid (7181 bp) contains a GFP tag (b).

The plasmid, pcDNA3.1/His/LacZ (Invitrogen) was used as a control and to determine transfection efficiency. The LacZ gene encodes for the enzyme β-galactosidase that cleaves the substrate X-gal (5-bromo-4-chloro-3-indolyl-β–galactopyranoside) into galactose and an insoluble blue product that can be visualized and quantified. To calculate transfection efficiency, the cells nucleofected with pcDNA3.1/His/LacZ were fixed and stained for β- galactosidase activity using a β-gal staining kit (Invitrogen). Under bright field microscopy, the percent of stained cells was determined from 5 random fields at 20X magnification of at least 20 cells. A different vector, pmax-GFP (Lonza, Basel, Switzerland), was used as a control for GFP expression.

In Vitro Transcription/Translation

In vitro transcription/translation was performed to verify protein production using the TnT Quick Coupled Transcription/Translation system according to manufacturer's recommendations (Promega, Madison, WI). Briefly, 1 μg of plasmid DNA was added to a nuclease-treated rabbit reticulocyte lysate in the presence of 10 mCi/ml [^{35}S] methionine ([^{35}S]Met) and then incubated for 60 minutes at 30°C. The supernatants were directly analyzed by SDS-polyacrylamide gel electrophoresis (SDS-PAGE), followed by autoradiography to detect the [^{35}S]Met-labeled reaction products and to determine product molecular weight.

Cell culture

Passage 13 C3H10T1/2 Clone 8 mouse mesenchymal stem cells (ATCC, Manassas VA) were expanded in Dulbecco's Modified Eagle's Medium high glucose (4,500 mg/L) (DMEM, Cellgro, Manassas, VA) supplemented with 10% fetal bovine serum (FBS, Cellgro), 2 mM L-glutamine (Cellgro) and 1% pencillin/streptomyocin (Cellgro), known as DMEM

growth media. Cells were trypsinized with 0.25% (w/v) trypsin/EDTA (Cellgro) and seeded at a density of 2,000 cells/cm^2 in DMEM growth medium prior to nucleofection.

Transfection and selection

C3H10T1/2 cells were nucleofected using the Cell Line Nucleofector® Kit V (Amaxa, Walkersville, MD) with program T-20 following the manufacturer's instructions. Six micrograms of scleraxis plasmid was used for nucleofection. Transfected cells were incubated for 10 minutes in warm growth medium at 37°C immediately after nucleofection. To increase transfection efficiency and/or improve protein yield, 20 μm MG132 (EMD Chemicals, Gibbstown, NJ) was added to the medium 24 hours post transfection.

For generation of stable clones, pcDNA3.1/His/SCX was linearized with *PvuI* (New England BioLabs, Ipswich, MA). The *PvuI* site was selected based on its interference with the ampicillin resistance gene and lack of interference with scleraxis and neomycin sequences in the vector. Cells were passaged 1:10 after 24 hours with DMEM growth medium. At 2 days post-transfection, 800 μg/mL gentamicin (G418, Invitrogen) was added to the DMEM growth medium to select for cells with resistance. After 10 to 12 days, individual colonies were selected and grown into clonal lines by limiting dilution.

Western Blot

Cell monolayers for western blot analysis were harvested 48 hours post-nucleofection. Cell lysates were collected by mechanical scraping following exchange of culture medium with Laemmli sample buffer containing 4% SDS, 10% 2-mercaptoethanol, 20% glycerol, 0.004% bromophenol blue, and 0.125 M Tris HCl (BioRad, Hercules, CA). Crude homogenates were then heated to 95°C for 5 minutes. In some instances, Ni-NTA Agarose beads (Qiagen, Valencia, CA) were used to purify His-tagged scleraxis prior to

heating, according to manufacturer's instructions. SDS-PAGE gel electrophoresis was performed on whole cell lysates. Thirty microliters of each sample were loaded into precast 15% polyacrylamide gels (8.7 x 13.3 cm, Criterion™ Precast Gel, BioRad). Diluted ProSieve® color protein markers (Lonza, Basel, Switzerland) and a positive control protein containing the Xpress ™ epitope (Positope™, Invitrogen) were also loaded. Proteins were separated at 200 V for approximately 60 minutes in 1X running buffer (25mM Tris base, 192mM glycine, 0.1% SDS w/v, pH 8.3) until the dye front reached the bottom of the gel. Once completed, gels were equilibrated with pre-chilled 1X transfer buffer (Towbin; 25mM Tris base, 192mM glycine and 10% methanol or CAPS; 10mM CAPS and 10% methanol) and transferred electrophoretically to Immobilon FL-polyvinylidene difluoride (PVDF) (Millipore, Billerica, MA) membranes at 100 V for 30 minutes in an ice bath. The predicted size of the scleraxis protein is 20-22 kDa [60]. Following transfer of fractionated proteins, membranes were washed in PBS for 5 minutes. PVDF membranes were agitated overnight in blocking buffer (Near Infrared Fluorescent Blocking Buffer, Rockland Immunochemicals, Inc., Gilbertsville, PA) at 4°C. After blocking, membranes were washed in 1X phosphate buffered saline (PBS) for 5 minutes, then incubated for 1 hour at room temperature with the primary antibody against the Xpress™-tag epitope (Invitrogen) diluted 1:5000 in 0.5X blocking buffer and 0.02% Tween-20 with agitation. Following primary antibody incubation, membranes were washed 4 times for 5 minutes/wash in PBS with 0.02% Tween-20 at room temperature with agitation. The membranes were then incubated in IRDye® 800 Conjugated Affinity Purified Anti-mouse IgG (H+L) (Rockland) diluted 1:12,500 in 0.5X blocking buffer and 0.02% Tween-20 for 1 hour at room temperature with

agitation. Finally, membranes were washed 4 times as above. The membranes were scanned using the Odyssey Infrared Imaging System (LI-COR Biotechnology, Lincoln, NE).

Real time PCR

For collection of total RNA, cells nucleofected with pcDNA3.1/His/SCX were plated at a density of 5,000 cells/cm^2 into 12 well plates for the early timepoints. Cells were seeded at 2,500 cells/cm^2 for 3 and 7 day collections. Total RNA was isolated from the cell layers using the RNeasy Mini Kit (Qiagen, Valencia, CA) following the manufacturer's instructions. Cells were washed twice with 1X PBS and collected in 350 µL Buffer RLT provided in the kit. Lysates were first homogenized with QIAShredder columns (Qiagen). Following homogenization an equal volume of 70% ethanol was added and the lysate was loaded onto the RNeasy silica spin columns and total RNA isolated according to the kit instructions. Samples were subjected to on-column DNase digestion using DNase I (Qiagen) prior to elution. Total RNA was quantified using the Quant-It RiboGreen® kit (Invitrogen) and a fluorescent plate reader (SpectraMax M2, Molecular Devices, Sunnyvale CA). Equal amounts of total RNA, approximately 500 ng, were then reverse transcribed to cDNA using the High Capacity cDNA Reverse Transcription kit (Applied Biosystems, Carlsbad CA) with random hexamers as primers, according to manufacturer's protocol.

Real time fluorescent PCR was performed using the ABI 7300 Real Time PCR System and Power Sybr® Green Master Mix (Applied Biosystems). Specific primers for mouse collagen type 1α1, decorin, and other ECM proteins were designed using Primer Express software v2.0 and published sequences (see Chapter 4, Table 4.1). β-actin was used as the reference gene. Equal quantities of total RNA, to test for genomic DNA contamination, and no template (nuclease-free H_20 in place of cDNA) were used as negative controls for the

reactions. Quantification of target gene expression was referenced to the reference/housekeeping gene (β-actin) using the comparative threshold cycle (ΔΔCt) method [151].

Imaging

For imaging, cells were transfected with either pCMV-AC-GFP-SCX or pmax GFP and plated into 6-well plates at 5,000 cells/cm^2. As early as 6 hours post transfection, cells were imaged using an inverted microscope (CKX41, Olympus, Center Valley, PA) equipped with a fluorescence illuminator and dual filters. For the first 24 hours following introduction of plasmid DNA, images were collected using a high resolution digital camera (Infinity 1-3C, Lumenera, Ottawa, ON) every 3 hours at 10X, 20X and 40X magnifications.

Cytotoxicity and apoptosis

Following nucleofection with the pcDNA3.1/His/SCX vector, cells were seeded at 31,250 cells/cm^2 (high density) or 7,812 cells/cm^2 (low density) into white, clear bottom 96-well tissue culture plates (Corning Life Sciences, Lowell, MA) and assayed. Cellular viability, cytotoxicity and apoptosis activity was detected using ApoTox-Glo multiplex assay (Promega, Madison, WI) at 6, 9, 12 and 24 hours post-transfection with Xpress-SCX, according to the manufacturer's recommendations. Fluorescence and luminescence were detected using a SpectraMax M2 microplate reader (Molecular Devices, Sunnyvale CA). Staurosporine, triton X-100 and digitonin were used as positive controls for apoptosis, cytotoxicity and necrosis respectively [267]. The positive control concentration in C3H10T1/2 cells was selected by determining the EC_{50} of a serial dilution assay of each compound using a nonlinear curve fitting algorithm at 6 (Figure 5.2) and 24 hours (Figure 5.3) (OriginPro 8.1, Northhampton MA). Using normalized raw values, an apoptotic index

was calculated by dividing the live-cell viability (RFU) by the caspase 3/7 activation value (RLU). A cytotoxicity index was also established at each timepoint dividing the dead-cell value (RFU) by the live-cell value (RFU) [186].

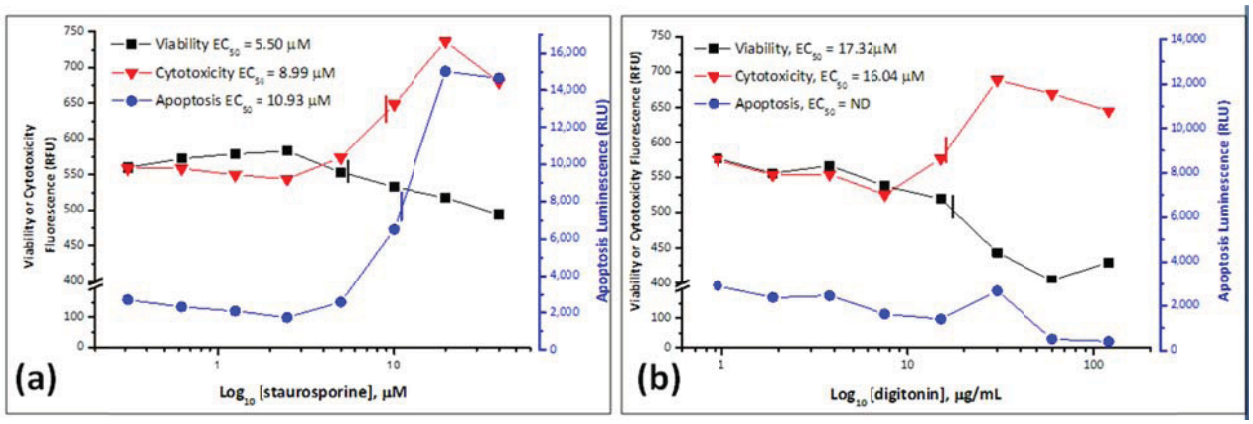

Figure 5.2: ApoTox-Glo assay results for staurosporine (a) or digitonin (b) treatment of C3H10T1/2 cells for 6 hours. Staurosporine treatment for 6 hours resulted in a dose-dependent decrease in viability, increase in cytotoxicity with an increase in caspase-3/7 activity consistent with apoptosis. Digitonin treatment for 6 hours resulted in a dose-dependent decrease in viability with an increase in cytoxicity but no caspase 3/7 activation.

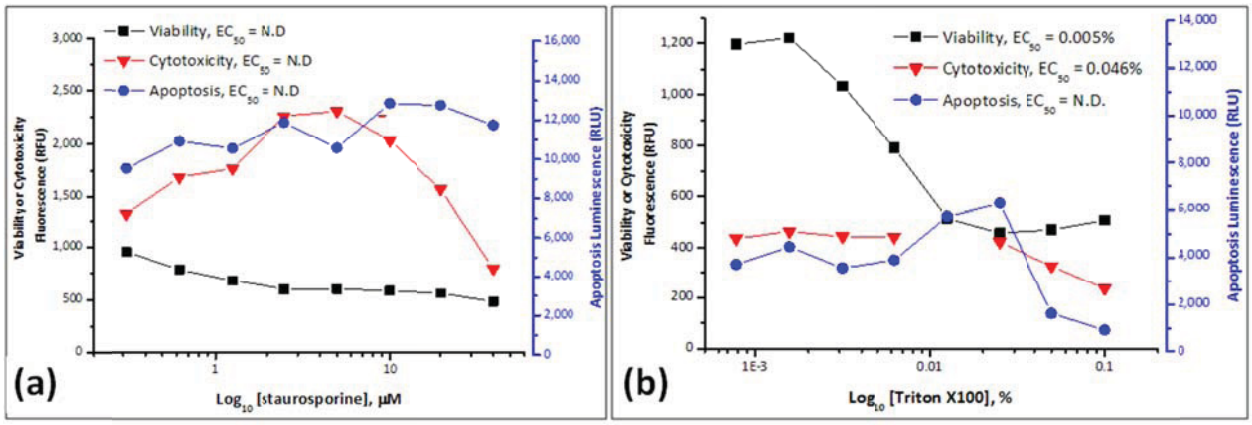

Figure 5.3: ApoTox-Glo assay results for staurosporine (a) or Triton X100 (b) treatment of C3H10T1/2 cells for 24 hours. Staurosporine treatment for 24 hours resulted in consistent caspase-3/7 activity at all concentrations tested. Triton X100 treatment for 24 hours resulted in a dose-dependent decrease in viability with an increase in cytoxicity and basal levels of caspase 3/7 activation.

Statistics

Results are reported as mean ± standard deviation unless otherwise noted. Statistical significance was determined using one-way ANOVA, followed by post-hoc

comparisons using the Fisher least significance difference method with a significance criterion of $p \leq 0.05$ (OriginPro 8.1, OriginLab, Northhampton, MA).

Results

To establish optimal transfection conditions in C3H10T1/2 cells, nucleofection was optimized using the control plasmid coding for the *lacz* gene. Following nucleofection using differing amounts of plasmid DNA (μg), cells were stained to quantify β-galactosidase activity (Figure 5.10). Transfection efficiency was found to increase linearly with the amount of plasmid DNA used for nucleofection with minimal increases in cytotoxicity. To conserve plasmid DNA, 6 μg was chosen to nucleofect cells, which corresponded to a transfection efficiency of 64%.

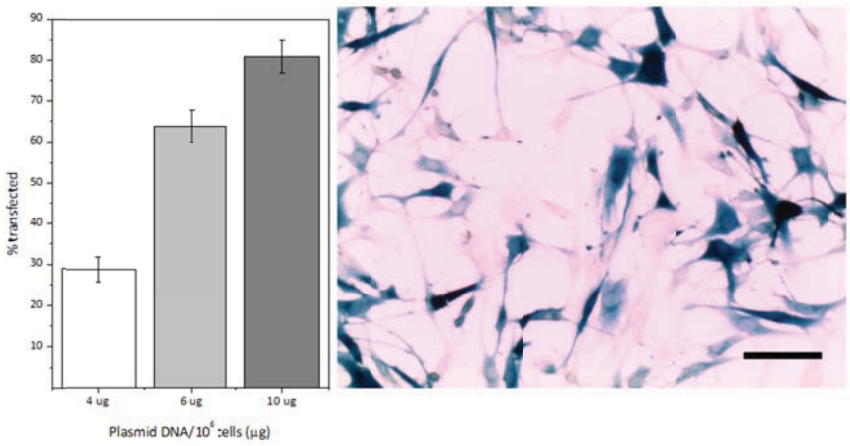

Figure 5.4: Optimization of nucleofection. Plasmid DNA was optimized by transfecting with pcDNA3.1/His/Lacz, then stained for β-galactosidase activity. Six micrograms of DNA was chosen as the optimal plasmid DNA amount (shown right). Scale bar: 100 μm.

Transient transfection of Xpress-SCX resulted in a significant upregulation in scleraxis mRNA transcripts at 24 hours post transfection (Table 5.1). C3H10T1/2 cells expressed basal levels of scleraxis with a Cycles to Threshold (Ct) value of 35. After transfection, the scleraxis Ct value decreased to 24. The Ct value for the housekeeping gene, β-actin, remained between 21 and 22 for all cells, transfected or not. PCR

amplification of total RNA isolated from Xpress-SCX transfected cells (without reverse transcription to cDNA, "no RT") had a Ct value of approximately 29, indicating an excess of scleraxis plasmid but undetectable amounts of β-actin. Control no RT reactions from untransfected cells had undetectable amounts of β-actin and scleraxis mRNA as expected.

Table 5.1: Cycles to threshold (Ct) values for scleraxis-transfected C3H10T1/2 cells. Using real time PCR, Cycles to threshold (Ct) values were measured for scleraxis gene expression 24 hours after transfection in C3H10T1/2 cells. SCX-transfected cells had a 1000-fold increase in transcript levels of scleraxis, indicating transcription of plasmid DNA.

	SCX-Transfected Cells	Non-Transfected Cells	SCX- Transfected Cells , No RT	Non-Transfected Cells , No RT
Scleraxis: Cycles to Threshold (Ct)	24.51 ± 0.14	35.52 ± 0.17	29.74 ± 0.25	Undetectable
Beta Actin: Cycles to Threshold (Ct)	22.66 ± 0.57	21.63 ± 1.32	Undetectable	Undetectable

Xpress-SCX stably transfected clones were not found following selection in G418 supplemented media (data not shown). At the end of the two week selection period, all Xpress-SCX transfected cells had died, similar to untransfected cells in the same conditions. In contrast, viable, stably expressing Xpress-LacZ cells were present at the end of selection.

Western blots were performed to verify expression of scleraxis protein following transient transfection. Because commercial antibodies to scleraxis are not currently available, the Anti-Xpress™ antibody was used to detect fusion proteins. Using the standard Towbin buffer, the Xpress-tagged protein encoding for β-galactosidase was detected (Figure 5.5a, Lanes 4 and 8) as well as the recombinant positive control protein (Figure 5.5a, Lanes 2 and 10). However, Xpress-SCX was not detectable (Figure 5.5a, Lanes

3 and 9). The Towbin buffer system with a pH of 7-8 predictably transfers most proteins from the gel to PVDF membrane. However, transfer will not occur if the protein has an isoelectric point (pI) above the buffer system and alterative buffers can be used. The isoelectric point of scleraxis is 10.9 [60]. Following transfer with the CAPS buffer system (pH 10-11), the positive control was detectable (Figure Figure 5.5b, Lanes 2 and 10) but Xpress-SCX was not (Figure 5.5b, Lanes 3 and 9). In this modified system, β-galactosidase was weakly detected (Figure 5.5b, Lanes 4 and 8). Inconclusive evidence of scleraxis protein production in cell lysates led to modifications of cell culture conditions and lysate collection. To determine if proteosome activity was degrading scleraxis protein in newly transfected cells, a non-specific proteosome inhibitor (20 μM MG132) was added to the medium 24 hours post transfection and cell lysates were collected for western blot 6 hours later [146]. However, scleraxis was not detected (data not shown). Separately, concentration of cell lysates with Ni-NTA agarose beads, which bind the 6X His sequence tag in pcDNA3.1/His vector, proved unsuccessful in detecting Xpress-SCX by western blot (data not shown).

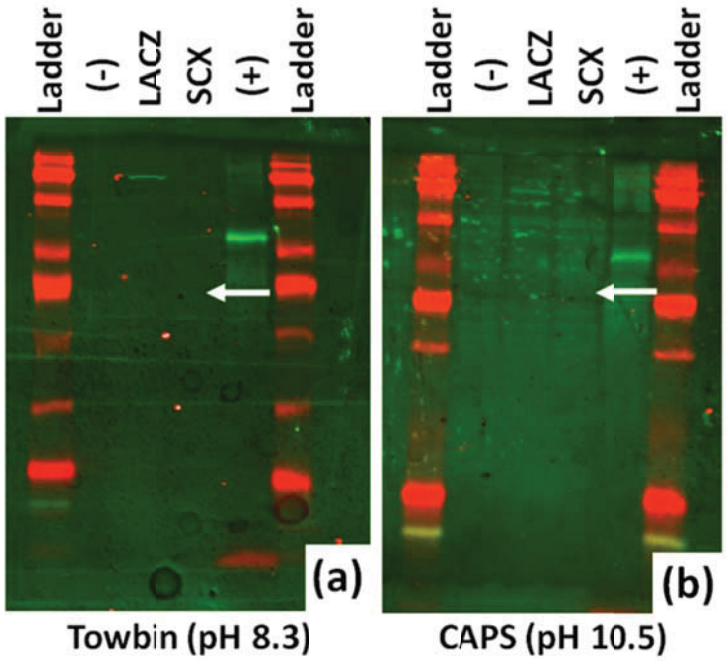

Figure 5.5: Western blots of whole cell lysates transfected with scleraxis or lacz detected using the Xpress epitope using traditional Towbin transfer buffer (a) or CAPS transfer buffer (b). A 150 kDa band for the Xpress-LacZ fusion protein is demonstrated. A 53 kDa band signifies the recombinant control Positope™ (+) protein. The white arrow depicts the predicted location for Xpress-SCX fusion protein at 39 kDa.

Temporal scleraxis gene expression was measured using fluorescent real time PCR following transient transfection with Xpress-SCX. At 6 hours, an approximately 1,300 fold upregulation in mRNA transcripts over controls was found (Figure 5.6a). At 12 hours, scleraxis transcripts were 800-fold greater than pcDNA3.1/His/LacZ and negative controls. By 72 hours post-transfection, scleraxis gene expression was equal to that of controls. Transient transfections were repeated in triplicate under identical conditions (e.g. cell passage, nucleofection conditions). Initial upregulation in scleraxis gene expression varied between experiments but the decrease in transcript levels followed a similar reduction in expression over time (Figure 5.6b).

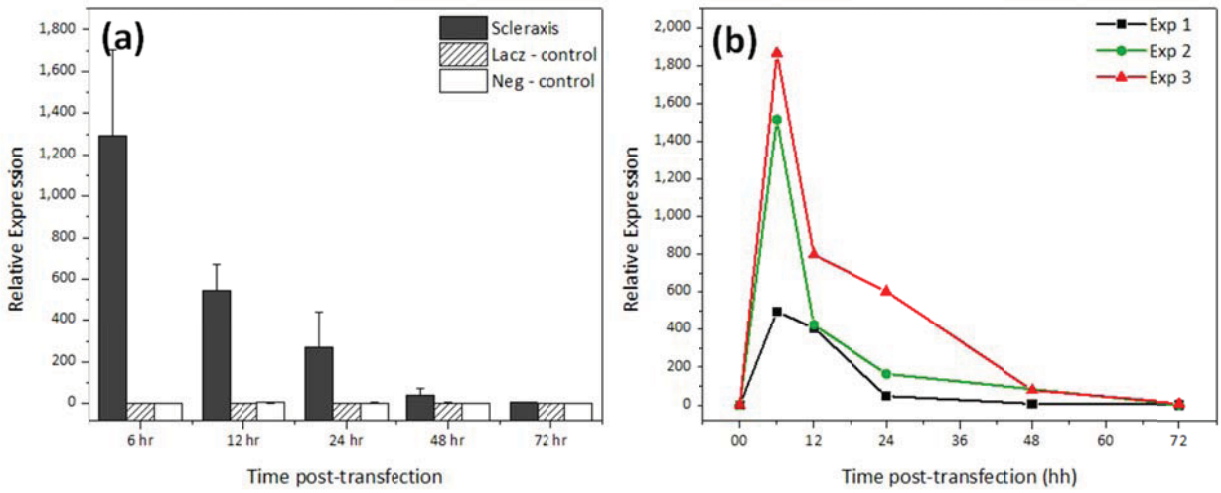

Figure 5.6: Temporal relative gene expression of scleraxis following transfection of C3H10T1/2 cells. Scleraxis gene expression was elevated 1,300 fold over controls at 6 hours post transfection then returned to basal levels by 72 hours post transfection (a). Scleraxis gene expression pattern following overexpression was similar over three separate experiments (b).

In addition to quantifying temporal scleraxis expression following transient transfection, expression of other tendon/ligament proteins was also quantified. Forced Xpress-scleraxis expression did not significantly alter collagen type I, 3 or 12 gene expression levels up to 72 hours post-transfection (Figure 5.7). Gene expression levels of collagen types 1 and 3 remained consistent over the 72 hour period. Scleraxis upregulation did not alter expression levels of decorin, tenascin-c or tenomodulin at the timepoints assessed (Figure 5.8). Decorin and tenomodulin gene expression decreased in a temporal manner in all groups.

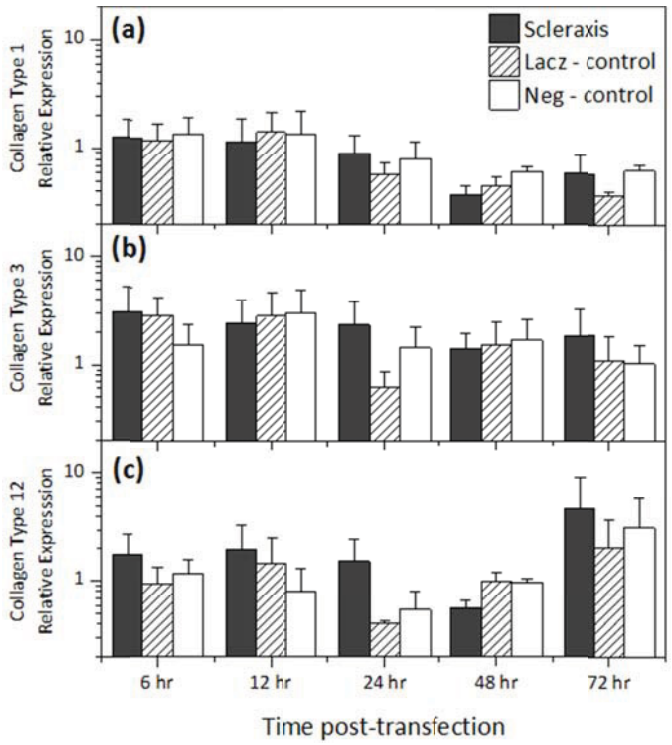

Figure 5.7: Temporal relative expression of collagen type I (a), type 3 (b) and type 12 (c) following transient transfection with scleraxis compared to lacz transfected and negative controls.

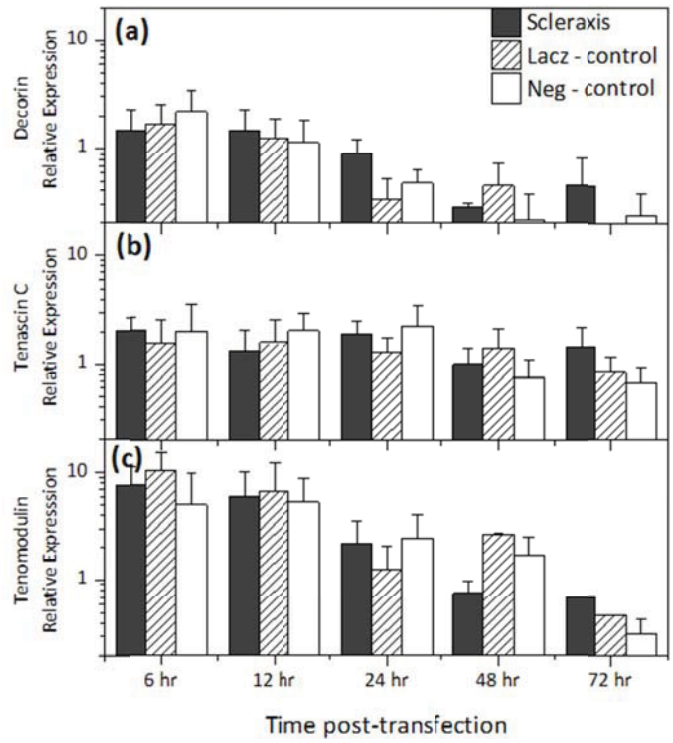

Figure 5.8: Temporal relative expression of decorin (a), tenascin-c (b) and tenomodulin (c) following transient transfection with scleraxis compared to lacz transfected and negative controls.

To confirm that the pcDNA3.1/His/SCX vector was producing the predicted protein, a cell-free system was used. Coupled *in vitro* transcription/translation revealed 39kDa and 120 kDa polypeptides, corresponding to the Xpress-tagged scleraxis (Xpress-SCX) and β-galactosidase proteins (Xpress-LacZ), respectively (Figure 5.9). Due to low abundance of the amino acid methionine in the scleraxis fusion protein, extended exposure (24 hrs) was required to detect the radiolabeled protein.

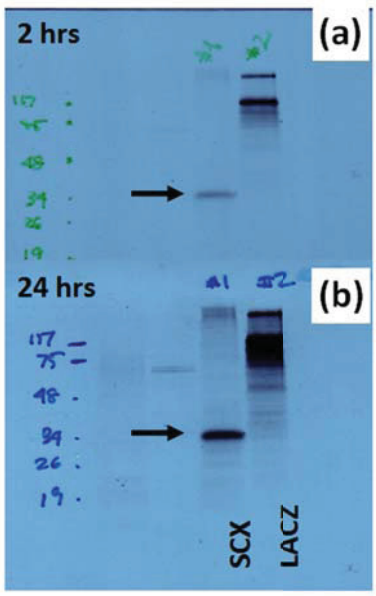

Figure 5.9: Autoradiography of [35S]-labeled *in vitro* transcription-translation products of plasmids (1 µg) containing cDNA of mouse scleraxis (lane 1) or lacz (lane 2) following 2 (a) or 24 (b) hours of exposure. As predicted, a 39 kDa band confirms presence of Xpress-scleraxis fusion protein (arrow).

Because the pcDNA3.1/His/SCX gene product (Xpress-SCX) was not detectable by western blot, a new vector encoding a GFP-scleraxis fusion protein was used to permit scleraxis detection by fluorescence microscopy. At 6 hours post transfection, the GFP-scleraxis protein was primarily localized to the nucleus with moderate signal intensity (Figure 5.10). Some expression was found in the cytoplasm but with faint signal intensity. As time progressed, GFP-scleraxis became compartmentalized to discrete areas within the nucleus and no expression was found in the cytoplasm. Starting at approximately 12 hours

post transfection, GFP-scleraxis positive cells became granulated and developed an altered morphology that was more round than stellate. By 24 hours, GFP-scleraxis positive cells were rounded and detached from the plate. In contrast, transfection with the GFP control vector (pCMV-AC-GFP) resulted in GFP positive cells with signal throughout the cytoplasm that intensified as time progressed (Figure 5.10, insets). Control GFP positive cells were viable and continued to express GFP for at least two weeks following transient transfection (data not shown). The expression pattern of SCX-GFP in the nucleus appeared to cause chromatin compaction. To test for activation of epigenetic regulation of plasmid DNA and to determine if cell viability could be improved, 5mM sodium butyrate was added to the medium following transfection. Sodium butyrate is a histone deacetylase inhibitor that can increase the efficiency of transfection and expression by preventing DNA methylation [98]. The expression pattern of GFP-SCX was not altered by sodium butyrate addition.

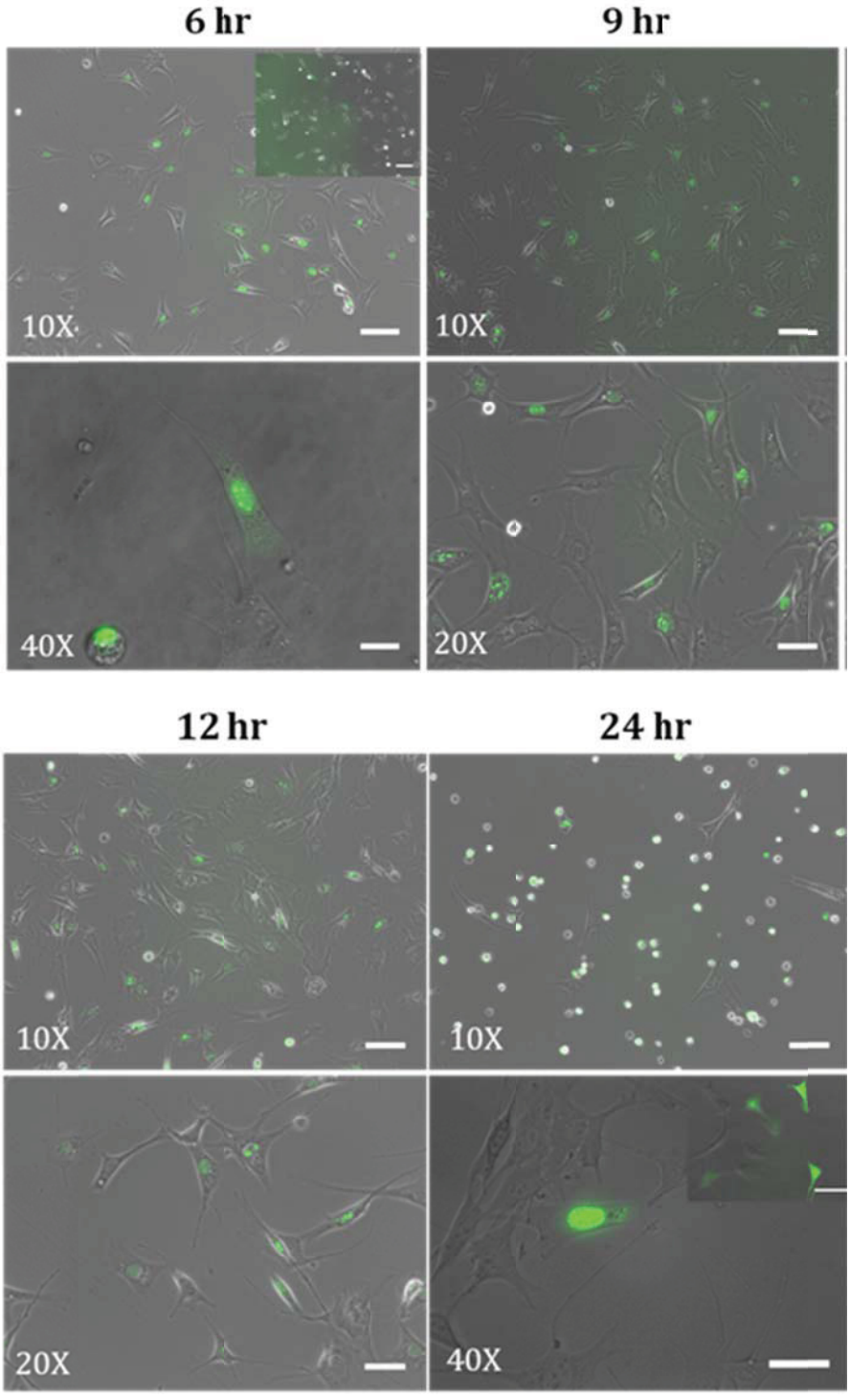

Figure 5.10: Temporal expression pattern of scleraxis-GFP fusion protein (green) in C3H10T1/2 cells following transient transfection with pCMV-GFP-SCX. Inset images show GFP expression in the control plasmid. Low resolution (10X) and high resolution (20X, 40X) micrographs are shown. Scale bars: 100um (10X), 50 um (20X) and 25 um (40X).

To further investigate the morphological changes seen following transfection with SCX-GFP, cellular viability, cytotoxicity and apoptosis activity was measured following transient transfection with Xpress-SCX. Transfection with SCX-GFP was not possible as the GFP excitation/emission wavelengths would overlap with the fluorescent substrates used in the assay. Using a multiplex assay, viability, cytotoxicity and caspase 3/7 activation events were assessed within a single assay well. Following transfection, the cytotoxicity index (C.I.) was similar between cells transfected with Xpress-SCX, LacZ or without plasmid DNA Figure 5.11b). However, the apoptotic index (A.I.) was higher in transfected cells where plasmid DNA was introduced at all timepoints measured (Figure 5.11a). Up to 24 hours post-transfection, Xpress-SCX transfected cells had a slightly greater apoptotic index than LacZ-transfected cells. The corresponding cytotoxicity index was similar between Xpress-SCX and LacZ-transfected cells but less than cells without exogenous plasmid DNA. Plating density following transfection did affect the calculated indices. At 6 hours, Xpress-SCX transfected cells had a significantly greater cytotoxicity index (12) and apoptotic index (112) than control transfectants (Xpress-LacZ cells, C.I. = 1.59, A.I. = 11.15) when plated a lower cell density (7,812 cells/cm^2) (Figure 5.12a, b). By 9 hours, both Xpress-SCX transfected cell indices were similar to controls.

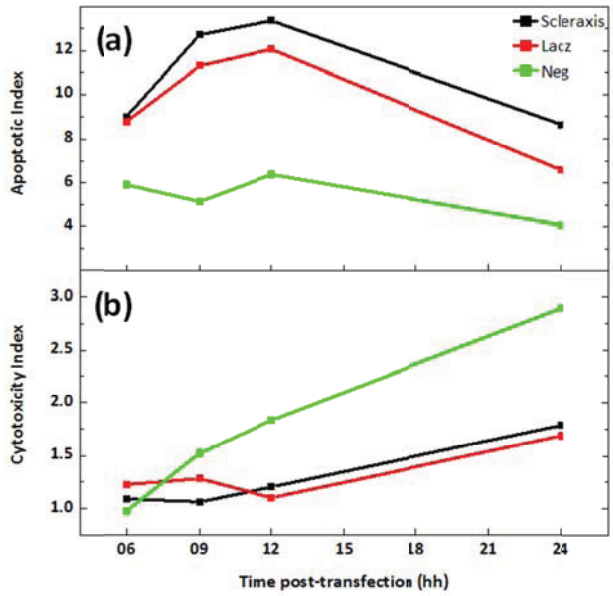

Figure 5.11: Analysis of viability, cytoxicity and caspase 3/7 activity in nearly-confluent C3H10T1/2 cells following transient transfection with pcDNA3.1/His/SCX using ApoTox-Glo triplex assay. C3H10T1/2 cells were seeded 31,250 cells/cm² following transfection then assayed over a 24 hour time period. The apoptotic index was calculated by dividing the live-cell viability (RFU) by the caspase 3/7 activation value (RLU) (a). A cytotoxicity index was established at each timepoint dividing the dead-cell value (RFU) by the live-cell value (RFU) (b).

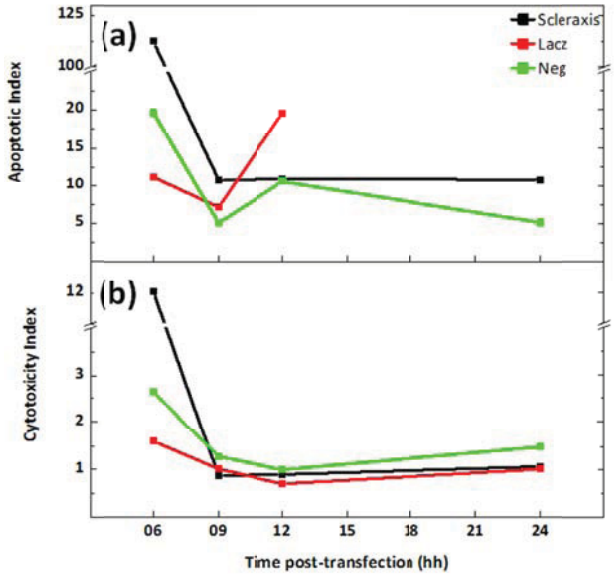

Figure 5.12: Analysis of viability, cytoxicity and caspase 3/7 activity in low density C3H10T1/2 cells following transient transfection with pcDNA3.1/His/SCX using ApoTox-Glo triplex assay. C3H10T1/2 cells were seeded 7,812 cells/cm² following transfection then assayed over a 24 hour time period. The apoptotic index was calculated by dividing the live-cell viability (RFU) by the caspase 3/7 activation value (RLU) (a). A cytotoxicity index was established at each timepoint dividing the dead-cell value (RFU) by the live-cell value (RFU) (b).

Discussion

To investigate scleraxis as a transcription factor responsible for inducing MSCs *in vitro* to differentiate along a ligament lineage, initial studies were performed to test the central hypothesis that overexpression of the transcription factor scleraxis induces mesenchymal stem cells to progress into the ligament/tendon fibroblasts lineage and to mature into tendon/ligament tissue. Considerable published support for this hypothesis derives from the following: (1) the basic helix-loop-helix proteins are known to play critical roles in differentiation and development by controlling tissue-specific gene expression [114, 136], (2) scleraxis is specifically expressed throughout tendon and ligament development [36, 212], and (3) scleraxis regulates the expression of two ligament-selective extracellular matrix proteins, tenomodulin and collagen type I [141, 218]. These data suggest that scleraxis is a major transcription factor associated with the early stages of tendon and ligament differentiation, and that its overexpression might accelerate differentiation along the tendon and ligament lineage.

In the current study, scleraxis was exogenously expressed in multipotent C3H10T1/2 cells. Vectors (pcDNA3.1/His/SCX or pCMV-GFP-SCX) containing scleraxis cDNA were transferred into cells using nucleofection, a modified electroporation technique used for many stem cell types. In both vectors used, scleraxis gene expression was directed from the constitutive cytomegalovirus (CMV) promoter. Following transient transfection, scleraxis transcript levels peaked at 6 hours post-transfection and then returned to baseline levels by 72 hours. Peak transcipt levels were 1,000-fold greater than untransfected cells but transcript levels of potential target ECM genes (e.g. collagen type I and tenomodulin) were unchanged. Using standard detection techniques, scleraxis protein

could not be identified in transfected cell lysates. Thus, a second plasmid fusing scleraxis with an easily detectable GFP tag was then used to identify scleraxis protein. GFP-SCX localized to the cell nucleus within 6 hours post-transfection and produced high levels of protein expression (as evidenced by signal intensity). However, cells expressing GFP-SCX appeared to undergo coordinated cell death by 24 hours post-transfection. Subsequent quantification of caspase 3/7 activity, an early marker for extrinsic (receptor-mediated) apoptosis, following introduction of Xpress-SCX to the cell was inconclusive.

Scleraxis fusion proteins were used to identify exogenous scleraxis protein because proven antibodies to native scleraxis proteins are not commercially available. Epitope tags were used to detect scleraxis fusion proteins during antibody-antigen reactions. Epitope tags have been fused at the n-terminus and c-terminus of scleraxis with no apparent loss of function. The pcDNA3.1/His/SCX vector introduced a short Xpress™ tag and 6X His sequence to the N-terminus of scleraxis cDNA. This identical vector has reportedly induced collagen 1α1 promoter activity in NIH/3T3 cells and C2 myoblasts and exhibited DNA-binding activity in COS-7 cells [141]. Anti- Xpress™ has also been successfully used in supershift assays. In this study, western blots performed to verify scleraxis protein production using anti-Xpress™ were unsuccessful for undetermined reasons.

The protein structure of scleraxis likely contributed to the inability to detect the protein in cell lysates using western blot. Western blotting is a common analytical technique to identify proteins, separated by SDS-PAGE electrophoresis. Electrophoresis separates proteins based on size, isoelectric point (pI) or both. The pI of scleraxis was calculated as approximately 10, owing to the large motif of basic amino acids within the structure. The common Towbin buffer system used for western blot techniques has a pH of

7.4. In this setup, scleraxis was undetectable; however; all controls were detected, confirming correct technique. A CAPS buffer system with a pH of 11 is preferred for high isoelectric point proteins and was tested with cell lysates expressing scleraxis (Figure 5.5b). With the CAPS buffer, scleraxis remained undetectable and the recombinant control was detected but Xpress-LacZ was only weakly detected. Further modifications, including concentration of cell lysates using Ni-NTA beads, were also unsuccessful, suggesting a possible error in the vector sequence.

Sequencing analysis confirmed the correct open reading frame to produce Xpress-SCX transcripts but additional validation was also performed. To further verify proper production of protein and discover potential pitfalls in the western blot method, coupled transcription/translation was performed in a cell-free system with pcDNA3.1/His/SCX. Using the *in vitro* translation product (labeled with [^{35}S]Met), Xpress-tagged scleraxis was found to migrate in the SDS-PAGE gel as expected (detected using autoradiography) but transfer to the PVDF membrane under standard conditions was unsuccessful. Scleraxis is a small protein of 207 amino acids with molecular weight of 22 kDa [60] or 39 kDa with the addition of the Xpress™ epitope tag and may pass through the membrane. The inability to detect scleraxis protein in cell lysates through this common analytical technique led to the use of another vector system.

GFP–scleraxis fusion protein was produced from a C-terminus GFP sequence in the pCMV-GFP-SCX vector. In general, GFP is considered non-toxic and more sensitive than other tags in labeling proteins. The specific GFP used in this study is derived from the copepod *Pontellina plumata* and has no known cellular toxicity [215]. Using non-destructive imaging to detect scleraxis following transfection, a scleraxis fusion protein

expressing GFP was used. Following transient tranfection, GFP positive cells, thus expressing the SCX-GFP fusion protein, were observed under fluorescent microscopy. As early as 6 hours post-transfection, GFP signal was predominately located in the nucleus with only very faint signal in the cytoplasm. In contrast, transfection of the control GFP vector (pmaxGFP) produced strong signal throughout the entire cell body. This suggests that the scleraxis protein is immediately translocated to the nucleus following translation in the cytoplasm. Using Nucleofector® technology, plasmid DNA can directly enter the nucleus as well as the cytoplasm. With plasmid DNA in the nucleus, the exogenous DNA can be integrated into the host genome despite all translation occuring in the cytoplasm. Translated products can then enter the nucleus. The absence of SCX-GFP signal in the cytoplasm suggests that following initial translation prior to 6 hours, either the plasmid DNA is inactivated or the protein is immediately degraded by regulatory mechanisms within the cell. Observations of SCX-GFP signals earlier post-transfection could provide further clues to this regulation.

Scleraxis-transfected cells with positive GFP signal underwent morphological changes resulting in cellular detachment from the culture plate. Starting at 12 hours post transfection, GFP-positive cells began to shrink and become less spindle-shaped. In addition, granulated bodies appeared within the cells and the SCX-GFP signal became compartmentalized to discrete areas of the nucleus. Recent advances have demonstrated that the nucleus is composed of a number of subnuclear structures including Cajal bodies, speckles and promyelocytic leukaemia bodies [269]. Whether SCX-GFP is localized to one of these subnuclear bodies is not clear and could be qualitatively determined by co-immunostaining in future experiments. As time progressed, SCX-GFP positive cells became

more condensed and the membrane structures began to bleb. By 24 hours, the majority of SCX-GFP positive cells were rounded and floating, suggesting cell death. In contrast, cells transfected with GFP alone showed continual expression and increased signal intensity for a minimum of 48 hours. Only a few reports have shown the morphology of scleraxis-transfected cells using microscopy. Cardiac myofibroblasts 24 hours after infection with adenovirus-encoding HA-tagged scleraxis were immunostained with anti-HA and showed localization of the scleraxis to the nucleus [77]. Transfection of HEK293T cells with the pCVM-GFP-SCX vector also indicated scleraxis localization to the nucleus after 48 hours [189]. Interestingly, further inspection of these images indicates irregular cellular morphology as well. The observations in the current study suggest activation of an apoptotic pathway [74]. However, only minimal increases in caspase 3/7, an early marker of the intrinsic apoptotic pathway, were found in scleraxis-transfected cells. Activation of other apoptotic or regulatory pathways is possible. In addition, the activity of this transcription factor may be dictated by other factors.

The scleraxis protein is a member of the bHLH transcription factor superfamily and can bind a consensus E-box (CANNTG) located in promoter/enhancer regions of tissue-specific genes. These DNA-binding proteins are important regulatory components in many cellular processes including developmental pathways, proliferation and sex determination [16, 177]. Specifically, scleraxis is a member of the Class B bHLH structural family of proteins, dictated by a large basic amino acid region. The helix-loop-helix (HLH) motif of primarily hydrophobic residues allows scleraxis and other bHLH proteins to interact and form homo and/or heterodimers. Heterodimerization with the *E2A* gene products E12 and E47 is preferred by the Class B proteins [136]. While the majority of literature regarding

regulation and function of bHLH proteins has focused on myoD, recent studies have reported increased DNA-binding activity when scleraxis is co-transfected with E12 or E47 [44, 60, 77, 141]. In these studies, scleraxis DNA-binding activity was measured using reporter systems harboring promoter regions of muscle creatine kinase [44], transferrin [174] , Col1α1 [141], and Col1α2 [77]. Without additional alterations, osteosarcoma Ros 17/2.8 cells with forced scleraxis expression under control of the SV40 promotor increased aggrecan, collagen type 2 and osteopontin levels [150]. With both osteogenic and chondrogenic gene expression changes, the results of the Ros 17/2.8 cell study are problematic. In the current study, mRNA expression levels of potential targets of scleraxis activity (e.g. collagen type 1α1) were unchanged following transfection (Figure 5.7 and Figure 5.8). The rate limiting component to DNA-binding activity may have been insufficient levels of E12/E47 within in the cell. Co-transfection with E12 or E47 may enhance downstream gene effects in the current design.

The combination of scleraxis-induced morphological changes and inability to detect scleraxis in cell lysates implies epigenetic regulation within the cell. The addition of sodium butyrate, a histone deacetylase inhibitor, did not improve cell survival following transfection with GFP-SCX as expected if methylation of plasmid DNA is occurring. Scleraxis activity may also be regulated by the dominant negative family of HLH proteins, including inhibitor of differentiation (Id) proteins, that antagonize dimerization and prevent DNA binding [129]. Finally, the CMV promoter used in the scleraxis vectors has been reported to be silenced *in vivo* and *in vitro* [201]. However, CMV silencing occurred over an extended period of time in these reports while scleraxis was almost immediately downregulated in this study.

The results of this study reveal the potential levels of control that cells have over transcription factor activity. The constitutive CMV promoter directs uninhibited scleraxis expression that appears detrimental to cell function. Future work will need to provide controlled gene expression in transfected MSCs. Transfection with an inducible vector carrying the scleraxis gene would permit expression only at discrete timepoints. Stable clones carrying an inducible scleraxis gene could be used to further explore the functional role of scleraxis in directing stem cell differentiation.

Conclusions

Intracellular signals may direct precursor cell differentiation into mature tendon or ligament fibroblasts. Transient transfection of scleraxis showed scleraxis gene expression peaking at 6 hours but returning to basal levels by 48 hours. Moderate expression changes in tendon/ligament genes were observed following transfection. Forced expression of GFP-tagged scleraxis indicated complete localization to the cell nucleus eventually resulting in cell death. However, only minimal increases in apoptotic activity were observed. Results from forced constitutive expression of the transcription factor, scleraxis, suggested activation of a complex, highly regulated pathway.

Acknowledgments

This project was funded in part by Virginia Tech Foundation and NIH fellowship #AR055872 to RDC. The authors thank Dr. William Huckle and Dr. Willard Eyestone for the helpful discussions and technical insights into this challenging project!

Chapter 6: Conclusions and Future Directions

Summary of Results

The main objective of this research project centered on the development of tissue engineered tendon/ligament grafts by directed differentiation of mesenchymal stem cells (MSCs) on fibrous elastomeric biomaterial scaffolds. Towards this goal, the effects of scaffold architecture, cyclic mechanical stretch and forced expression of the transcription factor scleraxis on cellular behavior were investigated.

In developing a strategy for a tissue engineered tendons and ligaments, the first objective was to identify biomaterial scaffold properties that maximized ECM gene expression and protein deposition while supporting cellular growth. The fibrous scaffolds tested in this project were fabricated by electrospinning a segmented poly(esterurethane urea) under different conditions to produce scaffolds with variations in fiber diameter and fiber alignment. Primary MSCs and the mesenchymal stem cell line, C3H10T1/2, were sensitive to the scaffold architecture. Individual fibers provided guidance cues to orient the cells and induce a spindle-shaped morphology. Elongation of primary MSCs increased with increasing fiber alignment. The mean fiber diameter within the scaffold affected cellular responses, including lineage differentiation, more substantially than the alignment of the fibers within the scaffold. Variation of the average fiber diameter within the matrix had pronounced effects on cellular morphology, growth and gene expression. Initially, both cell types had decreased cell density on the largest (≥ 2 μm) mean diameter fiber scaffolds but continued to proliferate. Expression of collagen type I and decorin genes was elevated on smaller (≤ 1 μm) mean diameter scaffolds. However, as culture continued, gene expression

on the largest (≥ 2μm) mean diameter scaffolds surpassed that on the smaller fiber scaffolds. These results suggest that large diameter fibers (≥ 2 μm) may be more suitable for development of a tendon/ligament graft *in vitro*.

In the second objective, mechanical stimulation was applied to cell-seeded scaffolds to determine if *in vitro* maturation of the tissue engineered constructs could be accelerated. Electrospun PEUUR scaffolds with two distinct mean fiber diameters in a semi-aligned orientation were prepared. C3H10T1/2 cells were seeded onto scaffolds using a custom platform. Following preloading, cyclic stretch was applied to 4% elongation for 30 minutes per day. Using the imaging modality of the bioreactor, cell attachment was verified during and after mechanical stress. Cells were found to change their morphology substantially following a short stimulation period, while gene expression differences between cyclically loaded, statically loaded, and unstretched cells were moderate. Results suggest that fiber diameter may play a role under dynamic culture as previously documented under static culture. In addition to use for accelerating cell differentiation and matrix development *in vitro*, the results of bioreactor studies might also be used for predicting constructs' physiologic responses to *in vivo* environments.

In the third objective, a tendon/ligament specific transcription factor, scleraxis, was over-expressed in MSCs to evaluate the potential of this signaling molecule in directed differentiation along a tendon/ligament lineage. Intracellular signals may direct precursor cell differentiation into mature tendon or ligament fibroblasts. Transient transfection resulted in scleraxis gene expression peaking at 6 hours but returning to basal levels by 48 hours. Moderate expression changes in tendon/ligament genes were observed following transfection. Using a second vector, forced expression of GFP-tagged scleraxis indicated

complete localization to the cell nucleus. This suggests that the constitutive expression of the gene product induced cell death; however, only minimal increases in apoptotic activity were observed. The combination of scleraxis-induced morphological changes and inability to detect scleraxis in cell lysates implies initiation of regulatory mechanisms within the cell.

Future Recommendations

The experimental methods and subsequent results developed during the course of this research project present promising approaches for the development of tendon/ligament tissue grafts. Further investigations in the following areas will extend this work in pursuit of developing approaches for directed differentiation of stem cells and the subsequent generation of a more robust tissue graft.

Improving cell ingress through scaffold modifications

The electrospun scaffolds used in this work need additional modifications in order to support formation of a fully functional ligament graft. The dense fibrous matrix formed by the electrospinning process provides a micropattern for directing cell and matrix growth, but physically impedes cellular infiltration from the top surface [157]. Increasing the rate of polymer degradation would assist cellular migration into the middle of the scaffold as culture time progresses. However, this approach would severely decrease the scaffold's mechanical properties. To maintain mechanical integrity of the elastomeric polyurethane, cells would need to be integrated during the formation of electrospun scaffolds. Integration could be accomplished through simultaneous electrospraying [229].

Alternatively, by modifying the polymer's backbone, individual fibers could be designed to swell under certain conditions, thereby increasing the pore size. Cell infiltration is improved when the pore size is increased. Swelling conditions of these

'smart' materials would need to be biocompatible, reversible and occur independently of an aqueous environment. Addition of another electrospun polymer with known swelling characteristics (e.g. uncrosslinked chitosan) into the scaffold, through the process of co-electrospinning, may facilitate this method. With an additional fiber type, the diameter could be made much larger than PEUUR fibers and serve as reinforcement to the scaffold. In addition, during swelling of the second polymer, the PEUUR inter-fiber space would be increased. After seeding, the swelling stimuli can be removed and fibers return to their 'as spun' diameter. Dynamic seeding on the scaffolds would also improve cell ingress [203, 247].

Improving integration in vivo

Clinically relevant tendon or ligament replacements will require integration at the bone-ligament, bone-tendon or muscle-tendon interfaces. For the ACL, osseous tunnels through the tibia and femur provide anchor points for the graft [89]. Grafts must integrate within these bone tunnels in order to provide stability to the knee joint. The current electrospun PEUUR scaffold does not contain graded fiber architectures or mechanical properties. Using multiple, offset spinnerets during electrospinning would allow construction of a scaffold with a gradient of fiber size or polymer type. Formation of transitional zones within the electrospun scaffolds would improve *in vivo* functional outcomes through ordered mechanical properties and directed differentiation to stem cells at each zone.

Enhancing matrix development by increasing duration of cyclic mechanical strain

In vitro mechanical stimulation is known to increase extracellular matrix deposition when applied for multiple weeks [7, 67]. In Chapter 4, cyclic stretch was applied for only 3 days, resulting in only moderate changes in gene expression of tendon/ligament matrix constituents. Increasing the magnitude or elongation of stretch has been shown to alter behavior in a number of cell types [65, 120]. Four percent elongation mimics native ACL tissue environment [31]. Increased magnitude and frequency of cyclic stimulation beyond normal tissue homeostasis has been associated with the etiology of tendon overuse injuries *in vivo* [13]. Without alterations in the regimen (magnitude, frequency), simply increasing the number of days or weeks of stress application would alter gene expression and matrix deposition in our constructs. In addition, each construct can be monitored to ensure cell attachment and development of collagenous matrix throughout the experiment using confocal microscopy to further optimize the stretch regimen. To facilitate *in situ* monitoring, cells could be labeled with a long term cell tracer or modified to constitutively express GFP or another fluorescent molecule. Using the current bioreactor system, second-harmonic generation microscopy can also be used to image collagen fibrillogenesis in the developing construct [258].

Initiating differentiation through regulated scleraxis expression

In the vector system described in Chapter 5, scleraxis was under control of the constitutive CMV promoter. Constitutive expression of scleraxis in progenitor cells was detrimental to cell survival and stable scleraxis-expressing cell lines could not be established, perhaps due to regulatory activity within the cell. The CMV promoter has

widespread use in directing 'always on' exogenous gene expression in mammalian cells but can be silenced by DNA methylation [201]. The results of this work suggest that forced, continuous expression of scleraxis might alter the epigenetics of the cell. During embryogenesis, scleraxis expression levels are variable during somite formation and development [60]. To further investigate this transcription factor, stem cell transfection with an inducible vector carrying the scleraxis gene would permit expression only at discrete timepoints. Using the pTUNE inducible vector (OriGene), scleraxis transcription can be induced following addition of isopropyl β-D-1-thiogalactopyranoside (IPTG) to the culture media [63]. Using pTUNE, the functional role of scleraxis in directing stem cell differentiation can be explored.

Alternatively, scleraxis activity could be regulated through co-transfection of known enhancers or antagonists. Basic helix-loop-helix transcription factors bind DNA through dimerization, either heterodimers or homodimers [122]. DNA binding properties differ between heterodimers and thus can elicit distinct biological activites [122]. In fact, scleraxis DNA binding activity is significantly increased when co-expressed with E47, another class of bHLH transcription factor [44]. Co-transfection of scleraxis with E47 may enhance transcriptional activation and thus increase expression of potential extracellular matrix genes. Alternatively, concurrent down regulation of dominant-negative HLH proteins (dnHLH) may induce differentiation. dnHLH proteins, such as inhibitor of differentiation (Id), dimerize with other bHLH proteins but cannot bind DNA [122]. Blocking Id activity during scleraxis overexpression could be achieved through siRNA methods. Forced expression of Id has been found to block differentiation of myeloid cells, which undergo subsequent apoptosis [129].

Modifying culture environment to synergistically enhance differentiation

The bulk of this work has built a foundation for inducing functional tendon/ligament constructs through directed differentiation of mesenchymal stem cells, exploring complementary methods. Scleraxis may play a role in the induction of tenocytes from progenitor cells and initial studies were performed to support this hypothesis during the course of this work. However, researchers have suggested that additional signals are required for final formation of the tendon/ligament tissue and that over-expression of scleraxis alone is not sufficient for a phenotypic change [150, 212]. The addition of mechanical stimuli, growth factor augmentation and a three-dimensional (3D) environment may facilitate induction of differention along the tendon/ligament fibroblast lineage. Preliminary studies using 3D type I collagen gels show increased gene expression of collagen types 1 and 3 in scleraxis-transfected cells, compared to non-transfected cells, suggesting a synergistic effect of scleraxis expression and the 3D culture conditions (Figure 6.1). These collagen gels can be untethered, tethered, or cyclically stretched using the FlexCell Tissue Train system [90]. The integration of scleraxis overexpression and mechanical stimulation through 3D collagen gels could improve matrix expression and production.

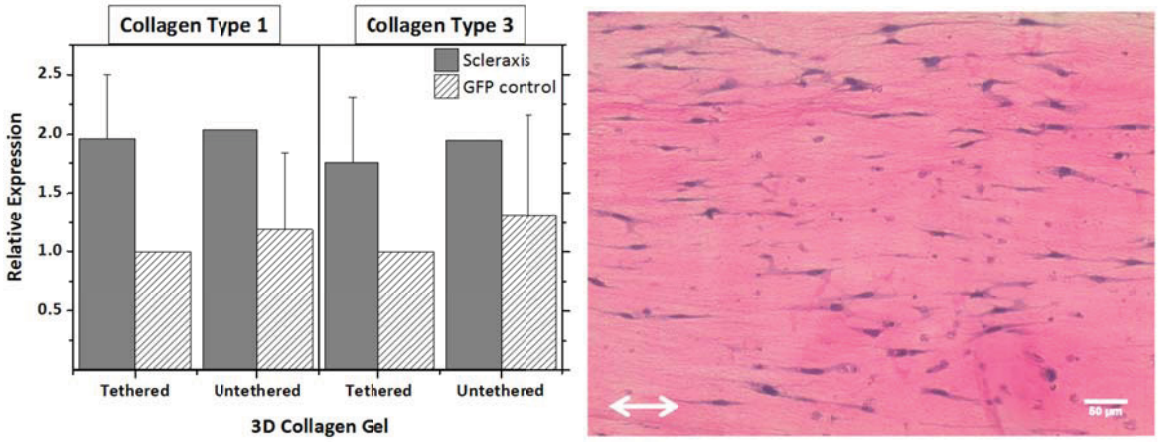

Figure 6.1: Preliminary data for scleraxis-transfected cells in 3D collagen gels. Gene expression of collagen types 1 and 3 was measured following culture of scleraxis transiently transfected cells in tethered or untethered collagen gels for 3 days (n= 1 or 2, mean ± SEM) (a). Photomicrograph of sectioned three-dimensional collagen gel stained with hematoxylin and eosin. This gel was seeded with C3H10T1/2 cells and cultured under static conditions for 4 days. The cells demonstrate the expected alignment parallel to the direction of tension (arrow) created by the anchors holding the ends of the three-dimensional construct (b).

Bibliography

1. Abe, S., et al., *Light and electron microscopic study of remodeling and maturation process in autogenous graft for anterior cruciate ligament reconstruction.* Arthroscopy, 1993. 9(4): p. 394-405.
2. Agarwal, C., et al., *Healing and normal fibroblasts exhibit differential proliferation, collagen production, alpha-SMA expression, and contraction.* Ann Biomed Eng, 2006. 34(4): p. 653-9.
3. Alhadlaq, A. and J.J. Mao, *Mesenchymal stem cells: isolation and therapeutics.* Stem Cells Dev, 2004. 13(4): p. 436-48.
4. Almarza, A.J., S.M. Augustine, and S.L. Woo, *Changes in gene expression of matrix constituents with respect to passage of ligament and tendon fibroblasts.* Ann Biomed Eng, 2008. 36(12): p. 1927-33.
5. Altman, G.H., et al., *Silk-based biomaterials.* Biomaterials, 2003. 24(3): p. 401-16.
6. Altman, G.H., et al., *Silk matrix for tissue engineered anterior cruciate ligaments.* Biomaterials, 2002. 23(20): p. 4131-41.
7. Altman, G.H., et al., *Cell differentiation by mechanical stress.* Faseb J, 2002. 16(2): p. 270-2.
8. Altman, G.H., et al., *Advanced bioreactor with controlled application of multi-dimensional strain for tissue engineering.* J Biomech Eng, 2002. 124(6): p. 742-9.
9. Amiel, D., et al., *Tendons and ligaments: a morphological and biochemical comparison.* J Orthop Res, 1984. 1(3): p. 257-65.
10. Archambault, J.M., et al. *Identification of Tendon and Ligament Specific Genes*. in *52nd Annual Meeting of the Orthopaedic Research Society*. 2006.
11. Archambault, J.M., et al. *Identification of tendon and ligament specific genes*. in *Trans Orthop Res Soc*. 2006.
12. Arnoczky, S.P., *Blood supply to the anterior cruciate ligament and supporting structures.* Orthop Clin North Am, 1985. 16(1): p. 15-28.
13. Arnoczky, S.P., M. Lavagnino, and M. Egerbacher, *The mechanobiological aetiopathogenesis of tendinopathy: is it the over-stimulation or the under-stimulation of tendon cells?* Int J Exp Pathol, 2007. 88(4): p. 217-26.
14. Aslan, H., et al., *Molecular targets for tendon neoformation.* J Clin Invest, 2008. 118(2): p. 439-44.
15. Asou, Y., et al., *Coordinated expression of scleraxis and Sox9 genes during embryonic development of tendons and cartilage.* 2002.
16. Atchley, W.R. and W.M. Fitch, *A natural classification of the basic helix-loop-helix class of transcription factors.* Proc Natl Acad Sci U S A, 1997. 94(10): p. 5172-6.
17. Awad, H.A., et al., *In vitro characterization of mesenchymal stem cell-seeded collagen scaffolds for tendon repair: effects of initial seeding density on contraction kinetics.* J Biomed Mater Res, 2000. 51(2): p. 233-40.
18. Ayres, C.E., et al., *Measuring fiber alignment in electrospun scaffolds: a user's guide to the 2D fast Fourier transform approach.* J Biomater Sci Polym Ed, 2008. 19(5): p. 603-21.
19. Badami, A.S., et al., *Effect of fiber diameter on spreading, proliferation, and differentiation of osteoblastic cells on electrospun poly(lactic acid) substrates.* Biomaterials, 2006. 27(4): p. 596-606.

20. Badylak, S., et al., *Naturally occurring extracellular matrix as a scaffold for musculoskeletal repair.* Clin Orthop Relat Res, 1999(367 Suppl): p. S333-43.
21. Baker, B.M., et al., *The potential to improve cell infiltration in composite fiber-aligned electrospun scaffolds by the selective removal of sacrificial fibers.* Biomaterials, 2008. 29: p. 2348-2358.
22. Baker, B.M. and R.L. Mauck, *The effect of nanofiber alignment on the maturation of engineered meniscus constructs.* Biomaterials, 2007. 28(11): p. 1967-77.
23. Balestrini, J.L. and K.L. Billiar, *Equibiaxial cyclic stretch stimulates fibroblasts to rapidly remodel fibrin.* J Biomech, 2006. 39(16): p. 2983-90.
24. Banes, A., et al., *Mechanical forces and signaling in connective tissue cells: cellular mechanisms of detection, transduction, and responses to mechanical deformation.* Current Opinion in Orthopaedics, 2001. 12: p. 389-396.
25. Banos, C.C., A.H. Thomas, and C.K. Kuo, *Collagen fibrillogenesis in tendon development: current models and regulation of fibril assembly.* Birth Defects Res C Embryo Today, 2008. 84(3): p. 228-44.
26. Bashur, C.A., *Effect of electrospun mesh diameter, mesh alignment, and mechanical stretch on bone marrow stromal cells for ligament tissue engineering*. 2009, University Libraries, Virginia Polytechnic Institute and State University: Blacksburg, Va.
27. Bashur, C.A., L.A. Dahlgren, and A.S. Goldstein, *Effect of fiber diameter and orientation on fibroblast morphology and proliferation on electrospun poly(D,L-lactic-co-glycolic acid) meshes.* Biomaterials, 2006. 27(33): p. 5681-8.
28. Bashur, C.A., et al., *Effect of fiber diameter and alignment of electrospun polyurethane meshes on mesenchymal progenitor cells.* Tissue Eng Part A, 2009. 15(9): p. 2435-45.
29. Bellincampi, L.D., et al., *Viability of fibroblast-seeded ligament analogs after autogenous implantation.* J Orthop Res, 1998. 16(4): p. 414-20.
30. Benjamin, M., E. Kaiser, and S. Milz, *Structure-function relationships in tendons: a review.* J Anat, 2008. 212(3): p. 211-28.
31. Beynnon, B.D. and B.C. Fleming, *Anterior cruciate ligament strain in-vivo: a review of previous work.* J Biomech, 1998. 31(6): p. 519-25.
32. Bhandari, M., et al., *Treatment of acute Achilles tendon ruptures: a systematic overview and metaanalysis.* Clin Orthop Relat Res, 2002(400): p. 190-200.
33. Birk, D.E. and R. Mayne, *Localization of collagen types I, III and V during tendon development. Changes in collagen types I and III are correlated with changes in fibril diameter.* Eur J Cell Biol, 1997. 72(4): p. 352-61.
34. Borkenhagen, M., et al., *In vivo performance of a new biodegradable polyester urethane system used as a nerve guidance channel.* Biomaterials, 1998. 19(23): p. 2155-65.
35. Brandau, O., et al., *A novel gene, tendin, is strongly expressed in tendons and ligaments and shows high homology with chondromodulin-I.* Dev Dyn, 2001. 221(1): p. 72-80.
36. Brent, A.E., R. Schweitzer, and C.J. Tabin, *A somitic compartment of tendon progenitors.* Cell, 2003. 113(2): p. 235-48.
37. Brown, C.H., Jr. and E.W. Carson, *Revision anterior cruciate ligament surgery.* Clin Sports Med, 1999. 18(1): p. 109-71.
38. Butler, D.L., et al., *Using functional tissue engineering and bioreactors to mechanically stimulate tissue-engineered constructs.* Tissue Eng Part A, 2009. 15(4): p. 741-9.

39. Butler, D.L., et al., *Functional tissue engineering for tendon repair: A multidisciplinary strategy using mesenchymal stem cells, bioscaffolds, and mechanical stimulation.* J Orthop Res, 2008. 26(1): p. 1-9.
40. Byers, B.A., et al., *Cell-type-dependent up-regulation of in vitro mineralization after overexpression of the osteoblast-specific transcription factor Runx2/Cbfal.* J Bone Miner Res, 2002. 17(11): p. 1931-44.
41. Cacou, C., et al., *A system for monitoring the response of uniaxial strain on cell seeded collagen gels.* Med Eng Phys, 2000. 22(5): p. 327-33.
42. Caplan, A.I., *Adult mesenchymal stem cells for tissue engineering versus regenerative medicine.* J Cell Physiol, 2007. 213(2): p. 341-7.
43. Carlberg, A.L., et al., *Efficient chondrogenic differentiation of mesenchymal cells in micromass culture by retroviral gene transfer of BMP-2.* Differentiation, 2001. 67(4-5): p. 128-38.
44. Carlberg, A.L., R.S. Tuan, and D.J. Hall, *Regulation of scleraxis function by interaction with the bHLH protein E47.* Mol Cell Biol Res Commun, 2000. 3(2): p. 82-6.
45. Carlstedt, C. and M. Nordin, *Biomechanics of tendons and ligaments*, in *Basic Biomechanics of the Musculoskeletal System*, M. Nordin and V. Frankel, Editors. 1989, Lea & Febiger: Malvern, PA. p. 59-74.
46. Caruso, A.B. and M.G. Dunn, *Changes in mechanical properties and cellularity during long-term culture of collagen fiber ACL reconstruction scaffolds.* J Biomed Mater Res A, 2005. 73(4): p. 388-97.
47. Chamberlain, G., et al., *Concise review: mesenchymal stem cells: their phenotype, differentiation capacity, immunological features, and potential for homing.* Stem Cells, 2007. 25(11): p. 2739-49.
48. Charest, J.L., A.J. Garcia, and W.P. King, *Myoblast alignment and differentiation on cell culture substrates with microscale topography and model chemistries.* Biomaterials, 2007. 28(13): p. 2202-10.
49. Chen, J., et al., *Monitoring Mesenchymal Stromal Cell Developmental Stage to Apply On-Time Mechanical Stimulation for Ligament Tissue Engineering.* Tissue Eng, 2006.
50. Chen, M., et al., *Role of fiber diameter in adhesion and proliferation of NIH 3T3 fibroblast on electrospun polycaprolactone scaffolds.* Tissue Eng, 2007. 13(3): p. 579-87.
51. Chen, Y.J., et al., *Effects of cyclic mechanical stretching on the mRNA expression of tendon/ligament-related and osteoblast-specific genes in human mesenchymal stem cells.* Connect Tissue Res, 2008. 49(1): p. 7-14.
52. Chew, S.Y., et al., *The effect of the alignment of electrospun fibrous scaffolds on Schwann cell maturation.* Biomaterials, 2008. 29(6): p. 653-61.
53. Chia, S.L., et al., *Biodegradable Elastomeric Polyurethane Membranes as Chondrocyte Carriers for Cartilage Repair.* Tissue Eng, 2006.
54. Chiquet, M., A. Sarasa-Renedo, and V. Tunc-Civelek, *Induction of tenascin-C by cyclic tensile strain versus growth factors: distinct contributions by Rho/ROCK and MAPK signaling pathways.* Biochim Biophys Acta, 2004. 1693(3): p. 193-204.
55. Christopherson, G.T., H. Song, and H.Q. Mao, *The influence of fiber diameter of electrospun substrates on neural stem cell differentiation and proliferation.* Biomaterials, 2009. 30(4): p. 556-64.

56. Connelly, J.T., et al., *Tensile loading modulates bone marrow stromal cell differentiation and the development of engineered fibrocartilage constructs.* Tissue Eng Part A, 2010. 16(6): p. 1913-23.
57. Cooper, J.A., Jr., et al., *Evaluation of the anterior cruciate ligament, medial collateral ligament, achilles tendon and patellar tendon as cell sources for tissue-engineered ligament.* Biomaterials, 2006. 27(13): p. 2747-2754.
58. Cooper, J.A., et al., *Fiber-based tissue-engineered scaffold for ligament replacement: design considerations and in vitro evaluation.* Biomaterials, 2005. 26(13): p. 1523-32.
59. Courtney, T., et al., *Design and analysis of tissue engineering scaffolds that mimic soft tissue mechanical anisotropy.* Biomaterials, 2006. 27(19): p. 3631-8.
60. Cserjesi, P., et al., *Scleraxis: a basic helix-loop-helix protein that prefigures skeletal formation during mouse embryogenesis.* Development, 1995. 121(4): p. 1099-110.
61. Curtis, A. and C. Wilkinson, *Topographical control of cells.* Biomaterials, 1997. 18: p. 1573-1583.
62. Dalby, M.J., et al., *The control of human mesenchymal cell differentiation using nanoscale symmetry and disorder.* Nat Mater, 2007. 6(12): p. 997-1003.
63. Deans, T.L., C.R. Cantor, and J.J. Collins, *A tunable genetic switch based on RNAi and repressor proteins for regulating gene expression in mammalian cells.* Cell, 2007. 130(2): p. 363-72.
64. den Braber, E.T., et al., *Scanning electron microscopic, transmission electron microscopic, and confocal laser scanning microscopic observation of fibroblasts cultured on microgrooved surfaces of bulk titanium substrata.* Journal of Biomedical Materials Research, 1998. 40: p. 425-433.
65. Devkota, A.C., et al., *Distributing a fixed amount of cyclic loading to tendon explants over longer periods induces greater cellular and mechanical responses.* J Orthop Res, 2007. 25(8): p. 1078-86.
66. Docheva, D., et al., *Tenomodulin is necessary for tenocyte proliferation and tendon maturation.* Mol Cell Biol, 2005. 25(2): p. 699-705.
67. Doroski, D.M., M.E. Levenston, and J.S. Temenoff, *Cyclic Tensile Culture Promotes Fibroblastic Differentiation of Marrow Stromal Cells Encapsulated in Poly(Ethylene Glycol)-Based Hydrogels.* Tissue Eng Part A, 2010.
68. Ducy, P., et al., *Osf2/Cbfa1: a transcriptional activator of osteoblast differentiation.* Cell, 1997. 89(5): p. 747-54.
69. Dunn, M.G., et al., *Development of fibroblast-seeded ligament analogs for ACL reconstruction.* J Biomed Mater Res, 1995. 29(11): p. 1363-71.
70. Duquin, T.R., C. Buyea, and L.J. Bisson, *Which method of rotator cuff repair leads to the highest rate of structural healing? A systematic review.* Am J Sports Med, 2010. 38(4): p. 835-41.
71. Edom-Vovard, F., et al., *Fgf4 positively regulates scleraxis and tenascin expression in chick limb tendons.* Dev Biol, 2002. 247(2): p. 351-66.
72. Ekdahl, M., et al., *Graft healing in anterior cruciate ligament reconstruction.* Knee Surg Sports Traumatol Arthrosc, 2008. 16(10): p. 935-47.
73. Eliasson, P., T. Andersson, and P. Aspenberg, *Rat Achilles tendon healing: mechanical loading and gene expression.* J Appl Physiol, 2009. 107(2): p. 399-407.
74. Elmore, S., *Apoptosis: a review of programmed cell death.* Toxicol Pathol, 2007. 35(4): p. 495-516.

75. Engelmayr, G.C., Jr., et al., *Cyclic flexure and laminar flow synergistically accelerate mesenchymal stem cell-mediated engineered tissue formation: Implications for engineered heart valve tissues.* Biomaterials, 2006. 27(36): p. 6083-95.
76. Engler, A.J., et al., *Matrix elasticity directs stem cell lineage specification.* Cell, 2006. 126(4): p. 677-89.
77. Espira, L., et al., *The basic helix-loop-helix transcription factor scleraxis regulates fibroblast collagen synthesis.* J Mol Cell Cardiol, 2009. 47(2): p. 188-95.
78. Fan, H., et al., *In vivo study of anterior cruciate ligament regeneration using mesenchymal stem cells and silk scaffold.* Biomaterials, 2008. 29(23): p. 3324-37.
79. Farah, M.H., et al., *Generation of neurons by transient expression of neural bHLH proteins in mammalian cells.* Development, 2000. 127(4): p. 693-702.
80. Farng, E., et al., *The Effects of GDF-5 and Uniaxial Strain on Mesenchymal Stem Cells in 3-D Culture.* Clin Orthop Relat Res, 2008.
81. Ferdous, Z., et al., *Decorin-transforming growth factor- interaction regulates matrix organization and mechanical characteristics of three-dimensional collagen matrices.* J Biol Chem, 2007. 282(49): p. 35887-98.
82. Fischer, L., G. Boland, and R.S. Tuan, *Wnt-3A enhances bone morphogenetic protein-2-mediated chondrogenesis of murine C3H10T1/2 mesenchymal cells.* J Biol Chem, 2002. 277(34): p. 30870-8.
83. Fithian, D.C., et al., *Prospective trial of a treatment algorithm for the management of the anterior cruciate ligament-injured knee.* Am J Sports Med, 2005. 33(3): p. 335-46.
84. Fong, H., I. Chun, and D.H. Reneker, *Beaded nanofibers formed during electrospinning.* Polymer, 1999. 40: p. 4585-4592.
85. Franchi, M., et al., *Different crimp patterns in collagen fibrils relate to the subfibrillar arrangement.* Connect Tissue Res, 2008. 49(2): p. 85-91.
86. Frank, C.B. and D.W. Jackson, *The science of reconstruction of the anterior cruciate ligament.* J Bone Joint Surg Am, 1997. 79(10): p. 1556-76.
87. Freeman, J.W., M.D. Woods, and C.T. Laurencin, *Tissue engineering of the anterior cruciate ligament using a braid-twist scaffold design.* J Biomech, 2007. 40(9): p. 2029-36.
88. Fu, F.H., et al., *Current Trends in Anterior Cruciate Ligament Reconstruction Part I: Biology and Biomechanics of Reconstruction.* The American Journal of Sports Medicine, 1999. 27(6): p. 821-830.
89. Fu, F.H., et al., *Current Trends in Anterior Cruciate Ligament Reconstruction Part II: Operative Procedures and Clinical Correlations.* The American Journal of Sports Medicine, 2000. 28(1): p. 124-130.
90. Garvin, J., et al., *Novel system for engineering bioartificial tendons and application of mechanical load.* Tissue Eng, 2003. 9(5): p. 967-79.
91. Gaur, T., et al., *Canonical WNT signaling promotes osteogenesis by directly stimulating Runx2 gene expression.* J Biol Chem, 2005. 280(39): p. 33132-40.
92. Gentleman, E., et al., *Development of Ligament-Like Structural Organization and Properties in Cell-Seeded Collagen Scaffolds in vitro.* Ann Biomed Eng, 2006: p. 1-11.
93. Gerecht, S., et al., *The effect of actin disrupting agents on contact guidance of human embryonic stem cells.* Biomaterials, 2007. 28(28): p. 4068-77.
94. Gilbert, S.F., *Developmental biology*. 9th ed. 2010, Sunderland, Mass.: Sinauer Associates. xxi, 711, 80 p.

95. Gilbert, T.W., et al., *Gene expression by fibroblasts seeded on small intestinal submucosa and subjected to cyclic stretching.* Tissue Eng, 2007. 13(6): p. 1313-23.
96. Gisselfalt, K., B. Edberg, and P. Flodin, *Synthesis and properties of degradable poly(urethane urea)s to be used for ligament reconstructions.* Biomacromolecules, 2002. 3(5): p. 951-8.
97. Goldstein, A.S., et al., *Effect of convection of osteoblastic cell growth and function in biodegradable polymer foam scaffolds.* Biomaterials, 2001. 22: p. 1279-1288.
98. Gorman, C.M., B.H. Howard, and R. Reeves, *Expression of recombinant plasmids in mammalian cells is enhanced by sodium butyrate.* Nucleic Acids Res, 1983. 11(21): p. 7631-48.
99. Guan, J., et al., *Preparation and characterization of highly porous, biodegradable polyurethane scaffolds for soft tissue applications.* Biomaterials, 2005. 26(18): p. 3961-71.
100. Guan, J., et al., *Synthesis, characterization, and cytocompatibility of elastomeric, biodegradable poly(ester-urethane)ureas based on poly(caprolactone) and putrescine.* J Biomed Mater Res, 2002. 61(3): p. 493-503.
101. Guelcher, S.A., *Biodegradable polyurethanes: synthesis and applications in regenerative medicine.* Tissue Eng Part B Rev, 2008. 14(1): p. 3-17.
102. Guelcher, S.A., et al., *Synthesis of biocompatible segmented polyurethanes from aliphatic diisocyanates and diurea diol chain extenders.* Acta Biomater, 2005. 1(4): p. 471-84.
103. Gupta, P., et al., *Electrospinning of linear homopolymers of poly(methyl methacrylate): exploring relationships between fiber formation, viscosity, molecular weight and concentration in a good solvent.* Polymer, 2005. 46: p. 4799-4810.
104. Halasz, K., et al., *COMP acts as a catalyst in collagen fibrillogenesis.* J Biol Chem, 2007. 282(43): p. 31166-73.
105. He, L., et al., *Synergistic effects of electrospun PLLA fiber dimension and pattern on neonatal mouse cerebellum C17.2 stem cells.* Acta Biomater, 2010. 6(8): p. 2960-9.
106. Hedbom, E. and D. Heinegard, *Interaction of a 59-kDa connective tissue matrix protein with collagen I and collagen II.* J Biol Chem, 1989. 264(12): p. 6898-905.
107. Heino, J., *The collagen receptor integrins have distinct ligand recognition and signaling functions.* Matrix Biology, 2000. 19(4): p. 319-323.
108. Henshaw, D.R., et al., *Canine ACL fibroblast integrin expression and cell alignment in response to cyclic tensile strain in three-dimensional collagen gels.* J Orthop Res, 2006. 24(3): p. 481-90.
109. Hewett, T.E., G.D. Myer, and K.R. Ford, *Reducing knee and anterior cruciate ligament injuries among female athletes: a systematic review of neuromuscular training interventions.* J Knee Surg, 2005. 18(1): p. 82-8.
110. Hoffmann, A. and G. Gross, *Tendon and ligament engineering in the adult organism: mesenchymal stem cells and gene-therapeutic approaches.* Int Orthop, 2007. 31(6): p. 791-7.
111. Hoffmann, A., et al., *Neotendon formation induced by manipulation of the Smad8 signalling pathway in mesenchymal stem cells.* J Clin Invest, 2006. 116(4): p. 940-52.
112. Hsieh, A.H., et al., *Time-dependent increases in type-III collagen gene expression in medical collateral ligament fibroblasts under cyclic strains.* J Orthop Res, 2000. 18(2): p. 220-7.

113. Hu, J.J., J.D. Humphrey, and A.T. Yeh, *Characterization of engineered tissue development under biaxial stretch using nonlinear optical microscopy.* Tissue Eng Part A, 2009. 15(7): p. 1553-64.
114. Hu, J.S., E.N. Olson, and R.E. Kingston, *HEB, a helix-loop-helix protein related to E2A and ITF2 that can modulate the DNA-binding ability of myogenic regulatory factors.* Mol Cell Biol, 1992. 12(3): p. 1031-42.
115. Humphrey, J.D., et al., *A theoretically-motivated biaxial tissue culture system with intravital microscopy.* Biomech Model Mechanobiol, 2008. 7(4): p. 323-34.
116. Iatridis, J.C., J.J. MaClean, and D.A. Ryan, *Mechanical damage to the intervertebral disc annulus fibrosus subjected to tensile loading.* J Biomech, 2005. 38(3): p. 557-65.
117. Jackson, D.W., G.E. Windler, and T.M. Simon, *Intraarticular reaction associated with the use of freeze-dried, ethylene oxide-sterilized bone-patella tendon-bone allografts in the reconstruction of the anterior cruciate ligament.* Am. J. Sports Med., 1990. 18: p. 1-11.
118. Jarvinen, T.A., et al., *Tenascin-C in the pathobiology and healing process of musculoskeletal tissue injury.* Scand J Med Sci Sports, 2000. 10(6): p. 376-82.
119. Jelinsky, S.A., et al., *Tendon-selective genes identified from rat and human musculoskeletal tissues.* J Orthop Res, 2010. 28(3): p. 289-97.
120. Joshi, S.D. and K. Webb, *Variation of cyclic strain parameters regulates development of elastic modulus in fibroblast/substrate constructs.* J Orthop Res, 2008. 26(8): p. 1105-1113.
121. Juncosa-Melvin, N., et al., *Mechanical stimulation increases collagen type I and collagen type III gene expression of stem cell-collagen sponge constructs for patellar tendon repair.* Tissue Eng, 2007. 13(6): p. 1219-26.
122. Kadesch, T., *Consequences of heteromeric interactions among helix-loop-helix proteins.* Cell Growth Differ, 1993. 4(1): p. 49-55.
123. Kapoor, A., et al., *Microtopographically patterned surfaces promote the alignment of tenocytes and extracellular collagen.* Acta Biomater, 2010. 6(7): p. 2580-9.
124. Kasperczyk, W.J., et al., *Age, activity and strength of knee ligaments.* Unfallchirurg, 1991. 94: p. 372-375.
125. Kavlock, K.O., et al., *Synthesis and characterization of segmented poly(ester urethane)urea (PEUUR) elastomers for bone tissue engineering.* Acta Biomaterialia, 2007. 3: p. 475-484.
126. Kim, B.S., et al., *Cyclic mechanical strain regulates the development of engineered smooth muscle tissue.* Nat Biotechnol, 1999. 17(10): p. 979-83.
127. Kim, S.G., et al., *Gene expression of type I and type III collagen by mechanical stretch in anterior cruciate ligament cells.* Cell Struct Funct, 2002. 27(3): p. 139-44.
128. Kluge, J.A., et al., *Versatile Bioreactor System for Biomaterial Design Studies Using Real-time Mechanical and Imaging Modalities*. 2010.
129. Kreider, B.L., et al., *Inhibition of myeloid differentiation by the helix-loop-helix protein Id.* Science, 1992. 255(5052): p. 1700-2.
130. Kreke, M.R. and A.S. Goldstein, *Hydrodynamic shear stimulates osteocalcin expression but not proliferation of bone marrow stromal cells.* Tissue Eng, 2004. 10(5-6): p. 780-8.

131. Kreke, M.R., W.R. Huckle, and A.S. Goldstein, *Fluid flow stimulates expression of osteopontin and bone sialoprotein by bone marrow stromal cells in a temporally dependent manner.* Bone, 2005. 36(6): p. 1047-55.
132. Ku, C.H., et al., *Collagen synthesis by mesenchymal stem cells and aortic valve interstitial cells in response to mechanical stretch.* Cardiovasc Res, 2006. 71(3): p. 548-56.
133. Kumbar, S.G., et al., *Electrospun poly(lactic acid-co-glycolic acid) scaffolds for skin tissue engineering.* Biomaterials, 2008. 29(30): p. 4100-7.
134. Kuo, C.K. and R.S. Tuan, *Mechanoactive tenogenic differentiation of human mesenchymal stem cells.* Tissue Eng Part A, 2008. 14(10): p. 1615-27.
135. Langer, R. and J.P. Vacanti, *Tissue engineering.* Science, 1993. 260(5110): p. 920-6.
136. Lassar, A.B., et al., *Functional activity of myogenic HLH proteins requires hetero-oligomerization with E12/E47-like proteins in vivo.* Cell, 1991. 66(2): p. 305-15.
137. Laurencin, C.T., et al., *Tissue engineering: orthopedic applications.* Annu Rev Biomed Eng, 1999. 1: p. 19-46.
138. Laurencin, C.T. and J.W. Freeman, *Ligament tissue engineering: an evolutionary materials science approach.* Biomaterials, 2005. 26(36): p. 7530-6.
139. Lee, C.H., et al., *Nanofiber alignment and direction of mechanical strain affect the ECM production of human ACL fibroblast.* Biomaterials, 2005. 26(11): p. 1261-70.
140. Lee, I.C., et al., *The differentiation of mesenchymal stem cells by mechanical stress or/and co-culture system.* Biochem Biophys Res Commun, 2007. 352(1): p. 147-52.
141. Lejard, V., et al., *Scleraxis and NFATc regulate the expression of the pro-alpha1(I) collagen gene in tendon fibroblasts.* J Biol Chem, 2007. 282(24): p. 17665-75.
142. Li, D., Y. Wang, and Y. Xia, *Electrospinning of polymeric and ceramic nanofibers as uniaxially aligned arrays.* Nano Letters, 2003. 3: p. 1167 - 1171.
143. Li, W.J., et al., *Engineering controllable anisotropy in electrospun biodegradable nanofibrous scaffolds for musculoskeletal tissue engineering.* J Biomech, 2007. 40(8): p. 1686-93.
144. Liljensten, E., et al., *Studies of polyurethane urea bands for ACL reconstruction.* J Mater Sci Mater Med, 2002. 13(4): p. 351-9.
145. Liu, H., et al., *A comparison of rabbit mesenchymal stem cells and anterior cruciate ligament fibroblasts responses on combined silk scaffolds.* Biomaterials, 2008. 29(10): p. 1443-53.
146. Liu, M., X.L. Li, and B.A. Hassel, *Proteasomes modulate conjugation to the ubiquitin-like protein, ISG15.* J Biol Chem, 2003. 278(3): p. 1594-602.
147. Liu, W.F. and C.S. Chen, *Cellular and multicellular form and function.* Adv. Drug Deliv. Rev., 2007. 59: p. 1319-1328.
148. Liu, Y., et al., *Sclerotome-related helix-loop-helix type transcription factor (scleraxis) mRNA is expressed in osteoblasts and its level is enhanced by type-beta transforming growth factor.* J Endocrinol, 1996. 151(3): p. 491-9.
149. Liu, Y., et al., *Effects of fiber orientation and diameter on the behavior of human dermal fibroblasts on electrospun PMMA scaffolds.* J Biomed Mater Res A, 2008.
150. Liu, Y., et al., *Overexpression of a single helix-loop-helix-type transcription factor, scleraxis, enhances aggrecan gene expression in osteoblastic osteosarcoma ROS17/2.8 cells.* J Biol Chem, 1997. 272(47): p. 29880-5.

151. Livak, K.J. and T.D. Schmittgen, *Analysis of relative gene expression data using real-time quantitative PCR and the 2(-Delta Delta C(T)) Method.* Methods, 2001. 25(4): p. 402-8.
152. Lohmander, L.S., et al., *The long-term consequence of anterior cruciate ligament and meniscus injuries: osteoarthritis.* Am J Sports Med, 2007. 35(10): p. 1756-69.
153. Lu, H.H., et al., *Anterior cruciate ligament regeneration using braided biodegradable scaffolds: in vitro optimization studies.* Biomaterials, 2005. 26: p. 4805-4816.
154. Ma, J., X. He, and E. Jabbari, *Osteogenic Differentiation of Marrow Stromal Cells on Random and Aligned Electrospun Poly(L: -lactide) Nanofibers.* Ann Biomed Eng, 2010.
155. Mascarenhas, R. and P.B. Macdonald, *Anterior cruciate ligament reconstruction: a look at prosthetics - past, present and possible future.* Mcgill J Med, 2008. 11(1): p. 29-37.
156. Mattila, P.K. and P. Lappalainen, *Filopodia: molecular architecture and cellular functions.* Nat Rev Mol Cell Biol, 2008. 9(6): p. 446-54.
157. Mauck, R.L., et al., *Engineering on the straight and narrow: the mechanics of nanofibrous assemblies for fiber-reinforced tissue regeneration.* Tissue Eng Part B Rev, 2009. 15(2): p. 171-93.
158. Mauck, R.L., et al., *Regulation of cartilaginous ECM gene transcription by chondrocytes and MSCs in 3D culture in response to dynamic loading.* Biomech Model Mechanobiol, 2007. 6(1-2): p. 113-25.
159. Mauck, R.L., et al., *Functional tissue engineering of articular cartilage through dynamic loading of chondrocyte-seeded agarose gels.* J Biomech Eng, 2000. 122(3): p. 252-60.
160. Mauney, J.R., et al., *Mechanical stimulation promotes osteogenic differentiation of human bone marrow stromal cells on 3-D partially demineralized bone scaffolds in vitro.* Calcif Tissue Int, 2004. 74(5): p. 458-68.
161. McDevitt, T.C., et al., *Spatially organized layers of cardiomyocytes on biodegradable polyurethane films for myocardial repair.* J Biomed Mater Res A, 2003. 66(3): p. 586-95.
162. McNeilly, C.M., et al., *Tendon cells in vivo form a three dimensional network of cell processes linked by gap junctions.* J Anat, 1996. 189 (Pt 3): p. 593-600.
163. Miller, C., et al., *Oriented Schwann cell growth on micropatterned biodegradable polymer substrates.* Biomaterials, 2001. 22(11): p. 1263-9.
164. Min, B.M., et al., *Regenerated silk fibroin nanofibers: water vapor-induced structural changes and their effects on the behavior of normal human cells.* Macromol Biosci, 2006. 6(4): p. 285-92.
165. Miyasaka, K., D. Daniel, and M. Stone, *The incidence of knee ligament injuries in the general population. .* American Journal of Knee Surgery, 1991. 4: p. 43-48.
166. Mo, X.M., et al., *Electrospun P(LLA-CL) nanofiber: a biomimetic extracellular matrix for smooth muscle cell and endothelial cell proliferation.* Biomaterials, 2004. 25(10): p. 1883-1890.
167. Mohanty, M., et al., *Evaluation of soft tissue response to a poly(urethane urea).* Biomaterials, 1992. 13(10): p. 651-6.
168. Molkentin, J.D. and E.N. Olson, *Combinatorial control of muscle development by basic helix-loop-helix and MADS-box transcription factors.* Proc Natl Acad Sci U S A, 1996. 93(18): p. 9366-73.

169. Moreau, J.E., et al., *Sequential biochemical and mechanical stimulation in the development of tissue-engineered ligaments.* Tissue Eng Part A, 2008. 14(7): p. 1161-72.
170. Moreau, J.E., et al., *Growth factor induced fibroblast differentiation from human bone marrow stromal cells in vitro.* J Orthop Res, 2005. 23(1): p. 164-74.
171. Moreau, J.E., et al., *Sequential growth factor application in bone marrow stromal cell ligament engineering.* Tissue Eng, 2005. 11(11-12): p. 1887-97.
172. Moroni, L., et al., *Fiber diameter and texture of electrospun PEOT/PBT scaffolds influence human mesenchymal stem cell proliferation and morphology, and the release of incorporated compounds.* Biomaterials, 2006. 27(28): p. 4911-22.
173. Mow, V.C. and W.C. Hayes, *Basic orthopaedic biomechanics*. 1991, New York: Raven Press. x, 453 p.
174. Muir, T., I. Sadler-Riggleman, and M.K. Skinner, *Role of the basic helix-loop-helix transcription factor, scleraxis, in the regulation of Sertoli cell function and differentiation.* Mol Endocrinol, 2005. 19(8): p. 2164-74.
175. Murchison, N.D., et al., *Regulation of tendon differentiation by scleraxis distinguishes force-transmitting tendons from muscle-anchoring tendons.* Development, 2007. 134(14): p. 2697-708.
176. Murray, M.M., et al., *Collagen-platelet rich plasma hydrogel enhances primary repair of the porcine anterior cruciate ligament.* J Orthop Res, 2007. 25(1): p. 81-91.
177. Murre, C., et al., *Structure and function of helix-loop-helix proteins.* Biochim Biophys Acta, 1994. 1218(2): p. 129-35.
178. Murugan, R. and S. Ramakrishna, *Design strategies of tissue engineering scaffolds with controlled fiber orientation.* Tissue Eng, 2007. 13(8): p. 1845-66.
179. Nagineni, C.N., et al., *Characterization of the intrinsic properties of the anterior cruciate and medial collateral ligament cells: an in vitro cell culture study.* J Orthop Res, 1992. 10(4): p. 465-75.
180. Nair, L.S., et al., *Fabrication and optimization of methylphenoxy substituted polyphosphazene nanofibers for biomedical applications.* Biomacromolecules, 2004. 4: p. 2212-2220.
181. Nau, T., P. Lavoie, and N. Duval, *A new generation of artificial ligaments in reconstruction of the anterior cruciate ligament. Two-year follow-up of a randomised trial.* J Bone Joint Surg Br, 2002. 84(3): p. 356-60.
182. Nebelung, W. and H. Wuschech, *Thirty-five years of follow-up of anterior cruciate ligament-deficient knees in high-level athletes.* Arthroscopy, 2005. 21(6): p. 696-702.
183. Neidlinger-Wilke, C., H.J. Wilke, and L. Claes, *Cyclic stretching of human osteoblasts affects proliferation and metabolism: a new experimental method and its application.* J Orthop Res, 1994. 12(1): p. 70-8.
184. Nieponice, A., et al., *Mechanical stimulation induces morphological and phenotypic changes in bone marrow-derived progenitor cells within a three-dimensional fibrin matrix.* J Biomed Mater Res A, 2007. 81(3): p. 523-30.
185. Nigg, B.M., B.R. MacIntosh, and J. Mester, *Biomechanics and biology of movement*. 2000, Champaign, Ill.: Human Kinetics. xvii, 465 p.
186. Niles, A., et al., *Multiplexed Viability, Cytotoxicity and Apoptosis Assays for Cell-based Screening*, in *Cell Notes*. 2006, Promega Corporation.

187. Nirmalanandhan, V.S., et al., *Combined effects of scaffold stiffening and mechanical preconditioning cycles on construct biomechanics, gene expression, and tendon repair biomechanics.* Tissue Eng Part A, 2009. 15(8): p. 2103-2111.
188. Noyes, F.R. and E.S. Grood, *The strength of the anterior cruciate ligament in humans and Rhesus monkeys.* J Bone Joint Surg Am, 1976. 58: p. 1074-1082.
189. OriGene Technologies, I., *Transfection of HEK293T cells with pCMV-GFP-SCX*. 2009: Rockville, MD.
190. Oshima, Y., et al., *Expression and localization of tenomodulin, a transmembrane type chondromodulin-I-related angiogenesis inhibitor, in mouse eyes.* Invest Ophthalmol Vis Sci, 2003. 44(5): p. 1814-23.
191. Park, S.A., et al., *Biological responses of ligament fibroblasts and gene expression profiling on micropatterned silicone substrates subjected to mechanical stimuli.* J Biosci Bioeng, 2006. 102(5): p. 402-12.
192. Peperzak, K.A., T.W. Gilbert, and J.H. Wang, *A multi-station dynamic-culture force monitor system to study cell mechanobiology.* Med Eng Phys, 2004. 26(4): p. 355-8.
193. Petersen, W. and B. Tillmann, *Structure and vascularization of the cruciate ligaments of the human knee joint.* Anat Embryol (Berl), 1999. 200(3): p. 325-34.
194. Petrigliano, F.A., et al., *The effects of local bFGF release and uniaxial strain on cellular adaptation and gene expression in a 3D environment: implications for ligament tissue engineering.* Tissue Eng, 2007. 13(11): p. 2721-31.
195. Petrigliano, F.A., D.R. McAllister, and B.M. Wu, *Tissue engineering for anterior cruciate ligament reconstruction: a review of current strategies.* Arthroscopy, 2006. 22(4): p. 441-51.
196. Pham, Q.P., U. Sharma, and A.G. Mikos, *Electrospun poly(epsilon-caprolactone) microfiber and multilayer nanofiber/microfiber scaffolds: characterization of scaffolds and measurement of cellular infiltration.* Biomacromolecules, 2006. 7(10): p. 2796-805.
197. Pittenger, M.F., et al., *Multilineage potential of adult human mesenchymal stem cells.* Science, 1999. 284(5411): p. 143-7.
198. Potier, E., J. Noailly, and K. Ito, *Directing bone marrow-derived stromal cell function with mechanics.* J Biomech, 2010. 43(5): p. 807-17.
199. Praemer, A., S. Furner, and D. Rice, *Musculoskeletal condition in the United States*. 1992, Park Ridge: Am Acad Orthop Surg. 199.
200. Prodromos, C.C., et al., *A meta-analysis of the incidence of anterior cruciate ligament tears as a function of gender, sport, and a knee injury-reduction regimen.* Arthroscopy, 2007. 23(12): p. 1320-1325 e6.
201. Prosch, S., et al., *Inactivation of the very strong HCMV immediate early promoter by DNA CpG methylation in vitro.* Biol Chem Hoppe Seyler, 1996. 377(3): p. 195-201.
202. Pryce, B.A., et al., *Generation of transgenic tendon reporters, ScxGFP and ScxAP, using regulatory elements of the scleraxis gene.* Dev Dyn, 2007. 236(6): p. 1677-82.
203. Radisic, M., et al., *High-density seeding of myocyte cells for cardiac tissue engineering.* Biotechnol Bioeng, 2003. 82(4): p. 403-14.
204. Rahaman, M.N. and J.J. Mao, *Stem cell-based composite tissue constructs for regenerative medicine.* Biotechnology and Bioengineering, 2005. 91: p. 261-284.
205. Raif el, M., et al., *Cyclic straining of cell-seeded synthetic ligament scaffolds: development of apparatus and methodology.* Tissue Eng, 2007. 13(3): p. 629-40.

206. Reilly, G.C. and A.J. Engler, *Intrinsic extracellular matrix properties regulate stem cell differentiation.* J Biomech, 2010. 43(1): p. 55-62.
207. Rezgui, F., et al., *Deformation and damage upon stretching of degradable polymers (PLA and PCL).* Polymer, 2005. 46: p. 7370-7385.
208. Reznikoff, C.A., D.W. Brankow, and C. Heidelberger, *Establishment and characterization of a cloned line of C3H mouse embryo cells sensitive to postconfluence inhibition of division.* Cancer Res, 1973. 33(12): p. 3231-8.
209. Riboldi, S.A., et al., *Electrospun degradable polyesterurethane membranes: potential scaffolds for skeletal muscle tissue engineering.* Biomaterials, 2005. 26: p. 4606-4615.
210. Saber, S., et al., *Flexor tendon tissue engineering: bioreactor cyclic strain increases construct strength.* Tissue Eng Part A, 2010. 16(6): p. 2085-90.
211. Saez, A., et al., *Rigidity-driven growth and migration of epithelial cells on microstructured anisotropic substrates.* Proc. Natl. Acad. Sci. USA, 2007. 104: p. 8281-8286.
212. Schweitzer, R., et al., *Analysis of the tendon cell fate using Scleraxis, a specific marker for tendons and ligaments.* Development, 2001. 128(19): p. 3855-66.
213. Seghatoleslami, M.R., et al., *Progression of chondrogenesis in C3H10T1/2 cells is associated with prolonged and tight regulation of ERK1/2.* J Cell Biochem, 2003. 88(6): p. 1129-44.
214. Seidel, J.O., et al., *Long-term culture of tissue engineered cartilage in a perfused chamber with mechanical stimulation.* Biorheology, 2004. 41(3-4): p. 445-58.
215. Shagin, D.A., et al., *GFP-like proteins as ubiquitous metazoan superfamily: evolution of functional features and structural complexity.* Mol Biol Evol, 2004. 21(5): p. 841-50.
216. Shukunami, C., Y. Oshima, and Y. Hiraki, *Molecular cloning of tenomodulin, a novel chondromodulin-I related gene.* Biochem Biophys Res Commun, 2001. 280(5): p. 1323-7.
217. Shukunami, C., et al., *Chondromodulin-I and tenomodulin are differentially expressed in the avascular mesenchyme during mouse and chick development.* Cell Tissue Res, 2008. 332(1): p. 111-22.
218. Shukunami, C., et al., *Scleraxis positively regulates the expression of tenomodulin, a differentiation marker of tenocytes.* Dev Biol, 2006. 298(1): p. 234-47.
219. Silver, F.H., *Mechanosensing and mechanochemical transduction in extracellular matrix : biological, chemical, engineering, and physiological aspects*. 2006, New York, NY: Springer. xvi, 292 p.
220. Silver, F.H., J.W. Freeman, and G.P. Seehra, *Collagen self-assembly and the development of tendon mechanical properties.* J Biomech, 2003. 36(10): p. 1529-53.
221. Silver, F.H., et al., *Analysis of mammalian connective tissue: relationship between hierarchical structures and mechanical properties.* J Long Term Eff Med Implants, 1992. 2(2-3): p. 165-98.
222. Sisson, K., et al., *Fiber diameters control osteoblastic cell migration and differentiation in electrospun gelatin.* J Biomed Mater Res A, 2010. 94(4): p. 1312-20.
223. Skarja, G.A. and K.A. Woodhouse, *Synthesis and characterization of degradable polyurethane elastomers containing and amino acid-based chain extender.* J Biomater Sci Polym Ed, 1998. 9(3): p. 271-95.

224. Sodersten, F., et al., *Ultrastructural immunolocalization of cartilage oligomeric matrix protein (COMP) in relation to collagen fibrils in the equine tendon.* Matrix Biol, 2005. 24(5): p. 376-85.
225. Sommer, L., Q. Ma, and D.J. Anderson, *neurogenins, a novel family of atonal-related bHLH transcription factors, are putative mammalian neuronal determination genes that reveal progenitor cell heterogeneity in the developing CNS and PNS.* Mol Cell Neurosci, 1996. 8(4): p. 221-41.
226. Spaans, C.J., et al., *Solvent-free fabrication of micro-porous polyurethane amide and polyurethane-urea scaffolds for repair and replacement of the knee-joint meniscus.* Biomaterials, 2000. 21(23): p. 2453-60.
227. Spaans, C.J., et al., *High molelcular weight polyurethanes and a polyurethane urea based on 1,4-butanediisocyanate.* Polymer Bulletin, 1998. 41: p. 131-138.
228. Stankus, J., J. Guan, and W. Wagner, *Fabrication of biodegradable elastomeric scaffolds with sub-micron morphologies.* J Biomed Mater Res, 2004. 70A: p. 603-614.
229. Stankus, J.J., et al., *Microintegrating smooth muscle cells into a biodegradable, elastomeric fiber matrix.* Biomaterials, 2006. 27(5): p. 735-44.
230. Stella, J.A., et al., *On the biomechanical function of scaffolds for engineering load-bearing soft tissues.* Acta Biomater, 2010. 6(7): p. 2365-81.
231. Strauss, W.M., *Preparation of Genomic DNA from Mammalian Tissue*. Current Protocols in Molecular Biology. 2001: John Wiley & Sons, Inc.
232. Stylianopoulos, T., et al., *Computational predictions of the tensile properties of electrospun fibre meshes: effect of fibre diameter and fibre orientation.* J Mech Behav Biomed Mater, 2008. 1(4): p. 326-35.
233. Subbiah, T., et al., *Electrospinning of nanofibers.* Journal of Applied Polymer Science, 2005. 96: p. 557-569.
234. Thayer, M.J., et al., *Positive autoregulation of the myogenic determination gene MyoD1.* Cell, 1989. 58(2): p. 241-8.
235. Thomas, T.W. and P.A. DiMilla, *Spreading and motility of human glioblastoma cells on sheets of silicone rubber depend on substratum compliance.* Medical and Biological Engineering and Computing, 2000. 38: p. 360-370.
236. Tian, F., et al., *Quantitative analysis of cell adhesion on aligned micro- and nanofibers.* J Biomed Mater Res A, 2008. 84(2): p. 291-9.
237. Tibbitt, M.W. and K.S. Anseth, *Hydrogels as extracellular matrix mimics for 3D cell culture.* Biotechnol Bioeng, 2009. 103(4): p. 655-63.
238. Tozer, S. and D. Duprez, *Tendon and ligament: development, repair and disease.* Birth Defects Res C Embryo Today, 2005. 75(3): p. 226-36.
239. Tuan, R.S., G. Boland, and R. Tuli, *Adult mesenchymal stem cells and cell-based tissue engineering.* Arthritis Res Ther, 2003. 5(1): p. 32-45.
240. Valeriani, M., et al., *Clinical and neurophysiological abnormalities before and after reconstruction of the anterior cruciate ligament of the knee.* Acta Neurol Scand, 1999. 99(5): p. 303-7.
241. van Eijk, F., et al., *The effect of timing of mechanical stimulation on proliferation and differentiation of goat bone marrow stem cells cultured on braided PLGA scaffolds.* Tissue Eng Part A, 2008. 14(8): p. 1425-33.

242. Van Eijk, F., et al., *Tissue engineering of ligaments: a comparison of bone marrow stromal cells, anterior cruciate ligament, and skin fibroblasts as cell source.* Tissue Eng, 2004. 10(5-6): p. 893-903.
243. Vanderploeg, E.J., et al., *Oscillatory tension differentially modulates matrix metabolism and cytoskeletal organization in chondrocytes and fibrochondrocytes.* J Biomech, 2004. 37(12): p. 1941-52.
244. Vogel, K.G., M. Paulsson, and D. Heinegard, *Specific inhibition of type I and type II collagen fibrillogenesis by the small proteoglycan of tendon.* Biochem J, 1984. 223(3): p. 587-97.
245. Vogel, K.G. and J.A. Trotter, *The effect of proteoglycans on the morphology of collagen fibrils formed in vitro.* Coll Relat Res, 1987. 7(2): p. 105-14.
246. Vunjak-Novakovic, G., et al., *Tissue engineering of ligaments.* Annu Rev Biomed Eng, 2004. 6: p. 131-56.
247. Vunjak-Novakovic, G., et al., *Dynamic cell seeding of polymer scaffolds for cartilage tissue engineering.* Biotechnol Prog, 1998. 14(2): p. 193-202.
248. Wang, H., et al., *Cell orientation response to cyclically deformed substrates: experimental validation of a cell model.* J Biomech, 1995. 28(12): p. 1543-52.
249. Wang, J.H., *Mechanobiology of tendon.* J Biomech, 2006. 39(9): p. 1563-82.
250. Wang, J.H. and B.P. Thampatty, *An introductory review of cell mechanobiology.* Biomech Model Mechanobiol, 2006. 5(1): p. 1-16.
251. Wang, J.H., et al., *Mechanoregulation of gene expression in fibroblasts.* Gene, 2007. 391(1-2): p. 1-15.
252. Wang, J.H., G. Yang, and Z. Li, *Controlling cell responses to cyclic mechanical stretching.* Ann Biomed Eng, 2005. 33(3): p. 337-42.
253. Waters, C.M., et al., *A system to impose prescribed homogenous strains on cultured cells.* J Appl Physiol, 2001. 91(4): p. 1600-10.
254. Webb, K., et al., *Cyclic strain increases fibroblast proliferation, matrix accumulation, and elastic modulus of fibroblast-seeded polyurethane constructs.* J Biomech, 2006. 39(6): p. 1136-44.
255. WebMD. *Anterior Cruciate Ligament (ACL) Injuries*. May 16, 2008 [cited 2009 January 25].
256. Weintraub, H., et al., *Activation of muscle-specific genes in pigment, nerve, fat, liver, and fibroblast cell lines by forced expression of MyoD.* Proc Natl Acad Sci U S A, 1989. 86(14): p. 5434-8.
257. Whitlock, P.W., et al., *A naturally derived, cytocompatible, and architecturally optimized scaffold for tendon and ligament regeneration.* Biomaterials, 2007. 28(29): p. 4321-9.
258. Williams, R.M., W.R. Zipfel, and W.W. Webb, *Interpreting second-harmonic generation images of collagen I fibrils.* Biophys J, 2005. 88(2): p. 1377-86.
259. Woo, S.L., et al., *Biomechanics of knee ligaments.* Am J Sports Med, 1999. 27(4): p. 533-43.
260. Woo, S.L., et al., *Injury and repair of ligaments and tendons.* Annu Rev Biomed Eng, 2000. 2: p. 83-118.
261. Woo, S.L., et al., *Tensile properties of the human femur-anterior cruciate ligament-tibia complex. The effects of specimen age and orientation.* Am J Sports Med, 1991. 19(3): p. 217-25.

262. Woolfson, D.N. and M.G. Ryadnov, *Peptide-based fibrous biomaterials: Some things old, new and borrowed.* Curr Opin Chem Biol, 2006. 10(6): p. 559-67.
263. Yang, F., et al., *Electrospinning of nano/micro scale poly(L-lactic acid) aligned fibers and their potential in neural tissue engineering.* Biomaterials, 2005. 26(15): p. 2603-10.
264. Yang, G., R.C. Crawford, and J.H. Wang, *Proliferation and collagen production of human patellar tendon fibroblasts in response to cyclic uniaxial stretching in serum-free conditions.* J Biomech, 2004. 37(10): p. 1543-50.
265. Yim, E.K., S.W. Pang, and K.W. Leong, *Synthetic nanostructures inducing differentiation of human mesenchymal stem cells into neuronal lineage.* Exp Cell Res, 2007. 313(9): p. 1820-9.
266. Yin, Z., et al., *The regulation of tendon stem cell differentiation by the alignment of nanofibers.* Biomaterials, 2010. 31(8): p. 2163-75.
267. Yun, S.I., H.Y. Yoon, and Y.S. Chung, *Glycogen synthase kinase-3beta regulates etoposide-induced apoptosis via Bcl-2 mediated caspase-3 activation in C3H10T1/2 cells.* Apoptosis, 2009. 14(6): p. 771-7.
268. Zhang, G., et al., *Decorin regulates assembly of collagen fibrils and acquisition of biomechanical properties during tendon development.* J Cell Biochem, 2006. 98(6): p. 1436-49.
269. Zhao, R., M.S. Bodnar, and D.L. Spector, *Nuclear neighborhoods and gene expression.* Curr Opin Genet Dev, 2009. 19(2): p. 172-9.
270. Zong, X.H., et al., *Electrospun fine-textured scaffolds for heart tissue constructs.* Biomaterials, 2005. 26(26): p. 5330-5338.

Appendix A Effect of Growth Factor on Rat Bone Marrow-derived Mesenchymal Stem Cell Gene Expression

To determine if growth factors, specifically FGF-2 and TGFβ-1, increase the differentiation of MSCs in culture, a preliminary study was conducted. FGF-2 and TGFβ-1, growth factors present in normal and healing ligaments, have been shown to increase cell proliferation and ECM synthesis, respectively. Passage 2 MSCs were seeded at 5,000 cells/cm^2 and were cultured in growth media containing 2 mM ascorbate-2-phosphate (hereafter, A2P media) plus either 2 ng/mL FGF-2, 5 ng/mL TGFβ-1 or both for 3 or 7 days. Cell density (n=3) at day 3 was lowest with TGFβ-1 alone but was not statistically significant. By day 7, FGF-2 addition increased cell number while TGFβ-1 groups were similar to control (Figure A.1). Real-time PCR (n=3) was used to determine the relative expression levels of two ligament ECM genes, collagen 1α1 and decorin on day 7 (Figure A.2). Collagen 1α1 expression increased in the presence of TGFβ-1 alone and was further increased with the addition of FGF-2. Decorin expression levels were increased in the presence of the FGF-2, but was significantly decreased with the addition of TGFβ-1. In addition, TGFβ-1 cultures were observed to "peel" from the culture surface after 1 week. While TGFβ-1 increased collagen 1α1 expression, TGFβ-1 diminished decorin expression and cell number. This study showed the addition of two growth factors may be beneficial to increasing ECM production. Another substrate may alleviate cell detachment from the culture plate. Electrospun polymers may prevent cell peeling, as the culture surface would no longer be smooth.

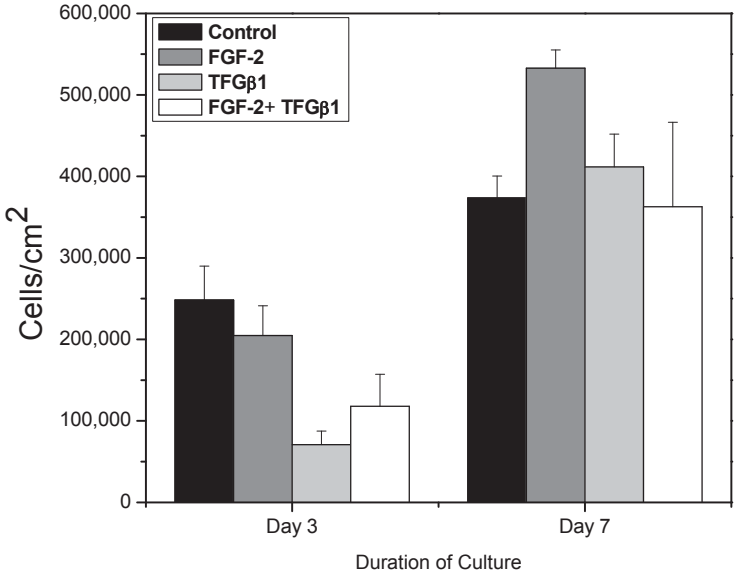

Figure A.1: Effect of growth factor supplementation on MSC proliferation

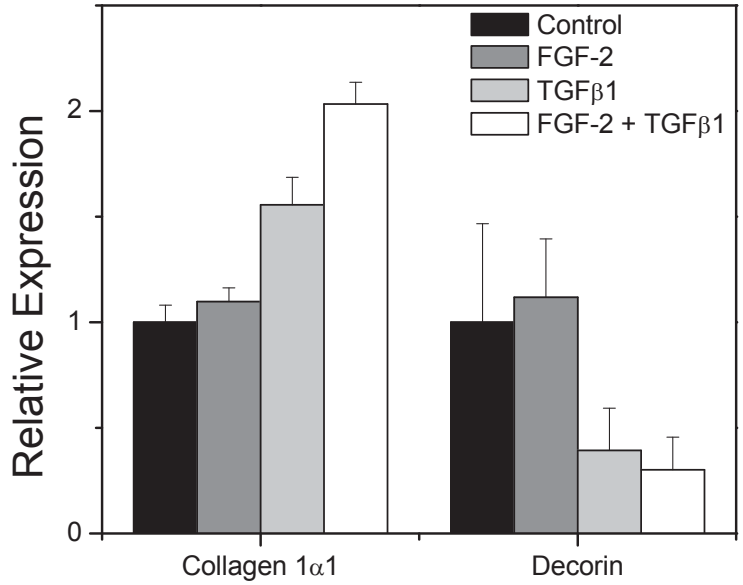

Figure A.2 Effect of growth factor supplementation on MSC gene expression of collagen type I and decorin

To determine if the expression of ligament tissue phenotypic markers (collagen 1α1 and decorin) is affected by polymer (PLGA) and fiber (electrospun) morphology when cultured in the presence of TGFβ-1 and FGF-2, a preliminary study was performed. PLGA was spincoated or electrospun (fiber diameter 1.02 ± 0.336 μm) onto rigid glass coverslips.

Passage 3 or 4 rat bone marrow-derived mesenchymal stem cells were cultured in A2P media plus either 2 ng/mL FGF-2, 5 ng/mL TGFβ-1 or both for 3, 7 or 12 days. As shown in Figure A.3, spincoated and electrospun scaffolds with supplemental growth factors did slightly increase collagen 1α1 and decorin relative expression levels compared to spincoated surfaces without growth factors (n=3). However, the electrospun scaffold with the addition of either FGF-2 or TGFβ-1 had statistically significant increases of collagen 1α1 as compared to the spincoated group without growth factors ($p \leq 0.05$). Decorin expression was also significantly increased in all electrospun scaffold groups as compared to the spincoated group without growth factors. Finally, the electrospun + TGFβ-1 group had statistically significant increases in decorin expression levels as compared to the spincoated + TGFβ-1. In this preliminary study, growth factors did not affect cell number or gene expression significantly but the electrospun scaffolds did have significant effects on cellular gene expression as compared to the spincoated surfaces. Based on this study, growth factors will not be used for future studies.

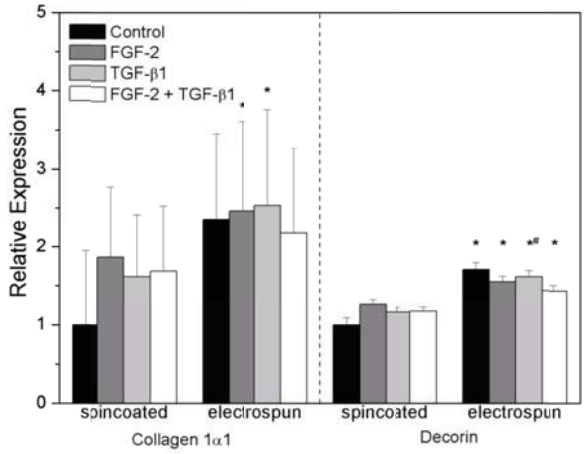

Figure A.3: Effect of growth factor treatment on MSC relative gene expression of collagen 1α1 and decorin as a function of PLGA scaffold type (spincoated vs. electrospun fibers). Data was normalized relative to cells on spincoated PLGA films after 7 days of culture. Statisical significance ($p \leq 0.05$) relative to Spincoated/No Growth factor control is indicated by *, and statisical significance relative to Spincoated/TGFβ-1 is indicated by # (n=3).

Appendix B Molecular Techniques

B.1 RNA Isolation – using QIAGEN RNeasy Mini Columns

Supplies Needed:

RNeasy Mini Kit (Qiagen):
- RNeasy Mini Spin Columns (pink)
  - Buffer RLT
  - Buffer RWI
- Buffer RPE (with ethanol)
- 2mL collection tubes

RNase free DNase I Kit (Qiagen):
- DNase I Stock Solution
- RDD Buffer

70% ethanol made with nuclease-free water
Nuclease-free Water
Nuclease-free Micro-centrifuge tubes (~1.2mL)
QIAshredder Spin Columns (purple)
β-mercaptoethanol

Before Starting:

- Place PBS in 37°C water bath
- Prepare 50 mL of 70% ethanol (35mL EtOH + 15mL nuclease-free water)
  - Label: 70% ethanol Nuclease-Free
- Prepare Buffer RLT + β-merc in hood in 15mL conical tube (lasts 2-3 days at RT)
  - 10µL β-merc to 1mL Buffer RLT - Need 350µL per sample – make (n+1)
    - Buffer RLT = (# samples +1) x 350µL
  - β-merc = 10µL per mL Buffer RLT
- Prepare DNase I + Buffer RDD in micro-centrifuge tube (store on ice)(make fresh)
  - Buffer RDD = (# samples +1) x 70µL
  - DNase I solution = (# samples +1) x 10µL
- Label QIAshredders (purple) with sample numbers (side and top)
- Bring labeled QIAshredders (purple) and Buffer RLT to hood
- Wipe hands and pipets with RNase Away

Procedure:

1. Aspirate media from cell plate
2. Wash each well 2x with ~1 mL PBS
3. Add 350µL Buffer RLT (with B-merc) to each well (Pre-made)
   Wash down sides of well with the liquid to capture all cells to be put on QIAshredder
4. Pipet cell lysate directly onto pre-labeled QIAshredder (purple)

Use new tip for each well, make sure to get al.l liquid from well into QIAshredder

5. Centrifuge for 2 minutes at max speed at room temperature
   (Can be used as a stopping point, put QIAshredder caps on)
   Store at -80°C in pre-labeled box
   If above step is used as stopping point, be sure to thaw lysates on ice
6. Remove/discard spin column (purple) from collection tube
7. Slowly add 350µL 70% EtOH to each #1 collection tube
8. Pipet the 700µL into the RNeasy Mini Spin columns (pink)
9. Centrifuge at >8,000g (>10,000rpm) for 15 seconds at RT
10. Discard the flow through
11. Pipet 350µL Buffer RWI into spin column
12. Centrifuge at >8,000g (10,000rpm) for 15 seconds at RT
13. Discard the flow through
14. Mix DNase + Buffer RDD solution well (on ice)
    Pipet 80µL DNase + Buffer RDD solution directly onto spin column membrane
    Let stand at RT for 15 minutes
15. Pipet 350 µL Buffer RW1 into spin column
16. Centrifuge at >8,000g (10,000rpm) for 15 seconds at RT
17. Discard flow through
18. Transfer spin column to new 2mL collection tube
19. Pipet 500µL Buffer RPE (with EtOH!) onto spin column
20. Centrifuge at >8,000g (10,000rpm) for 15 seconds at RT
21. Discard flow through
22. Pipet another 500µL Buffer RPE (with EtOH!) onto spin column
23. Centrifuge at >8,000g (10,000rpm) for 2 minutes at RT
24. Transfer spin column to new 2mL collection tube
25. Discard flow through and old collection tube
26. Centrifuge at >8,000g (10,000rpm) for 1 minute at RT
27. Discard flow through and collection tube
28. Transfer spin column to new 1.5mL microfuge tube
29. Pipet 30µL RNase-free water directly onto membrane to elute RNA
30. Let stand at RT for 1-2 minutes
31. Centrifuge at >8,000g (10,000rpm) for 1 minute at RT
32. Discard spin columns
33. Label microfuge tubes: Sample #, Date, Initials
    Store at -80°C if finished, or keep on ice if quantifying

B.2 RNA Quantification Using RiboGreen Reagent or DNA Quantification using PicoGreen Reagent

**procedures are identical except for standards and reagent used*

Supplies Needed:

Quant-iT™ RiboGreen® RNA Reagent & Kit or Quant-iT™ PicoGreen® DNA Reagent & Kit (Invitrogen)

1X TE Buffer (Nuclease-free)
Diluted DNA/RNA Standard (DNA/RNA Std + Nuclease-free water)
Undiluted rRNA or lambda DNA Standard
RiboGreen or PicoGreen Dye
Isolated DNA/RNA Samples
Micro-centrifuge tubes
96-Well black assay plates (Costar)

Before Starting:

1. Thaw on ice:
    a. Isolated RNA
    b. RNA Standard (diluted and undiluted)
2. Prepare required amount of 1X TE Buffer in 50mL conical tube
    If from 20X TE Buffer:
    2mL TE Buffer +38mL water (Nuclease Free!)
3. Prepare RNA Standard (2ug/mL) in micro-centrifuge tubes
    980µL TE Buffer (nuclease-free)+20µL of100ug/mL RNA standard
4. Label nuclease-free micro-centrifuge tubes: Sample #, Date, Initials

Procedure:

1. Dilute the DNA/RNA samples in micro-centrifuge tubes:
    Dilute 1:X by adding (X-1) µL of TE Buffer and 1 µL of DNA/ RNA sample. A minimum of 200 µL of diluted sample is required for duplicate reactions (MIX WELL!)
2. Prepare 1:200 dilution of Dye with TE buffer in 15mL conical tube wrapped in Al foil:
    Remove aliquot of Dye from freezer, wrap in Al foil, place on ice
    Calculate required amount of dilution
        [2mL + 200µL per DNA/RNA sample (for duplicates)]
        Thaw Dye by hand (will not thaw on ice)
        1:200 Dilution:

Required Amount	2mL	3mL	4mL	5mL	10mL
Dye	10µL	15µL	20µL	25µL	50µL
1X TE Buffer	1990µL	2985µL	3980µL	4975µL	9950µL

3. Turn on plate reader to warm up
4. Add 1X Buffer TE to the following wells:

	1	2	3	4	5
A	100µL	100µL			
B	100µL	100µL			
C	100µL	100µL			
D	100µL	100µL			
E	100µL	100µL			
F	100µL	100µL			
G	100µL	100µL			
H	0µL	0µL			

5. Add DNA/RNA standard Stock (2 µg/mL) to row G, then serially dilute with multi-well pipet:

	1	2	
A			
B			Mix, Take 100 µL from "B" and discard
C			Mix, Take 100 µL from "C" to "B"
D			Mix, Take 100 µL from "D" to "C"
E			Mix, Take 100 µL from "E" to "D"
F			Mix, Take 100 µL from "F" to "E"
G			Mix, Take 100 µL from "G" to "F"
H	200µL	200µL	Take 100 µL from here to "G"

This is your final DNA/RNA Concentration (ng/µL):

	1	2
A	Blank	Blank
B	0.03125	0.03125
C	0.0625	0.0625
D	0.125	0.125
E	0.25	0.25
F	0.5	0.5
G	1	1
H	2	2

6. Add 100µL of dilutedDNA/ RNA samples to the following wells (MIX WELL!):

	1	2	3	4
A			100µL Sample 1	100µL Sample 1
B			100µL Sample 2	100µL Sample 2
C			100µL Sample 3	100µL Sample 3
D			100µL Sample 4	100µL Sample 4
E			100µL Sample 5	100µL Sample 5
F			100µL Sample 6	100µL Sample 6
G			etc	etc
H			etc	etc

7. Pour diluted Dye (1:200) from 15mL conical tube into plastic basin for multi-well pipet

Cover basin with Al foil

8. With 8-well multi-well pipet, add 100µL of Dye (1:200) to each well

Cover plate with Al foil

9. Read using plate reader with SoftMax Pro Software

On Computer:

Open Softmax Pro
Protocols
→Nucleic Acids
→RiboGreen OR PicoGreen
Plate 1 Template
Select A1-2 through H1-2 (Standards)
Series
→Bottom
Starting Value = 2
Step by / 2
Select A1-2
Standard value = 0µL
Select A-F 3,4 (Samples)
Unknowns
Top
Series
OK
OK
Put plate in plate reader (A1 in upper left corner)
Push "Drawer" button
Click "Read" (Green button on top of screen)
Analyze Results:

1. The points should fall along the line
2. The points should fall in the lower left corner of the graph
3. The R^2 value should be 0.98-0.99
4. RFU values are within the curve (Sample RFU values lie within the min and max values stated by the standards)

SAVE YOUR WORK, then save as .txt file → file import/export – export - .txt
Push "Drawer" (closes), Turn plate reader OFF

B.3 cDNA/ Reverse Transcription

Supplies Needed:

High Capacity cDNA Reverse Transcription Kit (Invitrogen)
10X RT Buffer
10X RT Random Primers
25X dNTP Mix (100mM)
MultiScribe Reverse Transcriptase
RNase Inhibitor (RNase Out)
H_2O (Nuclease-free)
1.5 mL Microcentrifuge tubes (Nuclease-free)
0.8 mL Microcentrifuge tubes (Nuclease-free)

Before Starting:

Thaw kit components on ice
Thaw isolated RNA samples
Label mini-microcentrifuge tubes with sample numbers and date

cDNA and 'no RT rxn' procedures are the same, EXCEPT 'no RT ' doesn't use master mix

Procedure:

1. Calculate, record, and prepare volumes needed to create Master Mix (n+1):
    a. H_2O (Nuclease Free 3.2 µL
    b. 10X RT Buffer 2.0 µL
    c. 10X RT Random Primers 2.0µL
    MultiScribe Reverse Transcriptase 1.0 µL
    RNase Inhibitor (RNase Out) 1.0 µL
    d. 25X dNTP Mix (100mM) 0.8 µL
2. Prepare RT Master Mix on ice
3. Pipette 10µL of Master Mix (MIX WELL) into mini microcentrifuge tubes used for cDNA only (not 'no RT rxn' microcentrifuge tubes)
4. According to calculated RNA quantifications, add required amount of water to each mini microcentrifuge tube (both cDNA and 'no RT rxn')
5. According to calculations, add required amount of original RNA sample (MIX WELL) into each mini microcentrifuge tube and mix (both cDNA and 'no RT rxn')
6. Mix tubes and briefly centrifuge the mini microcentrifuge tubes
7. Place mini microcentrifuge tubes for cDNA in thermocycler
8. Run following program:

	Step 1	Step 2	Step 3	Step 4
Temp (°C)	25	37	85	4
Time	10 min	120 min	5 sec	∞

9. Place mini microcentrifuge tubes for 'no RT rxn' in -80°C freezer. After Thermocycler finishes, store cDNA at -20 or -80°C

B.4 Real time PCR using SybrGreen chemistry

Supplies needed:

Nuclease-free filter pipet tips
1.5mL nuclease-free tubes
0.5mL nuclease-free tubes
8-tube strips
Power SybrGreen (Applied Biosystems)
10 μM primer sets (forward & reverse)
Nuclease-free H20
96-well optical PCR plate
Optical Adhesive Plate Seals

Before starting:

- Quantify RNA and determine ng to reverse transcribe to cDNA
- Make NO RT controls as needed
- Set up PCR plate, samples in triplicate or duplicate, including master mix/no RT controls
- Thaw 10uM primers at least 30 minutes before starting (can thaw at room temp.)

Procedure:

1. Primers, cDNA samples, SybrGreen should all be on ice!
2. Make master mix of SybrGreen for EACH primer set

For triplicate:

45 μL x (n + 1) SybrGreen
37.8 μL x (n+1) H20
2.7 μL x (n+1) primer, forward
2.7 μL x (n+1) primer, reverse

For duplicate:

31.25 μL x (n+1) SybrGreen
26.25 μL x (n+1) H20
1.875 μL x (n+1) primer, forward
1.875 μL x (n+1) primer, reverse
W*here n +1 is the number of samples (RT, NO RT, master mix control)*

3. Add 88.2 μL (for triplicate) or 61.25 μL (for duplicate) of Primer Set A master mix to each tube of an 8-tube strip labeled Primer Set A. Also add 88.2 μL (or 61.25 μL) of each master mix to 1 tube for no template control. Use new tip for *each*.
   For 3 primer sets, 3 8-tube strips will be used for 8 samples.
4. Dilute cDNA samples in separate 8-tube strip and spin to mix well.
   For 200ng cDNA, dilute 1/10 (1 μL sample in 9 μL H20)
   For 80ng cDNA, dilute 1/4 (3 μL sample in 9 μL H20)

5. Add 1.8 µL (for duplicate, 1.25 µL) cDNA of each sample to corresponding tube on each 8-tube strip. Also add 1.8 µL (or 1.25 µL) H20 to master mix controls.

Sample dilutions		Primers A	Primers B	Primers C
1	1.8 µL			
2				
3				
4				
5				
6				
7				
8				

6. Spin all strips of tubes to mix
7. Arrange 96-well plate, triplicate samples and pipet tips to decrease plate contamination.
8. Add 25 µL of reaction mixture to corresponding well on plate layout using a new tip *each* time. Be careful not to get bubbles in tips.
9. Place optically adhesive cover on top of 96 well plate.
   Only touch outer edges and be sure to not get to get air bubbles when sealing.
10. Spin plate in centrifuge for 1 min at low speed
    Set up computer and 7300….

Open new document in Software:
Relative Quantification (RQ) plate
Label wells using Well Inspector
    Be sure to label endogenous control (ENDO, BetaActin, GAPDH, etc.)
    All others are Target
    Label each sample exactly the same!
Change volume to 25µL in Instrument tab
Add dissociation curve when using SybrGreen
    Save File
    Start to run PCR (do not interrupt)
To start a new study file (.sdm)…
    RQ(ddCt) Study
    Add Plates (all plates in study)
    Analysis Settings→ Calibrator Sample (control sample) → ReAnalyze
    Export→ Both (.csv)

B.5 RNA Isolation– using TRIZOL and QIAGEN RNeasy Mini Columns

Supplies Needed:

TRIzol (Invitrogen)
RNeasy Mini Kit (Qiagen):
  RNeasy Mini Spin Columns (pink)
Buffer RLT
Buffer RWI
  Buffer RPE (with ethanol!)
  2mL collection tubes
RNase free DNase I Kit (Qiagen):
  DNase I Stock Solution
  RDD Buffer
70% ethanol made with nuclease-free water
Chloroform
Nuclease-free Water
Nuclease-free Micro-centrifuge tubes (~1.2mL)
Phase lock gel tubes- heavy
Nuclease-free Filter tips

Before Starting:

- Place PBS in 37°C water bath
- Prepare 50 mL of 70% ethanol (35mL EtOH + 15mL nuclease-free water)
  Label: 70% ethanol Nuclease-Free
- Prepare DNase I + Buffer RDD in micro-centrifuge tube (store on ice)(make fresh)
  Buffer RDD = (# samples +1) x 70µL
  DNase I solution = (# samples +1) x 10µL
- Label QIAshredders (purple) with sample numbers (side and top)
- Bring labeled QIAshredders (purple) and Buffer RLT to hood
- Wipe hands and pipets with RNase Away
- Thaw samples on ice (from -80C freezer)
- Spin phase lock gel-heavy tubes at 1500xg (12,000 rpm?) for 30 sec to spin gel to bottom of tube

Procedure:

1. Once samples are thawed, transfer to phase lock gel tubes
2. Incubate 5 minutes at for 5 minutes at 15-30°C (RT)
   If needed, STOPPING POINT: Freeze at -80°C

3. Add 200 µL chloroform per 1 mL TRIzol reagent. Cap the tube and shake vigorously for 15 seconds.

4. Incubate for 2-3 minutes at 15-30C.
5. Centrifuge at no more than 12000 x g for 15 minutes at 2-8°C.

Following centrifugation, the mixture separates into a lower red, phenol-chloroform phase, an interphase, and a colorless upper aqueous phase. RNA remains exclusively in the aqueous phase. The volume of the aqueous phase is ~60% of volume of TRIzol reagent used.

6. Transfer the upper aqueous phase to a new nuclease-free microcentrigure tube. Save the lower organic phase if isolation of DNA or protein is required. Record µl removed.

Do not get any material from the lower phases! It is better to sacrifice aqueous material than to risk contamination with the lower precipitate.

7. Precipitate the RNA from the aqueous phase by addition of an equal volume of 70% ethanol (~600 µL) and mix thoroughly. Do NOT centrifuge.

SLOWLY add ethanol to prevent local precipitation.

From here, the RNeasy Mini Kit procedure is followed….

Appendix C Plasmid Development Protocols & Nucleofection

C.1 TOP10 Transformations

To replicate pcDNA3.1/His/SCX and pcDNA3.1/His/LacZ plasmids, bacterial cells were used. Chemically competent OneShot® TOP10 *E.coli* cells (Invitrogen) are transformed to produce large quantities of plasmid DNA using standard methods. Ten nanograms of the pcDNA3.1/His/SCX plasmid dissolved in TE buffer is added to one 50 µL vial of cells and incubated for 30 minutes on ice. The ligation mixture is then heat-shocked at 42°C for exactly 30 seconds, to allow plasmid DNA to pass cell membrane, and then returned to incubate on ice. Next, 250 µL of room temperature Super Optimal broth with Catabolite repression (S.O.C, Life Technologies) medium was added to the mixture followed by shaking at 37°C for 1 hour at 225 rpm. Finally, 100 µL of the transformation mixture was spread on pre-made Luria Bertram (LB) agar plates containing 0.1 mg/mL ampicillin to select for pcDNA3.1/His/SCX positive colonies and incubated overnight at 37°C. Colonies were picked from the plates using sterile toothpicks and inoculated in a 1 ml LB broth with ampicillin at 100 µg/mL (LB-amp). Broth cultures were incubated overnight at 37°C while shaking at 160 rpm. All colonies were screened using restriction enzyme digests or PCR. To verify presence of the scleraxis cDNA, a selection of positive colonies will be screened using PCR.

To replicate the pCMV-GFP-SCX plasmid, chemically competent DH5α cells were used. Briefly, 5 ng of plasmid was added to an aliquot of DH5α cells, incubated for 30' on ice, warmed at 37°C for exactly 20 seconds and then placed back on ice for 2'. The remaining incubation proceeded as above.

C.2 PCR colony screening

To perform standard PCR, cells were pelleted from 200 µl of each LB-amp cultures (14,000 x g, at room temperature), resuspended in 100 µl 1X TE buffer and heated at 95°C for 5 minutes. Each PCR reaction (20 µl) contains an aliquot (1 µl) of the cell lysates in TE, primers at 0.25 µM, and 2X *Taq* PCR Master Mix (200 µM dNTPs, 1.5 mM $MgCl_2$, 0.5 units *Taq* DNA polymerase, and Tris HCl based buffer, Qiagen). Forward T7 (5' TAATACGACTCACTATAGGG 3') and reverse bovine growth hormone (BGH) primers (BH 246, 5' CACCCCCCAGAATAGAATGACACC 3') flank the scleraxis & LacZ cDNA insert in the pcDNA 3.1 vector and are used to screen the construct. After amplification, the products will be fractionated on a 1% agarose gel and stained with ethidium bromide (1.5 µg/mL in ddH_2O), and are viewed by a ultra-violet transilluminating light box. A subcloned culture that gives rise to products of the predicted size will be selected and 200 µL of the 'toothpick' culture will be added to 100 mL fresh LB-amp medium and will be incubated overnight at 37°C with shaking. Bacterial cell stocks are aliquoted from this overnight culture by adding 400 µL 50% glycerol to 400 µL of the bacterial culture and frozen at -80°C.

C.3 Plasmid Purification

For purification and elution of plasmid DNA, an adapted protocol will be used in conjunction with the Endotoxin-Free Maxi purification kit (Qiagen). The overnight culture (100 mL) will be centrifuged at 6,000 x g for 15 minutes at 4°C. The pellet will be resuspended in 10 ml of Buffer P1 (50 mM Tris-Cl (pH 8.0), 10 mM EDTA, and 100 µg/mL RNase A). Resuspended cells are lysed with the addition of 10 ml Buffer P2 (200 mM NaOH

and 1% SDS [w/v]), and protein and bacterial genomic DNA precipitated with 10 ml chilled neutralization Buffer P3 (3.0 M potassium acetate, pH 5.5). This mixture will be centrifuged at 15,000 x g for 30 minutes at 4°C. The supernatant will then be poured into the barrel of the QIAfilter Cartridge and incubated at room temperature for 10 minutes. The cell lysate (~25 mL) is gently filtered using the plunger included with the kit into a sterile 50 mL conical tube. Buffer ER (2.5mL) added to the lysate and incubation on ice for 30 minutes removes endotoxins.

The lysate, containing plasmid DNA, is adsorbed to the silica resin (QIAGEN-tip 100) pre-equilibrated with 10 ml Buffer QBT (750 mM NaCl, 50 mM MOPS, pH 7.0, 15% isopropanol [v/v], and 0.15% Triton® X-100 [v/v]). Bound plasmid DNA is washed twice with 30 ml Buffer QC (1.0 M NaCl, 50mM MOPS, pH 7.0, and 15% isopropanol [v/v]). The DNA is eluted with 15 ml of Buffer QN (1.6 M NaCl, 50 mM MOPS, pH 7.0, and 15% isopropanol [v/v]) into a sterile 50mL conical tube and precipitated by adding 10.5 mL of room-temperature isopropanol. The DNA pellet is collected by centrifugation (15,000 x g for 30 minutes at 4°C) then gently washed with 600 µL of endotoxin-free 70% ethanol and carefully transferred to a microcentrifuge tube. Pellets are recentrifuged at high speed for 2 minutes. The supernatant was decanted, and the pellet air dried for 15 minutes on the benchtop. The DNA pellet was re-dissolved in 200 µL of endotoxin, DNase, & RNase-free H_2O. The approximate concentration and purity of the DNA was estimated by measuring the absorbance at 260 nm and 280 nm ([DNA] µg/mL = A260 x dilution factor x 50 µg/mL [extinction coefficient]), using a .NanoDrop spectrophotometer (ThermoScientific, Wilmington DE). An aliquot at a concentration of 100 µg/mL was sent to the Virginia Bioinformatics Institute (VBI) Core Laboratory for full sequencing of the construct using

the T7 promoter primer (5' TAATACGACTCACTATAGGG 3') provided by VBI for pcDNA3.1 vector or OriGene's supplied primers (VP1.5: 5'GGACTTTCCAAAATGTCG 3', XL39: 5' ATTAGGACAAGGCTGGTGGG 3') for pCMV-GFP-SCX. Obtained sequences were compared to the predicted sequence and verified as the correct sequence prior to transfection.

C.4 Generation of Restriction Digest Maps

Following plasmid purification, the circular DNA is digested using specific restriction enzymes to further confirm identity of the construct. For the pcDNA3.1/His/SCX, the restriction enzymes *ApaI*, *BglII* and *NcoI* (New England Biolabs) will be used to cut the sequence at known locations using Lasergene v.7.2 software (DNASTAR). For the reporter plasmid pcDNA3.1/His/LacZ, the restriction enzymes *EcoRV*, *AleI* and *NcoI* (New England Biolabs) will be used. For the plasmid pCMV-GFP-SCX, the restriction enzymes *BamHI* and *XhoI* (New England Biolabs) were used. Each reaction contains 0.5 µg plasmid DNA, 1 µL enzyme (concentrations: *EcoRV* 20 U; *AleI* 5 U: *ApaI* 50 U; *BglII* 10 U; *NcoI* 10 U), 2 µL NE buffer (NE3 or NE4 as recommended by manufacturer), 2 µL 10X Bovine Serum Albumin if recommended (100 µL/mL, BSA, New England Biolabs) and nuclease-free water to a total reaction volume of 20 µL. Reactions are gently mixed and incubated for 60 minutes at 37°C or 25°C (*ApaI* only) according to the enzyme recommendations. Following digestion, 6 µL of Blue Loading Dye (Sigma) is added to each reaction and mixed. Fifteen microliters of each reaction and DNA ladder (Sigma) is loaded into the wells of a 1.5% agarose gel and gel electrophoresis is run at 100V for 30-45 minutes in 1X Tris-Borate-EDTA (TBE) buffer. Finally, the gel is stained with ethidium bromide and visualized under UV light as above. Vectors are verified by the appearance of bands that correspond to the predicted fragment sizes using the expected sequence.

C.5 Plasmid Mini Preps

Aliquots of the 'toothpick' broth cultures (1 mL) can be purified for restriction enzyme digests prior to large scale production. Following overnight growth, 500 µL of bacterial cultures is transferred to a microcentrifuge tube and centrifuged at maximum speed for 2' to pellet the cultures. The supernatant is aspirated and 100 µL of Buffer P1 (from the Qiagen Endotoxin-Free Maxi purification kit) is added to make a homogenous suspension. Next, 200 µL of Buffer P2 (also from the kit) is added and then the mixture is incubated on ice for 5'. One hundred fifty microliters of cold Buffer P3 (from kit) is then added, followed by another 5' incubation of ice. The mixture is then centrifuged at maximum speed for 5'. The supernatant is transferred to a clean microcentrifuge tube and precipitated in an equal volume of isopropanol (~400 µL). Following centrifugation at maximum speed for 5', a small DNA pellet is visible. The supernatant is aspirated and the pellet is then washed in 70% ethanol. Pellets are recentrifuged at high speed for 2 minutes. The supernatant was decanted, and the pellet air dried for 15 minutes on the benchtop. The DNA pellet was re-dissolved in 20 µL of endotoxin, DNase, & RNase-free H_2O. Dissolved DNA can be used for restriction enzyme digests or PCR.

C.6 Nucleofection

Supplies Needed:

Cell Line Nucleofector® Kit V (Lonza)
- Solution V
- Supplement
- Blue –cap cuvettes
- Sterile plastic pipettes

Plasmid DNA
Sterile pipet tips
Cultured cells in T75 flasks

Before starting:

- Warm PBS, media and Trypsin/EDTA in water bath
- Turn on Nucleofector device to warm up

Procedure:

1. Rinse flasks 2X with 1X PBS
2. Add 3 mL 1X Trypsin/EDTA to each flask and incubate 4' in the incubator
3. Add 5 mL DMEM growth media to each flask and collect in individual 15 mL conical tube.
    a. Take aliquot of each sample to count cell number
4. Centrifuge 1500rpm for 8'
5. Resuspend each at **1 x 10^6 cells/mL** with DMEM growth media and transfer to sterile microfuge tubes
6. Centrifuge at 90*g* for 10' in microcentrifuge
7. Resuspend in 100 µL Nucleofector Soln' V + Supplement
    a. Cells should not be in Soln' V + Supp for more than 15'
8. Add **x** µL plasmid DNA (circular or linear) for 6- 10 µg
9. Mix each by pipetting and transfer to blue-cap cuvette
10. Place in machine and nucleofect with program T-20
11. Add 500µL warm DMEM growth media with supplied *transfer pipette* and transfer to new microfuge tube. Repeat for all samples
12. Incubate all samples at 37°C for 10' (recovery step)
13. Use *transfer pipette* to transfer cells to T75 flask containing 10 mL DMEM growth media, rocking gently to distribute cells (or to conical tube filled with DMEM growth media to dilute cell suspension prior to plating)

Appendix D Bioreactor procedures

D.1 Sterilization procedures for Bioreactor Chambers:

From bottom to top, the following components make up each chamber:

1. Metal baseplate
2. PDMS gasket w/coverslip view port (clear)
3. Ultem machined chamber (amber)
4. Rubber gasket (black)
5. Polycarbonate lid (clear)

Other components:

1. Long screws for securing baseplate, PDMS gasket to chamber
2. Long screws wrapped in Teflon tape (4) for inner holes
3. Short screws for securing lid to chamber
4. Magnetic pull rod
5. Non-magnetic pull rod
6. Clamps (2)

Prepare in sets of two (2) chambers for STEAM sterilization in pouches:

1. Baseplates + Chambers + Rubber Gaskets
2. PDMS gaskets * handle carefully!
3. Non-magnetic pull rods
4. Screwdriver with plastic handle (2)
5. Tweezers (curved and straight)

Prepare in sets of two (2) for STEAM sterilization in Pyrex dishes:

1. Teflon long screws (8 total)
2. Long & short screws for 2 chambers

For non-steam sterilization, soak the following in denatured ALCOHOL in hood:

1. Lids
2. Magnetic pull rods

For ETHYLENE OXIDE sterilization of PEUUR scaffolds, prepare PEUUR scaffolds by securing in clamps (~4.5cm L x 1.5 cm W) then leech in 100% EtOH for 2 days, followed by DI water for 2 days (changing solutions every day). Once dry, E.O sterilize in pouches and de-gas for minimum 24 hrs.

D.2 Bioreactor Chamber Assembly

*In sterile surgical gloves (person 1)
*In clean lab gloves (person 2)
Bioreactor assembly is requires two people in the hood to maintain sterility. Chambers are sterilized in sets of two and therefore assembled in sets of two.
Before beginning

- Place magnetic pull-rods and clear lids in large basin filled with 70% denatured alcohol to sterilize.
- Open one or two sterile 245mm square bioassay dishes to use as work surface (NOT the hood surface)
- Place 1 pack of each sterilized chamber parts, PDMS gasket w/coverslip, pull rods, screws and Teflon-coated screws in hood (spray liberally with alcohol first)

To assemble:

1. **Open** pouch of chamber parts and PDMS gasket
2. **Remove** chamber parts and PDMS gasket to square dish
3. **Assemble** starting from bottom baseplate
4. Rubber gasket
5. Chamber
6. PDMS gasket
7. Baseplate w/countersunk screw holes OUT
8. **Remove** lid from alcohol, allowing to dry briefly and pass to sterile person
9. **Secure** lids to top of chambers with four short screws (not necessary to screw in completely)
10. **Flip** entire assembly over and place Teflon screws (4) in inner hole locations (keep sterile, as these will be in contact with media)
11. **Finish** securing all long screws on baseplate and return to upright
12. Repeat for all remaining chambers before securing clamps inside chamber

To place clamps,

1. From seeding device, aseptically **transfer** clamps inside chamber remembering to flip clamps
    a. All lids will need to be un-screwed and lifted by non-sterile person or put in sterile location
    b. If cells are seeded on scaffolds, do not handle roughly and try to maintain length of construct
2. Using sterile forceps, **grasp** one clamp at a time to hold stationary and thread pull rod into clamp from outside
3. **Remove** magnetic pull rod from alcohol and allow to air dry before applying grease

4. **Coat** upper 2/3 of pull rod with thin layer of antimicrobial grease first (using sterile spatula or pipet tip)
    a. It is very easy to cross-thread the pull rod into clamp – do not force it!
5. One magnetic pull rod and one normal pull rod per chamber, doesn't matter which side
    a. At this point, the sterile person is no longer sterile and should NOT reach inside chamber unless new gloves are used.
    b. For seeded constructs, be very careful to not overextend lengthwise
6. Once both pull rods are secured, do not disturb the construct! The lids of the bioassay dish work better than the bottoms because the side height is less.
7. The clamber is now ready for mechanical stimulation